# Thermal Management of Conductive Electric Road Systems

Abrahamsson, Philip

2020

*Document Version:*
Publisher's PDF, also known as Version of record

# Thermal Management of Conductive Electric Road Systems

PHILIP ABRAHAMSSON
FACULTY OF ENGINEERING | LUND UNIVERSITY

# Thermal Management of Conductive Electric Road Systems

By Philip Abrahamsson


LUND
UNIVERSITY

Thesis for the degree Doctor of Philosophy in Engineering
Thesis advisors: Prof. Mats Alaküla, Assoc. Prof. Avo Reinap,
Assistant Prof. Francisco J. Márquez-Fernández

Faculty opponent: Dr. Reno Filla

To be presented, with the permission of the Faculty of Engineering of Lund University, for public criticism in the MA:2 lecture hall, Math Annex Building, Sölvegatan 20 on Friday, the 4th of December 2020 at 10:00

| | |
|---|---|
| **Organization**<br>LUND UNIVERSITY<br>Division of Industrial Electrical Engineering and Automation<br>Box 118, SE–221 00 LUND, Sweden | **Document name**<br>DOCTORAL DISSERTATION<br>**Date of dissputation**<br>2020-12-04 |
| **Author(s)**<br>Philip Abrahamsson | Sponsoring organization |


**Title and subtitle**
Thermal Management of Conductive Electric Road Systems


**Abstract**
A transition from conventional vehicles to electric vehicles requires a well-developed charging infrastructure. Electric Road Systems (ERS) are designed to provide power to moving vehicles, both for propulsion and for charging the onboard batteries. By providing power to moving vehicles, the need for large onboard batteries is reduced as the batteries are only needed when there is no ERS present.

This thesis investigates an Alternating Short-Segmented ERS (ASSE), with respect to internal and surface temperature of the ASSE and lifetime estimations of the main power switches. A 3D FE thermal model is developed to assess how different charging cases affect the temperatures of the ASSE. This model is calibrated and validated with measurements from a full size ASSE. The model is then used to acquire the temperature profile for the heatsink of the main semiconductor switches, which is used as an input for the lifetime models. The lifetime models used in this thesis are developed for power modules and not discrete components. Due to this, experimental tests have been performed to recalibrate the lifetime models to better fit the components used in the ASSE.

The thermal model combined with the lifetime models are used to investigate both static and dynamic charging with regards to the temperature of the ASSE and the expected lifetime of the main switches. For static charging, the losses are localized to a small area, thus the risk of hot spots is larger than for dynamic charging. Since the vehicles are moving while performing dynamic charging, the losses are spread out over a larger area, minimizing the risk for hot spots.



**Key words**
Thermal modeling, Electric Road System, lifetime modeling

Classification system and/or index terms (if any)

| | | |
|---|---|---|
| Supplementary bibliographical information | | **Language**<br>English |
| **ISSN** and key title | | **ISBN**<br>978-91-985109-0-4 (print)<br>978-91-985109-1-1 (pdf) |
| Recipient's notes | **Number of pages** 145 | Price |
| | Security classification | |




Signature 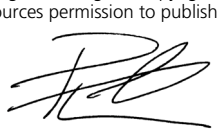 Date 2020-10-23

# Thermal Management of Conductive Electric Road Systems

by Philip Abrahamsson


LUND
UNIVERSITY

**Cover illustration:** Alternating Short-Segmented ERS



Div. Industrial Electrical Engineering and Automation
Department of Biomedical Engineering
Faculty of Engineering
Lund University

ISBN: 978-91-985109-0-4 (print)
ISBN: 978-91-985109-1-1 (pdf)
CODEN: LUTEDX/(TEIE-1093)/1-145/(2020)

Printed in Sweden by Media-Tryck, Lund University, Lund 2020

*"The way to get started is to quit talking and begin doing."*
*-Walt Disney*

# Contents

Acknowledgements . . . iii
Popular summary . . . v
Nomenclature . . . vii

**Chapter 1: Introduction** **1**
1.1 Background . . . 1
1.2 Objectives and limitations . . . 12
1.3 Contributions . . . 14
1.4 List of publications . . . 14

**Chapter 2: The ASSE design** **17**
2.1 Traffic flow and power requirement of vehicles . . . 17
2.2 Requirements . . . 22
2.3 Design . . . 25

**Chapter 3: Thermal modeling** **31**
3.1 Heat sources . . . 31
3.2 Heat dissipation . . . 42
3.3 Thermal model . . . 52
3.4 Thermal model calibration and validation . . . 60
3.5 Chapter summary . . . 69

**Chapter 4: Lifetime modeling** **71**
4.1 Mechanisms of failure . . . 71
4.2 Models to estimate lifetime . . . 73
4.3 Compensation factor for discrete IGBTs . . . 75
4.4 Lifetime model linked to the thermal model . . . 79

**Chapter 5: Analysis of Static charging** **81**
5.1 Reference cases . . . 81
5.2 Charging time . . . 83
5.3 Number of IGBTs . . . 87
5.4 Contact resistance . . . 91
5.5 Thermal conductivity of the contact segment . . . 94
5.6 External cooling . . . 97

5.7 Additional power from multiple vehicles . . . . . 101
5.8 Conclusions . . . . . 105

**Chapter 6: Analysis of dynamic charging** **107**
6.1 Reference parameters . . . . . 107
6.2 Distance between feed-in points . . . . . 109
6.3 Impact of traffic . . . . . 110
6.4 Number of IGBTs . . . . . 111
6.5 Vehicle speed . . . . . 113
6.6 Cooling from moving vehicles . . . . . 114
6.7 Location . . . . . 115
6.8 Conclusions . . . . . 117

**Chapter 7: Conclusions and future work** **119**
7.1 Conclusions . . . . . 119
7.2 Future work . . . . . 121

# Acknowledgements

Ever since I was a kid, I have wanted to get a PhD. Most children want to become firefighters or police officers, but I had my mind set on becoming an engineer with a PhD. I would like to thank Professor Mats Alaküla for giving me the opportunity to fulfill my childhood dream and guiding me throughout this experience. Whenever we had a meeting planned, I have learned to expect a few more things on my plate. However, no matter how many additional things there are to do after a meeting, the motivation you present makes it feel like the workload is less than before.

I would also like to thank my co-supervisors Assistant Prof. Francisco Marquez and Associate Prof. Avo Reinap. Fran, you have been a great support and your ideas and proofreading have been invaluable. I am very thankful for your decision of coming back to IEA after your rogue years in the UK. Avo, I know that we have not been working very closely together, but you have always been available if I ever needed help. Whenever I looked over towards Avo's office the door has always been fully open. It has been very reassuring to know that if I needed support you have always been there and that you have never been too busy for questions.

A special thank you to Getachew Darge who has been helping me in the lab over the last years. You always come up with clever solutions to fix laboratory setups and even though you have a million things in the different storage rooms, you always know where you have every piece of equipment.

I want to thank Dr. Gabriel Domingues for being my unofficial mentor. You are the one that has had to suffer from my questions about everything and nothing.

Lars Lindgren is another important person I would like to thank. It was always a joy when you came by my office and I have learned a lot from you. Lars you have probably forgotten more than I will ever learn.

A big thank you to Dan Zethraeus and Andreas Sörensen from Elonroad for answering questions and giving me access to the Elonroad test track.

Then there is also the entire division of Industrial Electrical Engineering and Automation (IEA) who have made this journey not only possible but also enjoyable. I will not list you all by name, but you know who you are, and I want to thank you all. I can hardly believe that this long journey is about to be over. When I started at the division, I did not really know anyone, but over the last few years I not only consider the people at IEA my colleagues but also my friends.

Throughout my life my mom, dad and brother have always been there for me, and during my PhD it has not been any different. The support you give does not only make getting a

PhD easier but also life itself. Fredrik Abrahamsson, even if you decide you do not want to follow in my footsteps and work towards getting a PhD of your own, now at least you have your name in one.

The last person I want to thank is my wonderful wife Katherine Morrow who has supported me and motivated me during this journey. You have been forced to read my "boring" and "they are all the same" papers and for that I am eternally grateful. Thank you for being there for me!

## Popular summary

The transition of not least road transport from combustible fossil fuels to electric energy supply requires a well developed charging infrastructure capable of supplying the vehicles with energy. The charging infrastructure can be composed of several different types of chargers, such as fast chargers and slow home chargers. Another type of energy supply, less well-known but yet interesting for mass electrification is Electric Road Systems (ERS), which are designed to charge vehicles while they are moving. The power transfer of an ERS, is just like any other charger, not perfect, resulting in e.g. generated heat. Due to this, the thermal properties of an ERS are of interest, as the heat losses may result in elevated temperatures which could damage the ERS or pose a safety risk to the surrounding environment. For an ERS located on ground level there is always a chance that someone touches a part of the ERS that have been thermally affected by the power transfer and can therefore be hot. To model the thermal behavior of an ERS a thermal model is developed, in order to predict the temperatures both on the surface of the ERS and also within the ERS. This model is calibrated and validated against measurements from a real world ERS test track. The measurements cover a variety of charging powers and external environmental conditions.

To thermally model an ERS, knowledge about the contact point losses between the current collector and the ERS is of high importance. This loss is especially important for static charging applications, as it is localized and not spread out over a larger area as when charging moving vehicles. To investigate this loss, a rotating test rig is used where two surfaces slide against each other and the resulting contact resistance is measured. This test rig is capable of testing different material combinations, current levels, speeds, and contact forces.

Another important input to the thermal model is the cooling effect by moving vehicles. When vehicles move the air around the vehicle is disturbed, causing forced convection on the ERS, and providing additional cooling. This additional cooling has been measured at different speeds to gain knowledge of how the moving vehicles on a road affect the heat dissipation from an ERS.

With a significant number of vehicles using the ERS everyday, it is important to consider the expected lifetime of the ERS. The ERS needs to be reliable and last long enough to be profitable. In this thesis an Alternating Short-Segmented ERS (ASSE) is investigated. An ASSE is based on having short contact segments arranged longitudinally along the road, with alternating potential. These segments can be energized individually and need to be short enough for a vehicle to connect to at least two contact segments at all times. To have such short contact segments the switching element that can switch a contact segment on or off needs to be placed inside the ASSE structure. This switching element experiences thermal cycling caused by the ASSE operation, and a switching element is not able to

handle an infinite amount of cycles. While different lifetime models for power modules can be found in literature, limited data is available regarding discrete components, which are used in the investigated ASSE. Due to this a lifetime test rig is built to investigate how the lifetime of the switching element is affected by different charging powers. The results from the lifetime test rig is combined with the existing lifetime models for power modules to estimate the discrete components' expected lifetime.

# Nomenclature

| | |
|---|---|
| $\alpha_s$ | Solar absorptivity [-] |
| $\alpha_{al}$ | Temperature coefficient of the resistivity for the aluminum foil [1/K] |
| $\alpha_{LESIT}$ | Coefficient used in the LESIT model [-] |
| $\beta$ | Coefficient of thermal expansion [1/K] |
| $\beta_{1...6}$ | Coefficient used in the CIPS model [-] |
| $\delta$ | Declination [°] |
| $\epsilon$ | Emissivity [-] |
| $\eta$ | Drivetrain efficiency [-] |
| $\theta_z$ | Solar zenith angle [°] |
| $\mu_f$ | Coefficient of friction [-] |
| $\mu_{fluid}$ | Dynamic viscosity [Pa·s] |
| $\rho$ | Density [kg/m$^3$] |
| $\rho_{electric}$ | Electrical resistivity [Ω m] |
| $\sigma$ | Stefan Boltzmann constant [W/(m$^2$K$^4$)] |
| $\phi$ | Latitude [°] |
| $A_{cross}$ | Cross-sectional area [m$^2$] |
| $A_{ERS}$ | Ground area covered by the ERS [m$^2$] |
| $A_{front}$ | Effective front area [m$^3$] |
| $A_{RMS}$ | RMS current [A] |
| $A_{surface}$ | Surface area [m$^2$] |
| $AM$ | Air mass [-] |
| $C$ | Cloud coverage [-] |
| $C_D$ | Drag coefficient [-] |
| $C_r$ | Roll resistance [-] |

| | |
|---|---|
| $C_p$ | Specific heat capacity [J/(kg K)] |
| $Coverage$ | The fraction between the ERS being shaded and not shaded [-] |
| $d_{Airgap}$ | Airgap thickness [m] |
| $d_{Asphalt}$ | Asphalt thickness [m] |
| $D$ | Diameter of the bondwire [$\mu$m] |
| $Day$ | Day of the year [-] |
| $E_a$ | Activation energy [J/mol] |
| $E_{off}$ | Turn off energy [J] |
| $E_{on}$ | Turn on energy [J] |
| $E_{thermal}$ | Incoming thermal radiation [W/m$^2$] |
| $f_{sw}$ | Switching frequency [Hz] |
| $F_N$ | Normal force [N] |
| $FractionDiffuse$ | The ratio between diffuse and total irradiance [-] |
| $g$ | Gravitational constant [m/s$^2$] |
| $G_R$ | Grashof number [-] |
| $h$ | Cooling coefficient [W/(m$^2$K)] |
| $h_{angle}$ | Hour angle [°] |
| $h_{Convection}$ | Convective heat tranfer coefficient [W/(m$^2$K)] |
| $h_{freeconv}$ | Convective heat tranfer coefficient for free convection [W/(m$^2$K)] |
| $Hour$ | Solar time [-] |
| $I$ | Current [A] |
| $I_{bondwire}$ | Current per bond wire [A] |
| $I_C$ | Collector current [A] |
| $I_D$ | Direct solar irradiance [W/m$^2$] |
| $I_G$ | Global solar irradiance [W/m$^2$] |

| | |
|---|---|
| $I_{solarAVG}$ | Average solar irradiance reaching the ERS [W/m$^2$] |
| $k$ | Thermal conductivity [W/(mK)] |
| $k_{Aluminum}$ | Thermal conductivity of the aluminum [W/(mK)] |
| $k_{Asphalt}$ | Thermal conductivity of the asphalt [W/(mK)] |
| $k_b$ | Boltzmann constant [J/K] |
| $k_{ERS}$ | Fraction of installed ERS [-] |
| $k_{Insulation}$ | Thermal conductivity of the soft insulation between the negative conductor and the PCB feeding rail [W/(mK)] |
| $k_{Rubber}$ | Thermal conductivity of the rubber [W/(mK)] |
| $K$ | Cloud height [-] |
| $K_{CIPS}$ | Coefficient used in the CIPS model [-] |
| $K_{LESIT}$ | Coefficient used in the LESIT model [-] |
| $L$ | Conductor length [m] |
| $L_{ch}$ | Characteristic length [m] |
| $m$ | Mass of the vehicle [kg] |
| $N_f$ | Number of cycles until failure [-] |
| $Nu$ | Nusselt number [-] |
| $P$ | Power [W] |
| $P_{aux}$ | Auxiliary power [W] |
| $P_{cond}$ | Average conduction loss [W] |
| $P_{drag}$ | Power to overcome airdrag [W] |
| $P_{friction}$ | Friction power [W] |
| $P_r$ | Prandtel number [-] |
| $P_{roll}$ | Power to overcome rolling resistance[W] |
| $P_{solarAVG}$ | Average solar power reaching the ERS [W] |

| | |
|---|---|
| $P_{sw}$ | Average switching loss [W] |
| $P_{vehicle}$ | Power needed by the vehicle [W] |
| $Q$ | Heat [W] |
| $R$ | Resistance [Ω] |
| $R_{PCB}$ | Electrical resistance of the PCB [Ω] |
| $R_{start}$ | Resistance at the start of an experiment [Ω] |
| $R_{thch}$ | Thermal resistance case-heatsink [K/W] |
| $Re$ | Reynolds number [-] |
| $RH$ | Relative humidity [%] |
| $t_{on}$ | On time of the solid state switch [s] |
| $T$ | Temperature [K] |
| $T_{\infty}$ | Bulk temperature [K] |
| $T_{ambient}$ | Ambient temperature [K] |
| $T_{ground-level}$ | Temperature at ground level [K] |
| $T_{heatsink}$ | Heatsink temperature [K] |
| $T_j$ | Solid state junction temperature [K] |
| $T_{low}$ | Lowest temperature during a power cycle [K] |
| $T_m$ | Average temperature during a power cycle [K] |
| $T_p$ | Period time for the solid state switch [s] |
| $T_s$ | Surface temperature [K] |
| $v_{air}$ | Air speed [m/s] |
| $v_{vehicle}$ | Vehicle speed [m/s] |
| $V_{CE}$ | Collector emittor voltage [V] |
| $v_{fluid}$ | Fluid speed [m/s] |
| $V_{rating}$ | Voltage rating of the IGBT divided by 100 [V] |

| | |
|---|---|
| $V_{RMS}$ | RMS voltage [V] |
| $U$ | Voltage [V] |
| $Z_{thjc}$ | Thermal impedance junction-case [K/W] |
| AC | Alternating current |
| $Al_2O_3$ | Aluminum oxide |
| ASSE | Alternating short segmented ERS |
| BEV | Battery electric vehicle |
| CIPS | Lifetime model for IGBT modules |
| $CO_2$ | Carbon dioxide |
| DC | Direct current |
| DUT | Device under test |
| EPA | Environmental Protection Agency |
| ERS | Electric road systems |
| EU | European Union |
| EV | Electric vehicle |
| FE | Finite element |
| HEV | Hybrid electric vehicle |
| IGBT | Insulated-gate bipolar transistor |
| IR | Infra red |
| LESIT | Lifetime model for IGBT modules |
| MOSFET | Metal oxide semiconductor field effect transistor |
| p.u. | Per unit |
| PCB | Printed circuit board |
| RC-network | Thermal network based on thermal resistances and thermal masses |
| RMS | Root mean square |

| | |
|---|---|
| TIM | Thermal interface material |
| TO-247 | A specific type of package for discrete semiconductor components |
| US | United States |
| Vdc | DC voltage |

# Chapter 1: Introduction

## 1.1 Background

The transport sector is responsible for about 25 % of the global $CO_2$ gas emissions out of which 75 % is from road transport [1]. A majority of today's vehicles are conventional vehicles [2], fueled with diesel or gasoline. With vehicle manufacturers replacing conventional vehicles with hybrid electric vehicles (HEVs) and battery electric vehicles (BEVs), the ratio of vehicles with electric propulsion is increasing [2]. This fast swing to HEVs and BEVs increases the need for batteries. By 2025 the yearly battery production can be nearly 500 GWh [3]. Since today's lithium ion batteries rely on rare metals, such as cobalt, the need for these materials will also increase, unless a new battery technology is developed. However, the labor conditions and environmental responsibility for the extraction of some of these metals from current sources are under question [4], which makes it difficult for manufacturers of equipment containing batteries to secure that their supply lines use ethically sourced cobalt [5].

Another problem with today's electric vehicles is the low energy density of batteries. Low energy density results in both large and heavy battery packs, which increase the energy consumption and limits the cargo capacity of the vehicle. Batteries are also expensive and even though battery prices are steadily decreasing [6], [7], the battery packs are a substantial part of the total vehicle cost for the near future. The battery pack is also responsible for a large amount of $CO_2$ emissions in a life-cycle perspective of an EV [8].

A solution to these problems could be a technology that facilitates energy supply while driving. Instead of carrying the energy in batteries on board the vehicles, it would be supplied from an external source and thus the need for on board energy storage could be reduced. Such a technology is called Electric Road Systems (ERS) and can be seen as a significant development of trolley bus supply technology. It is shown that with a well developed ERS network the need for batteries is significantly reduced [9]. However, the energy storage on board the vehicles can not be fully removed as the vehicles are not always connected to an ERS. While changing lanes there are likely short periods of time when the

energy supply is not available. Also installing ERS on 100 % of the roads is not economically optimal compared to covering a smaller fraction of the total road distance [10]. Therefore a realistic case would be to have a small energy storage to be able to drive some 10's of km without charging while driving on smaller roads.

### 1.1.1 Transportation electrification

Charging infrastructure is an important part of transportation electrification. Without a well implemented charging infrastructure electric vehicles will not be practical, and thus the rate of adoption of electric vehicles will remain low. There are three different types of charging:

- **Static charging** is when the vehicle is charging while standing still. This includes everything from AC charging at low power to fast DC charging and wireless charging, which can reach 100's of kW.
- **Dynamic charging** is energy supply when the vehicle is moving. The technology, known as Electric Road Systems (ERS), is developed to provide energy to moving vehicles that can be used for both charging and traction simultaneously. This system can be based on conductive, inductive or capacitive technology.
- **Battery swapping** is replacing an empty battery pack with another battery pack that is fully charged.

Static charging is the most common way of charging, similar to refueling a conventional vehicle. The main difference is in the magnitude of the power transfer. For example, assuming that a conventional gasoline powered car with a 60 l fuel tank can be filled in 2 minutes results in a flow rate of 0.5 l/s, which together with the high volumetric energy density of gasoline (34 MJ/l) yields a power transfer of 17 MW. Today commonly available fast charging for EVs are normally below 500 kW. Tesla's V3 Supercharger can charge with up to 250 kW [11]. As it can be seen from this comparison, the power transfer of gasoline is at least one order of magnitude greater compared to charging with electricity. This difference is to some extent compensated by the higher efficiency of an electric vehicle, which requires less energy than its fossil fueled counterpart to cover the same distance, but the difference in charging speed is still very high. The technology to build more powerful charging stations exists, but the limitation when fast charging a vehicle is in the battery onboard the vehicle. How fast a battery can be charged is mainly determined by the ability to prevent it from overheating. The battery chemistry determines the internal resistance, and thus the losses generated while fast charging, the cell design influences the heat dissipation and temperature gradient inside the battery cells, and the battery pack design and

cooling circuit affect the overall capability to keep the whole battery at the right temperature. The measure of how fast a battery can be charged is called C-rate, and it represents how long time (in hours) it takes to charge / discharge a battery completely. If an empty battery is charged with C-rate = 1, it means that it will take 1 hour to fully charge it. If it is charged with C-rate = 2 instead, it will take 1/2 of an hour to fully charge it. State of the art BEVs in 2019 [12] are capable of charging with C-rates up to 3, while most BEVs are commonly charging with a lower C-rate. In BEVs the batteries are usually energy optimized, which means they have a high energy density (kWh/kg) but have a limited power capability compared to a power optimized battery. Electric hybrid vehicles usually have smaller batteries that still need to deliver enough power to the vehicle. These batteries are power optimized and have a greater power density (W/kg) compared to energy optimized batteries. The choice between energy and power optimized batteries is not strictly one or the other. There is a continuous scale between the two and the degree of energy optimization or power optimization can be tailored to the application. An issue with high charging powers is that the electricity is difficult to store. This puts a heavy load on the local electric grid if the charging power is on the MW scale, especially if multiple vehicles are charging with high power simultaneously in the same area. Grid side energy storage can be used to stabilize the grid and even out the loads. Comparatively, for a conventional gas station the energy buffer is in an underground tank in the form of liquid fuel, which is very energy dense compared to even the most energy optimized batteries (>12 kWh/kg compared to about 0.25 kWh/kg at cell level in commercial EVs) [13], [14], [15].

Dynamic energy supply (with an ERS) is different since the vehicles are supplied with energy while they are moving. The power supplied to the vehicles is determined by the power needed to propel the vehicle plus any charging of the battery and supply of auxiliary loads. The power needed for propulsion is mostly determined by the type of vehicle, the load it may carry, the driving pattern and the road and weather conditions. The need to charge the battery is related to the fraction of the total trip distance that is covered with an ERS, i.e. enough energy needs to be transferred to the vehicle when charging to cover the distance when the energy supply is not available. The relative distance covered with an ERS is a design parameter when installing this form of infrastructure. By having a high coverage longer charging time is available to transfer the lower amount of energy needed, resulting in a lower supply power.

There are three fundamental ways of transferring energy from the ERS to the vehicle: through a capacitive or inductive coupling or through a conductive contact.

- In a **capacitive** solution the power transfer is through a coupled electric field (capacitive connection) between the vehicle and the ERS. One solution is to use a capacitive coupling between steel belts in the tires and a metal plate on the ground [16]. The impedance between the steel belt and the metal plate decreases with increased fre-

quency as the coupling is capacitive. To transfer energy with enough power to sustain a vehicle at highway speeds, the frequency and also the voltage need to be high [17]. This solution is not yet proven viable and is for now regarded as inferior to the other solutions.

- **Inductive** power transfer technology transfers power through a coupled magnetic field, by having at least one transmitter and one receiver coil that are inductively coupled. This technology is basically a transformer with a large airgap that couples the primary and the secondary winding [18]. The main difference with a normal transformer and an inductive ERS is that in the case of an ERS the coupling between the primary and secondary winding varies with the vehicle position [19]. Misalignment between the two coils due to the vehicle position is important to consider as it may be several 100's of mm off the center line [20].

- **Conductive** ERS are based on a physical contact between the current collector on the vehicle side and the ERS track. This connection can be located under, to the side of or above the vehicle. The main drawback of having the contact above the vehicle is that the contact needs to be high enough above the ground to allow tall vehicles to pass under it. This makes it very challenging for smaller vehicles to use the ERS as the contact point is located too high above the smaller vehicles. Road bound and side mounted conductive ERS do not have this drawback and are able to supply small and large vehicles with energy. A conductive ERS, no matter where the connection is, do not have a reliable electric protective earth connection to the vehicle, which can be used for safety [21]. Because of the unreliable or non existing ground connection the equipment on board the vehicle need to ensure a safe chassis potential.

Battery swapping is straight forward, where a discharged battery is replaced with a charged battery. This technique is used in e.g. forklifts and power tools but can also be applied to other vehicles. The discharged battery is swapped at a swapping station where there may be several batteries charging at the same time. This makes the effective charging power to a vehicle large if the swap is fast as the energy is physically moved into the vehicle. This allows for short charging times from the vehicle point of view as long as the swapping is performed quickly. The discharged battery can then slowly charge at the charging station, and when full it can be placed in another vehicle. Battery swapping implies that a specific battery does not belong to a specific vehicle and that there are more batteries than vehicles. It also requires a high degree of standardization of the battery shape and communication with the rest of the vehicle. These factors may complicate the ownership of the battery and is a question that needs to be solved in order to make battery swapping possible on a large scale.

### 1.1.2 Conductive road bound ERS

A conductive road bound ERS is a conductive ERS located on the ground level. Thus it can be utilized by light vehicles such as cars as well as heavy vehicles. Charging of two wheeled vehicles may be possible, but is more difficult compared to a vehicle with more wheels due to less stability of a two wheeled vehicle. By making it possible for almost all vehicles to utilize the ERS, the benefit of significantly reduced battery needs is maximized. Since the number of passenger cars and therefore the amount of batteries they require is at least an order of magnitude higher than that for trucks, it is essential that also cars can benefit from any ERS technology.

As with any conductive ERS there is a sliding contact between the current collector and the ERS track. This contact point is subjected to wear from the sliding as well as from the electric power transfer. Friction in the contact point generate heat as the contact is sliding, which also reduces the efficiency of the energy transfer. With a road bound solution the surface of the ERS may not be perfectly clean and there can be e.g. sand, dirt, leaves on the ERS. This needs to be taken in consideration as it can affect the performance of the sliding connection. The current collector needs to be designed in a way that it can handle the harsh environment it is being used in and last for the designed lifetime of the current collector.

Below are the most well known conductive road bound ERS technologies described:

- Alstom's ERS consists of two parallel tracks, separated by 15 cm [21]. The ERS structure is installed in the road with a depth of about 8 cm and reaches about 2 mm above the surface level [22], see Fig. 1.1. The ERS is split into segments, energized with 750 Vdc [21]. To either side of the track that is energized to 750 Vdc there is a grounded metal structure to act as a voltage barrier. On one side is a dedicated ground conductor and on the other is the return path of the current.


**Figure 1.1:** Shows the Alstom ERS, image taken from [23].

- Elonroad's solution is placed on top of the asphalt with a height of around 4 cm and

a width of 35 cm [24], see Fig. 1.2. The Elonroad ERS is divided into short segments placed in a longitudinal sequence [9]. The segments have a length of 1 m with an insulating separator between them. The contact segments have alternating potential in longitudinal direction where every other segment can be energized individually. The segments that can be energized are energized by power electronics located inside the ERS structure. The rest of the segments are connected to the return conductor, which is connected to ground in the transformer station. Due to the alternating voltage potential of the segments the current collector needs to have at least three contact points [21].

**Figure 1.2:** Shows the Elonroad ERS.

- Elways ERS design is based on having two slots into the ground, see Fig. 1.3. The energized contact track is located inside the slots, making it safe to walk on [25]. The top of the ERS structure is connected to ground [21]. With a ground potential at the top surface layer, there is a voltage barrier between the energized track and the environment surrounding the ERS. The ERS is split up into 50 m segments, which are fed with AC voltage and can be energized individually [26].

**Figure 1.3:** Shows the Elways ERS, image taken from [27].

- Honda is developing an ERS located to the side of the road, see Fig. 1.4. The ERS structure with two conductors are mounted on e.g. the guard rail [28]. A benefit of

having the ERS off the ground is the reduced problem with dirt and objects on the ERS. To have the ERS track located on the side of the road requires a current collector that extends to the side of the vehicle. The current collector Honda is developing connects to the two ERS tracks by using two spinning wheels, located on the end of the current collector arm [29].

Figure 1.4: Shows the Honda ERS, image taken from [29].

### 1.1.3 Supply potential

A conductive ERS can either be ground referenced or floating, depending on the impedances between the ERS power supply poles and ground. In a ground referenced ERS, one of the supply poles presents a low impedance to ground (it is "connected" to ground). In a floating ERS, both supply poles present a high impedance to ground. With a grounded system a dangerous situation can arise if there is an insulation fault between the not grounded pole and the chassis. This allows the high voltage to reach the chassis and is then exposed to the surroundings through the chassis of the vehicle. A floating system can handle insulation faults on one potential without causing a dangerous situation. The drawback is that if a fault occurs on the other potential, even if it is on a different vehicle, a dangerous situation arises. The Honda ERS is the only ERS described in this thesis that have both voltage potentials floating in relation to ground [30].

With road bound conductive ERS the exposed contact rails are in reach for humans and animals. Elways have a physical protection against electrocution by having the ERS track inside narrow slots in the ground. This prevents humans from accidentally reaching the energized track in a similar way as with conventional power outlets, e.g. the Schuko plug in Europe. Alstom and Elonroad use segmentation together with moving vehicles as their physical barrier. By only energizing segments close to a vehicle the risk of anyone coming too close to an energized segment is small. At low speeds or at standstill the vehicles do not prevent anyone from getting close to the energized segments. Elonroad uses 1 m segments, therefore they can make sure that the energized segment is always physically covered by a vehicle.

### 1.1.4 Segmented ERS

Segmentation of an ERS means that the ERS is split up into longitudinal segments, and that it is possible to energize individual segments. This improves safety of an ERS as only segments used by vehicles are energized. Depending on the length of the segments and the speed of the vehicles, the vehicles themselves act as protection from electrocution. With a segment length of e.g. 25 m and a vehicle speed of 90 km/h the time it takes for a vehicle to reach the other end of the segment is 1 seconds. With a vehicle passing in 1 seconds it is unlikely that someone is going to accidentally touch the energized ERS track without also being hit by the vehicle. One can think of the the vehicle as having a ”virtual length” that is the physical length plus the distance covered within a certain time (like 1 second) when moving, see Fig. 1.5. Any powered segment must be effectively covered by the ”virtual length” of a vehicle, which at zero speed equals the physical length of the vehicle.

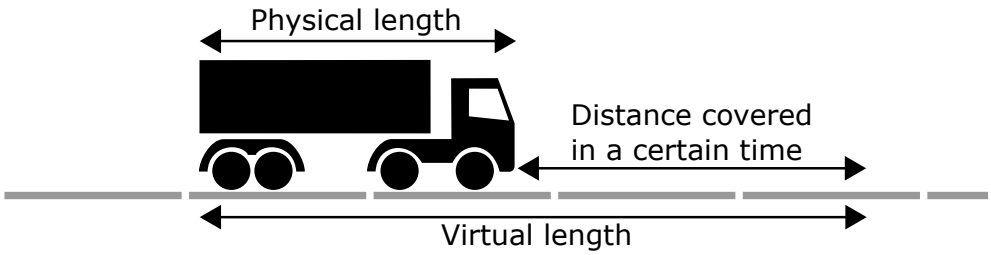


Figure 1.5: The virtual length is the physical length of the vehicle together with the distance covered by the vehicle in a certain time.

With longitudinal segmentation, positioning of the vehicles becomes more important compared to only having a continuous unsegmented ERS supply. Each individual segment need its own feeding and the system needs to know where the vehicles are to be able to turn on the correct segments when a vehicle passes. The longer the segments are the less the uptime is affected by late actuation of the segments. Uptime is here defined as the ratio between the real time supplying power and the desired time supplying power on a request from the vehicle. If a segment is broken this results in a reduced uptime as the vehicle requests to charge but the ERS can not deliver any power. If a loss in uptime due to late actuation of a segments of e.g. 1 % is allowed, the distance a vehicle can travel before the segment is energized is 1 % of the length of the segment. Figure 1.6 shows the uptime for different vehicle speeds and segment lengths if the actuation of a segment is 1 ms delayed. A delayed turn on time results in a reduced power transfer since the window of available charging is shortened.

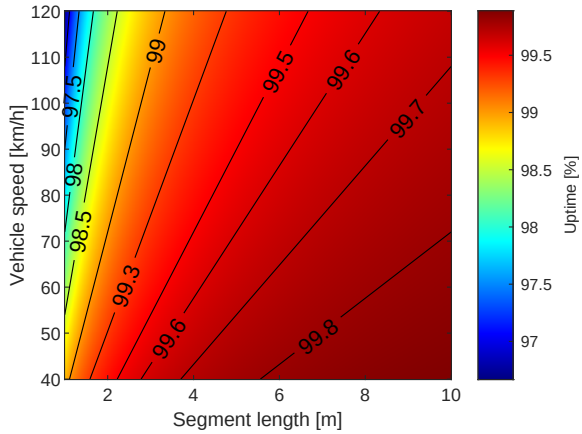


**Figure 1.6:** Shows the uptime when the turn on is delayed by 1 ms.

With the possibility to energize individual segments, they need individual feeding. Feeding of the segments is controlled with switches (either solid state or mechanical relays) placed next to the road or inside the ERS itself. For segments with a length of at least a few meters the switches can be placed next to the road in a switch box. These switch boxes need to be placed along the road with conductors crossing the road to feed the segments if the ERS is not located to the side of the road. Figure 1.7a shows an example of what it can look like with one switch box feeding one contact segment. The multiple switch boxes are fed by a feed-in station connected to a medium voltage line. This feed-in station is different from application to application and can e.g. include a rectifier if a DC voltage is required. In Fig. 1.7a a DC voltage is used, with red and blue lines marking the two voltage potentials. Each switch box can have multiple feeding conductors but these conductors need to be fed to the individual segments. For an ERS with shorter segments than a few meters it becomes inconvenient to have switch boxes next to the road as the number of feeding conductors becomes too large. One solution is then to move the switch box into the ERS structure. The ERS is fed in one end by the feed-in station and the main conductors run throughout the ERS structure, with power electronics energizing the individual segments from the inside of the structure, see Fig. 1.7b. Figure 1.7 presents two alternatives on how to feed an ERS. There are other ways, such as e.g. having conductors run along the road to extend the distance between the feed-in stations. The distance between feed-in stations should not be confused with distance between feed-in points, which is the distance between two consecutive points where the cables enter the ERS.

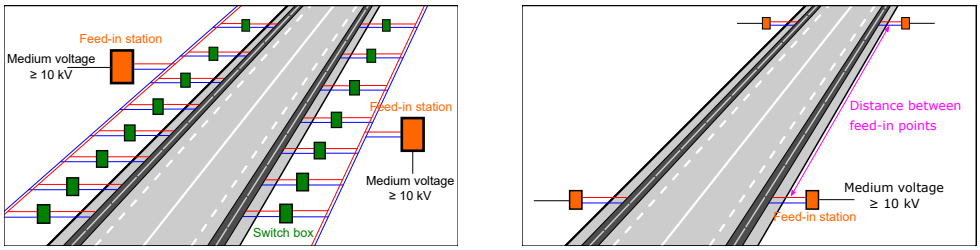


Figure 1.7: (a) shows an example of how switch boxes next to the road can feed individual segment of the ERS. (b) shows the usage of feed-in stations feeding the ERS only in one end and the power electronics are located inside the ERS structure.

By having short enough segments to only allow one vehicle per segment the charging power to individual vehicles can be monitored and measured. This simplifies billing and also detection of faulty equipment onboard a vehicle. If a vehicle tries to charge with faulty equipment, the segment the vehicle is trying to charge from can be disconnected. If the segment length allow for multiple vehicles, disconnecting a segment affects multiple vehicles. This can be an issue as it opens for the possibility of vehicles that are not authorized to use the ERS still are able to charge from it. Elonroad's solution have a segment length of 1 m which is well below the length of a vehicle. Such short segments allow for individual monitoring of the vehicles and also the possibility to disconnect individual vehicles.

### 1.1.5 Alternating short segmented ERS

An Alternating Short Segmented ERS (ASSE) is an ERS with one line of contact segments with alternating polarity. Every other segment can be energized to the working voltage in relation to the remaining segments. With an alternating potential of the ERS, the voltage the vehicle experience when moving along the ASSE is alternating. Due to this a rectifier is needed on board the vehicle to provide a voltage with a fixed polarity. In order for the principle of alternating polarity to work, a vehicle needs to be connected to at least two contact segments of different polarity at all times. This implies a segment length short enough for a vehicle to always be able to connect to at least two segments. With such a short segment length, individual vehicles can be monitored on an ASSE allowing e.g. billing and vehicle diagnostics of individual vehicles. Figure 1.8 shows an example of an ASSE design.

Between two contact segments an electric insulator is needed to separate the two potentials. The isolation distance needs to be at least the length of the current collector to prevent short circuit of the two potentials. Arcing may occur if there is a lost contact and can also cause a short circuit between the contact segments. An important aspect of having short contact segments with an insulator in between is that disturbing noise can be caused as the current

collector slides across the interface between contact segment and insulator. It is therefore important to consider the surface interfaces to minimize the noise from the interaction between the current collector and the surface to the ASSE.

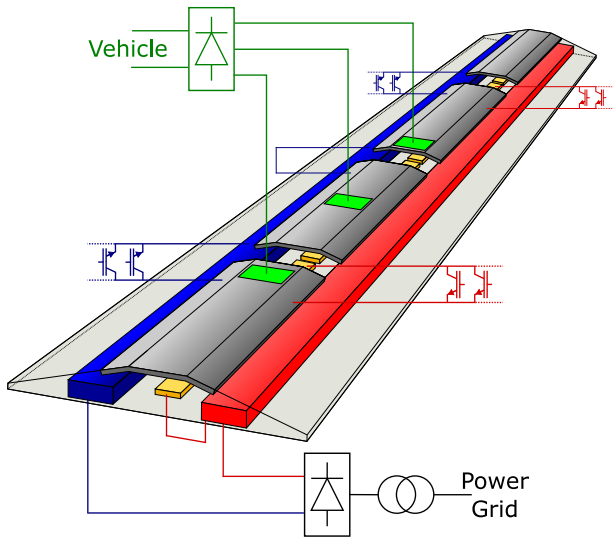


**Figure 1.8:** Shows a schematic example of an ASSE, figure from [31].

Figure 1.9 shows how the ASSE is divided into sections, subsections and segments. A stretch of an ASSE that is supplied with power in one end can be several 100's of meters and is called a section. Each section is composed by subsections that are joined together to form a section. The subsections are shorter than a section and allow shorter pieces of the ASSE to be handled during installation and maintenance. On each subsection there can be one or more contact segments depending on the length of the subsection and contact segment.

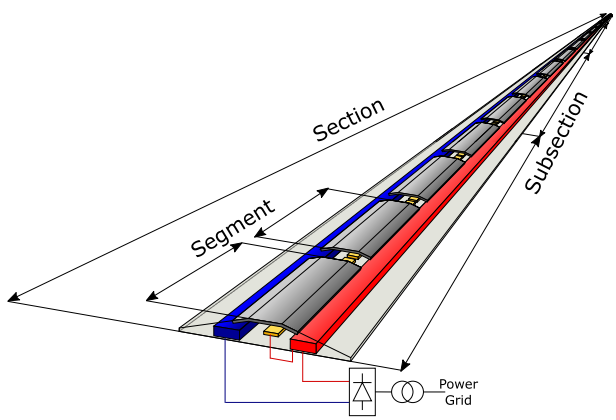


**Figure 1.9:** Shows how the ASSE is divided into sections, subsections and segments.

### 1.1.6 Current collector for an alternating short segmented ERS

The current collector for an ASSE needs to have at least three contact points with a certain distance from each other, see Fig. 1.8. The distance depends on the length of the contact segments and the insulator as the current collector needs to be connected to at least two contact segments, one of each polarity at all time. The three contact points are needed as one contact point may be on an insulator piece. Even more contact points may be preferable as it acts as redundancy in case one contact is glitching or breaks. A glitching contact with only three contact points causes arcing and disruption in the power transfer as there is no alternate path for the current. The exception to this is the short time two contacts are located on the same voltage potential as then there is a redundant connection. Arcing is harmful for both the ASSE and the current collector and must be kept at a minimum to reduce wear of the equipment. An arc also generates a bright light that can distract other drivers. With more contact points, the current path of individual contact points can be broken without arcing as long as the full current path is not broken. Stray inductance in the ASSE and the current collector results in small arcing even if the full current path is not broken. This arc is a low energy arc as the stored energy in the stray inductance in the specific current path of a single contact point is small.

Friction between the current collector and the contact segment of the ASSE is an important design parameter. Lower friction results in less losses, increasing the efficiency of the power transfer. To minimize the friction losses a contact material with a low coefficient of friction is needed. At the same time the contact material needs to be a good electrical conductor and be able to handle the wear from sliding across the ASSE surface. Aerodynamic performance of the current collector is also of great importance as losses due to air drag reduce the efficiency of the power transfer as well. Air drag of the current collector by itself may be of little importance, what is important is how the air drag of the entire vehicle changes. By adding a mechanical construction to a vehicle the airflow around the vehicle chassis may be disturbed, resulting in a higher air drag. There are also other parameters that are important to consider e.g. particle emissions, noise, looks and more.

## 1.2 Objectives and limitations

This thesis investigates the thermal behavior of an ASSE and evaluates the ASSE during different load conditions. The ASSE technology poses the most thermally challenging case, with the power electronics located inside the ASSE structure. The main power electronic switching element is confined in a small space with limited cooling. This gives a worst case even for the lifetime of the main switching element. With a faulty switching element the ASSE can not provide power to a vehicle. It is therefore important to understand how the lifetime of the switching element is related to different load conditions to properly

evaluate the ASSE. Tests at a full scale test site are performed to calibrate and validate the thermal model. Lifetime tests of the power electronic switching elements, in this case discrete IGBTs, are performed in lab conditions.

The main objectives of this thesis are:

- Develop a thermal model of an ASSE for both static and dynamic charging. The model should be able to estimate the temperature within the ASSE as well as on the surface at different conditions such as ambient temperature, location, traffic flow and other relevant parameters.
- Develop a lifetime model for discrete IGBTs, such as the ones used in the ASSE. The lifetime model is based on lifetime models for IGBT power modules together with a compensation factor obtained from experimental tests.
- Integrate the thermal model of the ASSE and the developed lifetime model for discrete IGBTs to evaluate the expected lifetime of the switching devices under different conditions.

The thermal model is limited to the ASSE only, and does not include any auxiliary powers within the ASSE or the feed-in point to the ASSE. Since the current collector is considered a vehicle component, its thermal behavior is only considered in enough detail to show how it affects the ASSE. The climatological aspects of heating and cooling of the ASSE are in this thesis limited to solar irradiation, cooling effect from the wind and cooling effect from the wake behind passing vehicles.

The expected lifetime of the ASSE depends on every component in the ASSE. In this thesis the lifetime investigation is limited to only the main switching element. There may be other components in the ASSE with shorter expected lifetime than the main switching elements, e.g. capacitors and solder connections on the PCB.

In real life vehicles tend to drive in groups instead of spreading out. The effect of vehicles driving in groups is not investigated or taken into consideration in this thesis. The result of this is an underestimation of the resistive losses in the main conductors as these losses are related to the resulting RMS current from the varying number of vehicles drawing power from the ASSE. The amount of underestimation is depending on the total current in the main conductors, a higher current results in a smaller error due to neglecting the influence of vehicles driving in groups.

## 1.3 Contributions

- Assessment of the different cooling and heating sources affecting an ASSE. The heat sources include electric losses as a result of supplying power to vehicles as well as heat from the sun and mechanical friction from the sliding current collector. Cooling from moving vehicles is experimentally investigated. The knowledge of cooling and heating sources is important to understand the implications of different design parameters of an ASSE.
- Providing a thermal model of an ASSE to evaluate performance based on load and external conditions. The model provides information about temperatures inside the ASSE as well as surface temperature. This model is developed to be able to handle both dynamic and static charging. A thermal model can be an important tool to optimize an ASSE both with regards to cost and performance.
- Experimental results from a real ASSE in different external conditions and with different loads. These results are used to calibrate and validate the thermal model and is important to increase the validity of the model.
- Experimental lifetime tests of discrete IGBTs. A test rig for power cycling of semiconductors is developed to estimate the lifetime of discrete IGBTs. The results from the tests are compared to existing lifetime models for power modules to achieve a compensation factor that is used with the existing models.
- Combining the output from the thermal model with the lifetime results from the test of discrete IGBTs to be able to predict IGBT lifetime based on load and external conditions. An ASSE using discrete IGBTs as the main switching element is likely to have a large amount of these switches. It is therefore of great interest to be able to accurately estimate the lifetime of these switches.
- Evaluation of the ASSE temperatures and IGBT lifetime based on different input parameters. These parameters range from design parameters that can be changed when designing or installing the ASSE to external parameters that can not be affected by design choices. This investigation of how different parameters affect the ASSE allows for a deeper understanding of the limitations of an ASSE and how the ASSE can be improved.

## 1.4 List of publications

Publications the thesis is based on, in chronological order:

I **P. Abrahamsson and M. Alaküla, "Sources of heat affecting an electric road system," 2017 IEEE 11th International Symposium on Diagnostics for Electrical Machines, Power Electronics and Drives (SDEMPED), Tinos, 2017, pp. 408-414.**

- I studied the different sources of heat affecting an ERS. Based on this information I calculated the heat generation and power losses in the different components of the ERS.

II **P. Abrahamsson and M. Alaküla, "Thermal design of an electric road system," EVS30 Symposium, Stuttgart, Germany, 2017.**

- I performed thermal measurements on an ERS prototype and developed a thermal model of the ERS prototype. With the thermal model I investigated how different parameters affect the temperature of an ERS.

III **P. Abrahamsson and M. Alaküla, "Thermal modeling of an ERS during static charging," 2018 IEEE International Conference on Electrical Systems for Aircraft, Railway, Ship Propulsion and Road Vehicles & International Transportation Electrification Conference (ESARS-ITEC), Nottingham, 2018, pp. 1-6.**

- I built the experimental setup to measure contact resistance. I further developed the thermal model from paper II and performed measurements to validate the thermal model. I used the model to simulate different charging cases.

IV **P. Abrahamsson, F. J. Márquez-Fernández and M. Alaküla, "Thermal Assessment of an ERS for Static Charging of Electric Vehicles," IEEE Transportation Electrification Conference and Expo (ITEC), Detroit, MI, USA, 2019, pp. 1-6.**

- I further developed the thermal model from paper III and linked it to a lifetime model to analyze aging properties of the ASSE for different charging cases by simulation.

V **P. Abrahamsson, F. J. Márquez-Fernández and M. Alaküla, "Thermal Modeling and Analysis of an Alternating Short-Segmented Conductive ERS," in IEEE Transactions on Transportation Electrification, vol. 5, no. 4, pp. 1078-1086, Dec. 2019.**

- I further developed the thermal model from paper IV and performed measurements to calibrate and validate the model. I also performed a sensitivity analysis of the thermal model.

VI **P. Abrahamsson, F. J. Márquez-Fernández and M. Alaküla, "Thermal Modeling of an ERS during Dynamic Charging," 2019 IEEE Vehicle Power and Propulsion Conference (VPPC), Hanoi, Vietnam, 2019, pp. 1-6.**

- I designed an experimental setup for evaluation of how the cooling coefficient for the ASSE surface is affected by the passage of a moving vehicle, based on an idea from fellow PhD student Lars Lindgren of using an aluminum foil. I developed the thermal model of the aluminum foil and performed tests to calibrate the model. I updated the thermal model from paper V with the results from the measurements and I used the lifetime modeling from paper IV to simulate different study cases.

Other publications:

VII **P. Abrahamsson, D, Wenander, M. Alaküla, F. J. Márquez-Fernández and Gabriel Domingues-Olavarría, "Automatic static charging of electric distribution vehicles using ERS technology," IEEE Transportation Electrification Conference and Expo (ITEC), Chicago, IL, USA, 2020, pp. 1191-1196.**

- I designed the measurement system to investigate charging performance of a distribution vehicle that use either a bit of an ASSE for automatic static charging or a more conventional manually connected AC charging. I estimated the power requirements for the distribution vehicle based on a logged drive cycle. I wrote an optimization algorithm to optimize cost based on choosing charging infrastructure and vehicle battery size.

# Chapter 2: The ASSE design

The idea of putting an ERS on the ground or close to the ground brings both advantages and disadvantages. By having it on ground level, small and large vehicle have the possibility to connect to the ERS and thereby get the energy they need for propulsion and battery charging. Having it on the road also require increased safety requirements such as e.g. for surface temperature, electrocution hazard, friction and surface evenness. With an ASSE the electrocution hazard is reduced since an ASSE uses short contact segments. Short contact segments also make it possible to monitor individual vehicles, allowing e.g. billing of electricity.

## 2.1 Traffic flow and power requirement of vehicles

### 2.1.1 Traffic flow

The characterization of the traffic flow is important in order to understand the power demand of and ASSE or any ERS. The number of vehicles traveling on the road where the ASSE is located is the main input parameter for the simulation model, although it should be noted that not all vehicles on that road necessarily draws power from the ASSE. Without vehicles the need for an ASSE disappears. This is why the traffic flow needs to be considered. Both vehicles utilizing the ASSE and vehicles driving without drawing power from the ASSE need to be considered since every vehicle affects the temperature of the ASSE. When a vehicle draws power from the ASSE, heat is generated and therefore the temperature is affected. A vehicle not utilizing the ASSE do not cause any losses but provides shade and wind drag, which also affects the temperature. The traffic flow is not only important for the thermal model but also for the economic validity of the ASSE. Enough vehicles need to utilize the ASSE in order for it to be profitable. The economic aspects of an ASSE are not investigated in this thesis. The vehicles in this thesis are divided into two categories, cars or trucks in order to simplify the traffic model.

The Swedish Traffic Administration measures traffic flows on the Swedish roads and makes this data available online [32]. Figure 2.1a shows the number of cars and trucks for one day on a busy 2-lane road south of the Swedish town of Helsingborg. As a rule of thumb many countries use the 2 second rule, which implies a time between two vehicles of 2 seconds is considered a safe distance [33]. The traffic flow in Fig. 2.1a results in a shorter time between two vehicles than 2 seconds on average. One reason for this is that the road is a 2-lane road. By assuming that the 2 second rule is obeyed and that all of the trucks drive in one lane, then some of the cars must drive in a different lane. Figure 2.1b shows how the traffic flow in the slow lane would look like if the 2 second rule is applied, considering that all cars are 4.76 m long, about the length of an Audi A4 [34] or Volvo V60 [35], and trucks 16.5 m, which is the maximum length for trucks in the EU [36], assuming that excess vehicles use another lane. The energy supplied to the vehicles in the slow lane do underestimate the total power demand from all of the vehicles on the road if only one lane is electrified. This is because the vehicles in the fast lane eventually must change to the slow lane to charge the batteries before moving over to the fast lane again. With the large amount of vehicles assumed in this thesis it is likely that both lanes are electrified, removing the need for vehicles to move to the slow lane in order to receive power.

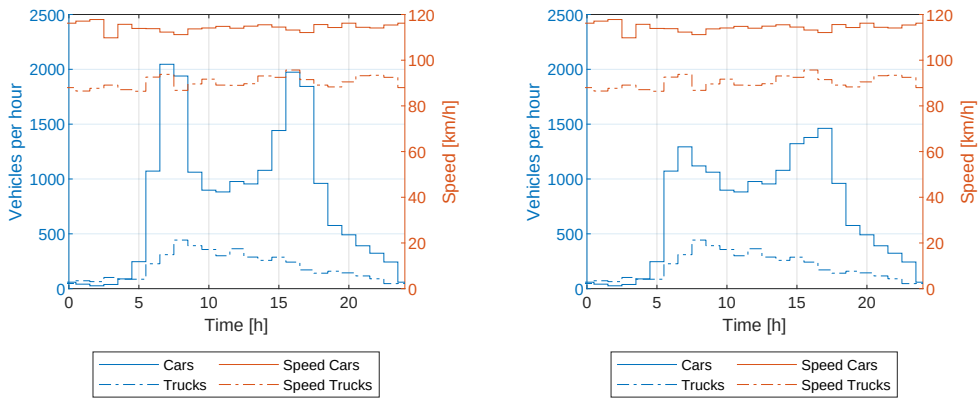


Figure 2.1: Shows traffic intensity and vehicle speeds. (a) shows the measured traffic flows for a 2-lane road south of Helsingborg in Sweden and (b) shows the resulting traffic intensity if the 2 second rule is applied and all of the trucks are driving in one lane.

### 2.1.2 Power requirements for vehicles

The power required to propel a vehicle is equal to the sum of the power needed to accelerate the vehicle, the power needed to climb or descend any potential slope, the rolling resistance and the air drag. When supplying power to the wheels the power needs to flow through

the powertrain of the vehicles. Losses in the powertrain must therefore be included in the calculations, resulting in a higher power demand. The electricity consumption of common electric cars is roughly 12-17 kWh/100km for the US combined regulatory test cycle, using 2016 US EPA data [37]. This electricity consumption is not measured at 120 km/h and a higher consumption can be expected at higher speeds. At 1.2-1.7 kWh/10km the power demand is roughly 14-20 kW at a speed of 120 km/h. The corresponding electricity consumption for a truck is about 12 kWh/10km for the EU long haul cycle [38], at 90 km/h this equals 108 kW at the wheels.

The power needed to keep a vehicle moving can be calculated analytically by eqn. (2.1), (2.2) and (2.3). The road is assumed to be completely flat, which is a simplification and neglects the increase in power demand from gravity. Table 2.1 shows the parameters of the assumed cars and trucks. These analytical equations give a power requirement of 25 kW for a car driving at 120 km/h and 118 kW for a truck driving at 90 km/h. These numbers are close to the measured power consumption from real drive cycles. The vehicles used for real world testing do not have exactly the same parameters as the vehicles used for the analytical equations, which could be one possible explanation to the differences between the two power estimations. For cars a power consumption of 25 kW is assumed and for trucks the power consumption is rounded up to 120 kW.

$$P_{drag} = \frac{1}{2}\,\rho\, C_D\, A_{front}\,(v_{vehicle} + v_{air})^2\, v_{vehicle} \tag{2.1}$$

$$P_{roll} = C_r\, g\, m\, v_{vehicle} \tag{2.2}$$

$$P_{vehicle} = \frac{P_{drag} + P_{roll}}{\eta} + P_{aux} \tag{2.3}$$

Table 2.1: Vehicle parameters used for the power calculations.

| Parameter | Car | Truck |
|---|---|---|
| **Mass [kg]** | 2100 | 40000 |
| **Drag coefficient** [-] | 0.24 | 0.5 |
| **Front area** [$m^2$] | 2.4 | 10 |
| **Roll resistance coefficient** [-] | 0.008 | 0.0045 |
| **Powertrain efficiency** [-] | 0.8 | 0.8 |
| **Auxiliary power [kW]** | 2 | 4 |

As previously mentioned, external conditions such as slope and wind do affect the power needed to propel a vehicle. Figure 2.2 shows the influence of headwind on the power requirement of the car and the truck from Table 2.1. With the battery in a vehicle acting as an energy buffer, the energy transfer from the ASSE to the vehicle can be less than the energy needed by the vehicle for some time. This is valid if there is a different charging opportunity, e.g. overnight charging, and if the battery is sufficiently large and powerful to supply the extra energy needed. To achieve a tough but realistic case it is assumed that the vehicles do not have access to any other charging opportunity. The energy transferred from the ASSE to a vehicle is then equal to the average energy consumption of that vehicle. Note again that the instantaneous power drawn from the ASSE is not equal to the instantaneous power consumption of the vehicle. Based on the complexity of the power requirement, which includes external factors, the onboard battery, and different charging solutions, the assumption is an overhead of 50 % of the power requirement. This is a simplification intended to compensate for external parameters that affect the power requirement. The influence of e.g. added drag and friction from the current collector, which is needed to draw power from the ASSE is not included in the power calculations. All of these external parameters need to be covered by the 50 % overhead in power. In order to get an accurate estimation of the required power from the ASSE for different vehicles, a thorough study of the power requirement for different conditions needs to be performed. This thorough study is not in the scope of this thesis, thus the simplified assumption of power requirement for the vehicles.

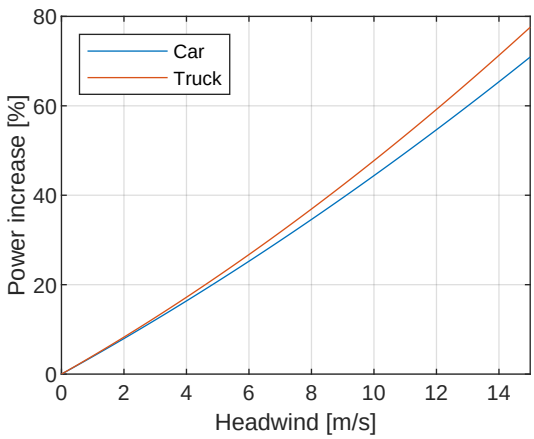


**Figure 2.2:** The increase in power requirement for cars and trucks at different headwinds. The speed of the car is 120 km/h and the truck 90 km/h.

### 2.1.3 ERS coverage factor

From the ASSE point of view the power drawn from the ASSE is of importance, not the power requirement to keep a vehicle moving. The drawn power is directly related to the fraction of the total road distance covered with an ASSE. With less ASSE the time for transferring energy to a vehicle is reduced, hence with a constant power demand the drawn power increases. Figure 2.3 shows the power from the ASSE needed for cars driving 120 km/h and for trucks going 90 km/h at different fractions of installed ERS, $k_{ERS}$, with the previously assumed drawn powers. $k_{ERS}$ is defined as the fraction of the total distance that is covered by an ERS, e.g. if 750 m of ERS is installed on a 1000 m distance the $k_{ERS}$ is 0.75 or 75 %, see Fig. 2.4. If considering a $k_{ERS}$ of 100 % then the power flow from the ERS to the vehicle does not have to be intermediately stored in the battery. At lower $k_{ERS}$ some of the energy is stored in the battery to be used when there is no ASSE to draw power from. With a battery efficiency lower than 1, the overall efficiency of the power transfer is reduced as the $k_{ERS}$ is reduced. In this thesis this effect is considered to be included in the 50 % drawn power overhead, which is also enough to cover the increased power demand from a headwind of about 10-11 m/s. Other external factors should also be covered by the overhead resulting in a lower acceptable headwind. A $k_{ERS}$ of 50 % is used based on the results presented in [10].

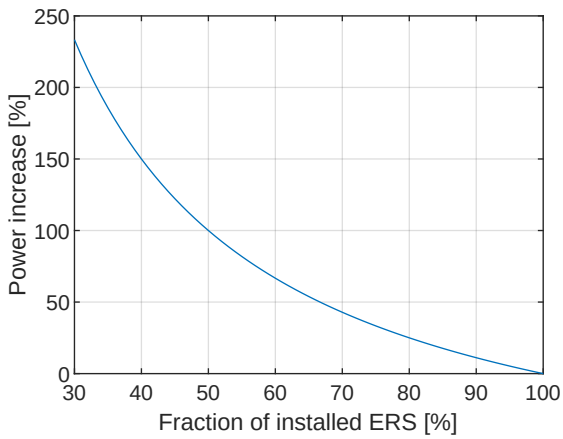


**Figure 2.3:** Power requirement of cars and trucks at different ERS coverage of the total distance. The vehicles are the same as in Fig. 2.2 and there is no headwind.

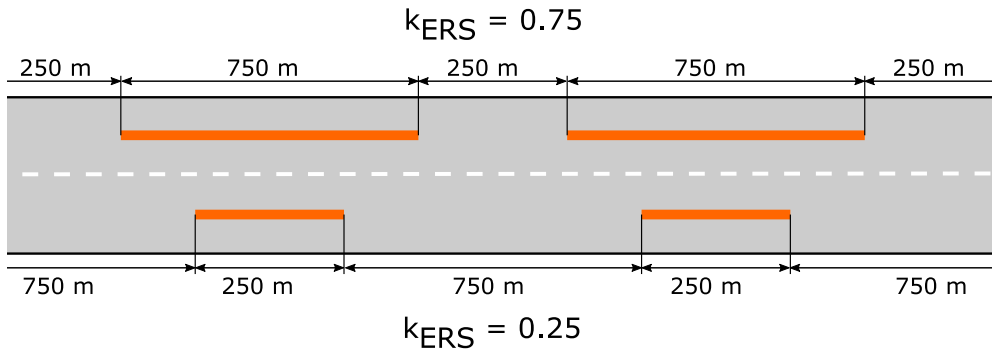


**Figure 2.4:** Shows $k_{ERS}$ for two different lanes equipped with ERS.

Using a $k_{ERS}$ of 50 % and also an overhead of 50 % on the resulting power drawn from the ASSE the final powers drawn from the ASSE are then 75 kW for cars and 360 kW for trucks. These values are based on a power requirement of 25 kW for a car and 120 kW for a truck. A truck is longer than a car and can therefore cover multiple segments of each polarity. It is then possible to draw power from at least 2 contact segments at the same time, reducing the power per contact segment to 180 kW. Thus, 180 kW is used in this thesis as power drawn by trucks from one contact segment. 360 kW is used when calculating the current inside the ASSE.

## 2.2 Requirements

There are multiple requirements of different nature when designing an ASSE. In this thesis only electrical, lifetime of the main switching elements and thermal requirements are considered. Mechanical requirements such as the structural integrity under load, the road-tire friction, or the wear of the contact rails, as well as other electrical requirements such as overvoltage / lightning protection or leakage current monitoring, and chemical / environmental requirements related to e.g. the exposure to different external agents are not within the scope of this thesis.

### 2.2.1 Electrical requirements

The electrical requirements considered in this thesis are voltage, power per contact segment, and voltage of exposed surfaces relative to ground. Tram applications,which use a technology similar to the ASSE, normally operate at a nominal voltage of 750 Vdc. 750 Vdc is therefore the voltage used for the ASSE in this thesis.

The maximum allowed voltage relative to ground is determined by what voltage is considered unsafe. In an ASSE like the one in Fig. 1.8, where every non energized contact segment is connected to the negative conductor, a voltage drop in the negative conductor results in different voltages on the non energized contact segments. If the negative conductor of the ASSE is grounded in the feed-in station then the exposed voltage relative to ground is equal to the voltage drop in the negative conductor. This is valid as long as the ground potential is the same along the ASSE. In vehicles a contact voltage below 60 Vdc is considered a safe voltage, and voltages below 60 Vdc is therefore commonly used in vehicles [39, 40, 41]. Based on this a safe touch potential is considered to be a 48 Vdc relative to ground. Any electrically conductive material that can be touched by a human or animal needs to be below 48 Vdc. Contact segments covered by a vehicle are not easily accessible and are allowed to have a higher potential than 48 Vdc relative to ground. In experimental tests a let go voltage of between 109-131 Vdc are observed [42]. Figure 2.5 shows two examples of how a person can come in contact with voltage from the ASSE by touching the contact segments directly or by touching a vehicle drawing power from the ASSE. In this thesis only the voltage drop in the negative conductor is considered and faults located on the vehicle side are not included.

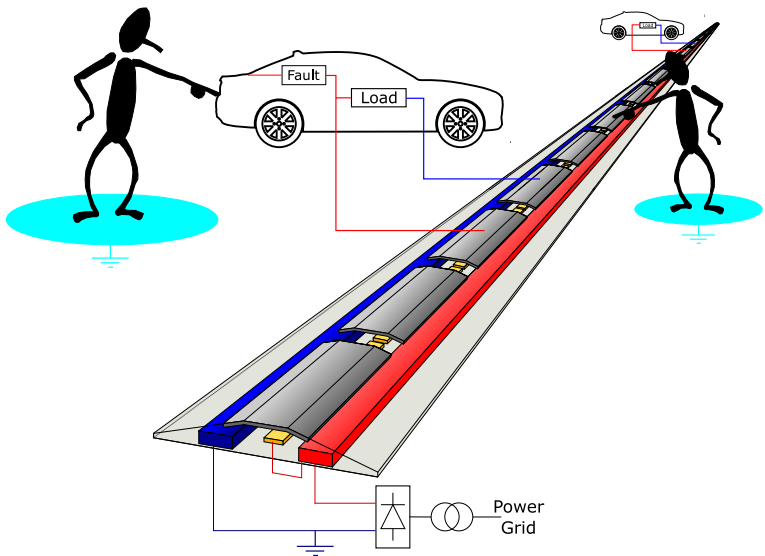


Figure 2.5: Shows two examples of how a person can come in contact with voltage related to ground by touching either the ASSE directly or by touching a vehicle drawing power from the ASSE.

**Requirements:**

- Voltage supplied to the ASSE from the feed-in station: 750 Vdc
- Power that can be supplied from one contact segment to a vehicle: 180 kW at the

nominal voltage of 750 Vdc

- Voltage relative to ground of any metal that are easily accessible: 48 Vdc

### 2.2.2 Lifetime requirements of main switches

The technical lifetime of a road paved with asphalt is 20 years [43]. This technical lifetime can be extended by maintenance of the top bitumen layers [43]. With road maintenance occurring with at least 20 year intervals the expected lifetime of the ASSE is assumed to be 20 years, the same as for an asphalt road. It should be noted that even if the ASSE as a system is assumed to have a lifetime of 20 years, individual components can have a longer lifetime. After 20 years it may be possible to replace the components with the shortest expected lifetime and extend the useful lifetime of the ASSE. In this thesis only the solid state switches are investigated. However, in order to ensure a system lifetime of at least 20 years, the other components in the system should also be taken into account.

**Requirements:**

- Expected lifetime of solid state switches: 20 years of operation

### 2.2.3 Thermal requirements

Two main thermal requirements are considered for the ASSE: a maximum internal temperature (inside the ASSE structure) and a maximum temperature for the exposed surfaces. The internal temperature limitation is based on the insulation of the conductors. Different insulation materials have different maximum operating temperatures and for many of them the maximum is 130 °C or greater [44], [45]. Based on this the internal temperature of the ASSE is limited to 130 °C.

The surface temperature is not limited by the maximum operating temperature of the material but is limited because of safety. A safe surface temperature is hard to define as it depends on several factors, e.g. thermal conductivity, exposure time and temperature. Metals have high thermal conductivity and it is therefore normally surface areas made of metal that are most dangerous. According to [46] an aluminum or steel surface at 80 °C can be touched by a human for about 0.5 seconds before the pain threshold is reached. For this thesis a touch time of a hot surface is considered to be up to 0.5 seconds. The requirement for the ASSE is then that the surface temperature of any exposed metal never exceeds 80 °C.

**Requirements:**

- Maximum temperature of the internal structure of the ASSE: 130 °C

- Maximum surface temperature of easily accessible metal surfaces: 80 °C

## 2.3 Design

An ASSE can have many different shapes and can e.g. be put down into the road, be placed on top of the road or next to the road. The only requirement of an ERS in order to call it an ASSE is that it needs to have alternating polarity of the contact segments. A result of having alternating polarity is that the contact segments need to be short enough for a vehicle to connect to at least one segment of each polarity. Short segments most likely need some sort of power electronics inside the ASSE to reduce the need for cables to the ASSE from the side of the road.

### 2.3.1 Contact segments

A contact segment is an electrically conductive surface with the purpose of transferring energy from the ASSE to a vehicle, see Fig. 2.6. The contact segments need to be designed with, friction, durability, contact resistance, length of segment and many more parameters in mind.

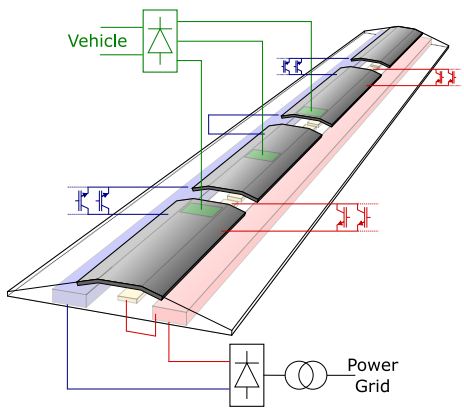


Figure 2.6: Highlights the contact segments from Fig. 1.8.

Friction between the ASSE contact segment and the current collector creates a braking force that causes both heat and lowers the efficiency of the power transfer. It is important to chose an appropriate material for the contact segment to have a low friction to the current collector, but at the same time high friction is necessary between the contact segment and the rubber tires of the vehicles to avoid losing traction and control of the vehicle. The contact segments are constantly exposed to wear from the sliding contact of the current

collector, both due to mechanical abrasion and electrical arcing caused by a poor electrical contact. The thickness of the contact segment need to allow for a long enough lifetime to meet the required lifetime or maintenance interval of the system.

The electric contact resistance is also material dependent [47]. This resistance causes losses in the contact point, generating heat both in the current collector and the contact segment. This heat is mostly an issue with static charging as for dynamic charging the contact losses are spread out over a larger area as the vehicle moves.

The maximum contact segment length is directly related to the minimum length of the vehicles using the ASSE. The vehicle needs to connect to at least one contact segment of each polarity at all times, which implies that at least 3 contact points are needed since the current collectors need to go over the insulation blocks between segments. At the same time, activated segments need to be physically covered by the vehicle to prevent animals and humans from being able to come in contact with an energized segment. The shorter the contact segments, the higher the requirements on position accuracy. A benefit of having short segments, shorter than the virtual length of the vehicle, is that an ASSE can be used for both dynamic and static charging. Both dynamic and static charging with an ERS with longer segments is possible but monitoring individual vehicles may not be possible from the ERS perspective. On board the vehicle the same equipment can also be used for both dynamic and static charging.

All of the above parameters except for the segment length are related to material selection and surface design. One material may not be the best material in every aspect but the different aspects need to be weighed against each other in order to select a suitable material. The surface design affects the interaction between the contact segment and the current collector. It may be possible to increase friction by making a pattern in the contact segment to allow the soft rubber tires to get better grip on the uneven surface. At the same time this may cause increased noise and wear. Leveling of the contact segment is important as even small differences in height can result in noise.

### 2.3.2 Main conductors

There are two main conductors, one positive and one negative, that provide each contact segment with power. These conductors run the entire length of the ASSE, from the feed-in point to the far end of the ASSE, see Fig. 2.7 where the main conductors are marked with blue and red. The longer the ASSE length the longer the main conductors have to be. With multiple vehicles drawing power from the ASSE the cumulative current in the main conductors is the highest close to the feed in point. This cumulative current causes resistive losses in the conductors, which are proportional to the electric resistance in the conductors. The resistance is material dependent and is also depending on the cross-sectional area and

the length of the conductors. A trade-off needs to be made between the length of the conductors and their cross-sectional area. A larger area allows for longer conductors at the cost of extra material, which increases both the size of the ASSE structure and the cost of the conductors. The length of the conductors is also limited by the capacity of the installed feeding station.

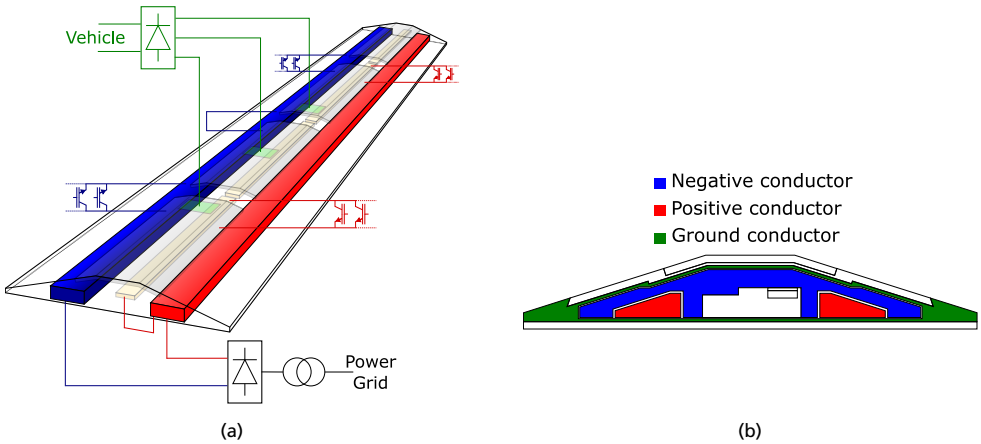


Figure 2.7: (a) highlights the main conductors from Fig. 1.8 and (b) illustrates how (a) can be implemented in a real design.

As previously explained the maximum voltage between any exposed / easily accessible surface and ground is 48 V. For an ASSE with the negative conductor grounded in the feed-in station the voltage drop in the negative conductor can not exceed 48 V. Due to this the cross-sectional area of the negative conductor can be made larger at the expense of the positive conductor. A larger negative conductor allows for more current to flow through it before a voltage drop of 48 V is reached. The drawback is that the combined heat generated in the positive and negative conductors from resistive losses is increased. This added heat can also limit the performance of the ASSE due to increasing temperatures. Yet again there is a trade-off, this time between voltage drop and losses in the conductors.

Commonly available conductor materials include aluminum and copper. Aluminum is relatively cheap with good electrical properties. Copper is even better than aluminum at conducting electric current and also heat, but to an increased cost [48]. The trade-off between aluminum and copper is mostly related to the value of reducing the size of the ASSE or increase the possible length of the conductors.

### 2.3.3 Ground conductor

A ground conductor can be used to add safety to the ASSE. By placing the conductor on both sides facing away from the energized segments, see Fig. 2.7b, a potential barrier

between the ASSE and the surroundings can be achieved. This potential barrier collects leakage currents and keep the voltage low for the surroundings of the ASSE. This can be of importance if there is e.g. a conductive layer of salt water between the energized segments and the surroundings.

The ground conductor is not necessary for the functionality of the ASSE. Ideally no current should flow through this conductor and it provides no function except for the extra safety for the system. If a ground conductor is used it is important that the conductor can handle the current during a short-circuit event without acting as a fuse.

### 2.3.4 Electric insulation

Materials used for electric insulation are materials with low electric conductivity [49]. The lower the conductivity the better an insulator a material is. Inside an ASSE the insulation needs to be able to withstand the working voltage together with any transients caused by a broken current path. The higher this voltage is the thicker the insulation needs to be. Physical properties such as electric conductivity of the insulation material determine the minimum thickness of the insulation layer. Another limiting factor is the durability of the material as there are small movements of the different layers, see Fig. 2.7b, inside the ASSE due to thermal expansion and compression from crossing vehicles. These movements may cause the insulation layer to wear over time. It is therefore important to consider wear of the insulation together with how long it is expected to last without maintenance. By only considering electrical performance and durability a thick insulation layer is preferred, but when also considering thermal performance a thick insulation layer is not optimal. With insulation around a conductor, heat generated inside the conductor needs to be dissipated through the insulation layer. Most insulation materials are poor thermal conductors, with a thick insulation layer the thermal resistance in the layer is large and there is a major thermal barrier in the cooling path. The thicker this layer is the more the temperature rises in the conductor. It is therefore important to find a good trade-off between electric and thermal performance while also considering the durability of the insulation.

Since the contact segments have alternating potential, there needs to be insulation between two consecutive segments. This insulation is different from the internal insulation layers as this insulation is subjected to direct contact with the current collector. A durable material is needed that can withstand wear from the sliding contact for the designed lifetime of the ASSE. The insulation must be wide enough to keep the insulation between the contact segments even when an electrically conductive current collector is on top of the insulation material, see Fig. 2.8.

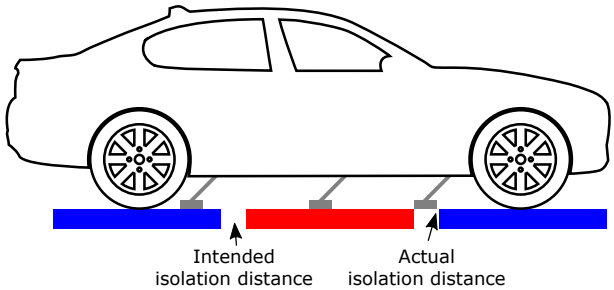


Figure 2.8: The actual isolation distance is smaller than the intended isolation distance when a conductive object is on top of the insulation material between two consecutive segments.

### 2.3.5 Switching element

An ASSE consists of many short contact segments that need to be able to be activated and deactivated individually. A crucial component of the ASSE is the switching element, which is the component that is able to energize the different contact segments. Since the segments need to be able to turn on individually there needs to be one switching element or multiple switching elements working as a combined switching solution per segment. Multiple switching elements in parallel can be used to reduce the stresses on each element for a given current. Switches in series increase the breaking voltage capability, as the voltage is divided among the switches. Having switches in series do not increase the current capabilities, which require the switches to be connected in parallel.

Switches can be either mechanical or solid state switches. Mechanical switches rely on a mechanical contact and moving parts. The connection inside the switch is from metal plates that are in physical connection, which allows for low conduction losses. One drawback of this type of switches is that the current path is broken by physically separating the metal plates. This is a relatively slow process and a switching event is in the ms range for a normal mechanical circuit breaker [50]. DC currents do not have zero crossings, like AC currents do, which makes it easier to extinguish any arcs that may occur when breaking the current to an inductive load. This makes DC breakers large and bulky compared to a solid state switch to have enough room to separate the two contact plates enough to extinguish the arc. Another drawback of mechanical switches is the limited number of switching events a switch can handle before it needs to be taken out of service.

Solid state switches rely on semiconductor technology to perform the switching. A solid state switch generally has higher conduction losses while conducting compared to a mechanical switch but they have an advantage when it comes to size, switching speed and number of switching events until failure. There are different types of solid state switches, with MOSFETs and IGBTs commonly used in power applications [51]. MOSFETs and IGBTs are both able to be actively controlled by a gate voltage [52]. By applying a voltage

to the gate the component starts to conduct. A MOSFET is usually used in applications with high switching frequency and when the voltage is rather low [53]. An IGBT does not have the same switching performance as the MOSFET but it is able to handle greater currents and voltages [53].

Another interesting topic is where the switching elements should be placed. Possible locations are inside the ASSE and outside the ASSE. A likely position outside the ASSE is next to the road in some sort of housing. This allows for good cooling and easy access to the components if maintenance is needed. Since the contact segments are energized individually there needs to be individual cabling to at least each contact segment that can be energized. Every other contact segment is connected to low potential and can be coupled together inside the ASSE without the need for any switches. This reduces the number of feed-in points for the low potential contact segments. This means that a single cable can be feed-in from next to the road to the ASSE every other segment or multiple cables have to be feed-in every few segments. It should be noted that if static charging is allowed, then each cable needs to be able to handle the static charging currents continuously. A benefit of having multiple feed-in points is that the need for main conductors is removed as the current does not flow along the ASSE but rather from the side of the road to the ASSE. By placing the switching elements inside the ASSE only one feed-in point is needed and then the switches are fed by the main conductors. This reduces the need for placing charging infrastructure next to the road, at the cost of placing the switching elements in a harsh environment inside the ASSE. With constraints in space the cooling inside the ASSE is limited, making it difficult to dissipate the heat generated by the switches. The ASSE is also subjected to vibrations and stresses from vehicles crossing the ASSE.

# Chapter 3: Thermal modeling

There are at least two reasons to motivate thermal modeling of an ASSE. The first is to be able to predict hot spot development that may cause burns on living beings and set fire to combustible material, and the second is to be able to predict thermal aging due to thermal cycling. The main focus of this chapter is to present the different heat sources, the heat dissipation mechanisms, as well as the models used to estimate the temperature distribution inside the ASSE structure.

## 3.1 Heat sources

There are several sources of heat affecting an ASSE. The main heat sources are from electric losses, friction and solar irradiance. Electric losses in e.g. the switching elements and conductors are directly related to the ASSE utilization, where higher usage results in more losses. Solar irradiance on the other hand is related to weather conditions and the total traffic flow, the more vehicles the less heat from the sun reaches the ASSE due to shading.

### 3.1.1 Solar irradiance

Heating from solar irradiance occurs when a material absorbing parts of the irradiance from the sun. This irradiance peaks at a wavelength of 0.5 $\mu$m, which is in the visible spectra of 0.4-0.7 $\mu$m [54]. Solar irradiance can be a major source of heat when the incoming irradiance is strong, e.g. midday in a clear summer day. Solar zenith angle, $\theta_z$, which is the solar angle away from its zenith position, see Fig. 3.1, is directly affecting the amount of solar irradiance reaching a surface on the ground, and is calculated with (3.4) [55]. $\phi$ is the latitude, $\delta$ is the declination angle of the sun, approximated with (3.5) [55], and $h_{angle}$ is the hour angle, approximated by (3.6) [56]. When calculating the hour angle correct solar time *Hour* must be used. Solar irradiance is also weather dependent as clouds can block the solar irradiance or even magnify the irradiance that reaches the ground [57].

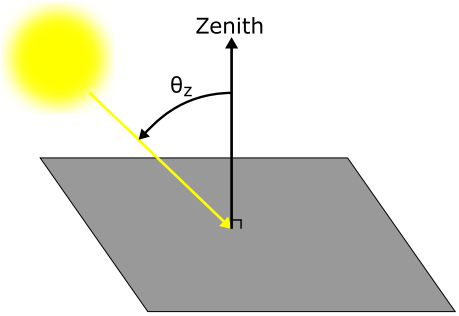


**Figure 3.1:** The solar zenith angle, $\theta_z$, is the angle away from the zenith position.

$$\theta_z = sin(\phi)\, sin(\delta) + cos(\phi)\, cos(\delta)\, cos(h_{angle}) \tag{3.4}$$

$$\delta = 23.45\, sin(\frac{360}{365}\,(284 + Day)) \tag{3.5}$$

$$h_{angle} = 15\, Hour \tag{3.6}$$

Based on the zenith angle the distance the solar rays travel through the atmosphere varies. As the rays are traveling in the atmosphere they are attenuated, resulting in less energy reaching the ground. The shortest distance through the atmosphere is in the zenith direction. In this direction the relative air mass, $AM$, is considered to be 1 [58]. $AM$ for different zenith angles can be approximated with (3.7) [59]. By knowing the air mass, the direct solar irradiance at ground level perpendicular to the rays, $I_D$, can be estimated with (3.8) [60].

$$AM = \frac{1}{cos(\theta_z) + 0.15\,(93.885 - \theta_z)^{-1.253}} \tag{3.7}$$

$$I_D = 1353 * 0.7^{\,AM^{0.678}} \tag{3.8}$$

Global solar intensity, $I_G$, at ground level is the combination of both direct solar irradiance, and diffuse solar irradiance. Diffuse irradiance is irradiance scattered by obstacles in the

solar rays path, e.g. by clouds or particles in the air. If the sky is clear the diffuse irradiance can be about 8 % of the total solar irradiance while it can be around 22 % for an urban location [60]. $I_G$ is calculated by using (3.9), where *FractionDiffuse* is the ratio between the diffuse irradiance and the global irradiance.

$$I_G = \frac{I_D}{1 - FractionDiffuse} \tag{3.9}$$

For an ASSE placed on a road, shading is important to consider. The heavier the traffic, the greater the fraction of the time the ASSE is shaded by vehicles, reducing the average solar irradiance, $I_{solarAVG}$. *Coverage* is defined as the fraction between the ASSE being shaded and not being shaded, where 1 means fully shaded and 0 not shaded at all. Equation 3.10 includes the coverage term to compensate for the shading effect and the gives an average solar irradiance reaching the ASSE.

$$I_{solarAVG} = I_G\,(1 - Coverage) \tag{3.10}$$

$I_{solarAVG}$ is the solar irradiance perpendicular to the solar rays. In order to get the total solar power reaching the ASSE, the angle between the rays and the ground needs to be considered. Also the ground area the ASSE is covering, $A_{ERS}$, needs to be considered. Equation (3.11) is used to calculate the average solar power, $P_{solarAVG}$, hitting the ASSE. Note that this assumes a completely flat ASSE that is placed in parallel with the ground. If the ASSE is positioned differently the incoming solar power reaching the ASSE is different.

$$P_{solarERS} = I_{solarAVG}\,A_{ERS}\,cos(\theta_z) \tag{3.11}$$

Only a fraction of the incoming $P_{solarAVG}$ is absorbed. The coefficient of solar absorptivity, $\alpha_s$, is the fraction of the total solar irradiance that is absorbed by a material. Light surfaces tend to reflect most of the visual light [61] and have low $\alpha_s$. Dark surfaces on the other hand tend to reflect less of the visual light [61] and have high $\alpha_s$. Table 3.2 gives some examples of $\alpha_s$ for different surfaces. These values depend on surface properties, which may change over time. Therefore it can be unreliable to use a coefficient of solar absorptivity that was measured for other conditions than for the intended application. For an ASSE lower values of $\alpha_s$ are preferred to minimize absorbed heat.

Table 3.2: Examples of coefficients of solar absorptivity [62].

| Material | $\alpha_s$ |
|---|---|
| **Machined stainless steel** | 0.47 |
| **Polished stainless steel** | 0.42 |
| **Buffed aluminum** | 0.16 |
| **Buffed copper** | 0.30 |
| **Hughson Black Paint L-300** | 0.95 |
| **3M Black Velvet Paint** | 0.97 |

### 3.1.2 Electric losses

Electric losses are the losses that occur when an electric current flows through a non-ideal electrical conductor, due to the resistivity of the material. In the ASSE, major losses occur in the large conductors and in the switching elements. The switching element that is considered is a solid state switch due to its size and reliability. Another source of losses that can be significant is the contact point between the ASSE and the current collector. These losses are highly dependent on the contact resistance between the two surfaces, which can vary greatly.

#### Conductors

The conductive losses are related to the material's electrical resistivity and the current squared, the larger the current the larger the losses, see (3.12). Close to the feed-in point the main conductors have to supply current to every vehicle on that ASSE section. This implies that with a longer ASSE (greater distance between feed-in points) the losses in the conductors may increase, as more vehicles can fit on the section of ASSE that is fed by one set of main conductors. Another reason why longer main conductors results in more losses is the voltage drop in the conductors. If a vehicle draws constant power from the ASSE the current increases as the voltage decreases. With an increase in current the losses increase.

$$P = UI = RI^2 = \frac{\rho_{electric} L}{A_{cross}} I^2 \tag{3.12}$$

In order for (3.12) to be correct the current must be the RMS equivalent. The RMS current is hard to estimate as it is directly linked to traffic flow. The ASSE can feed multiple vehicles simultaneously, and whenever a vehicle leaves or reach the ASSE there is a change in current. This results in a DC and an AC component of the current. The smaller the AC component in relation to the DC component is the closer the RMS value is to the average value. Based on this the longer the distance between the feed-in points the closer

the average is to the RMS as long as the traffic flow is constant. By using the average value the losses are underestimated, creating an easier case for the ASSE. Figure 3.2 shows two examples of what the current can look like for different lengths of the main conductors. In Fig. 3.2a the losses are underestimated by 15 % while in Fig. 3.2b the underestimation is only 2 %. Even in Fig. 3.2b the current is fairly small and higher currents can be expected during high traffic intensities. The expected underestimation of the losses is therefore less than 2 %. The influence of the voltage drop along the conductors is not included in Fig. 3.2. With the voltage drop included the shape of the curve would have a saw tooth shape due to the vehicles moving along the ASSE, drawing more current the further away from the feed-in point they are.

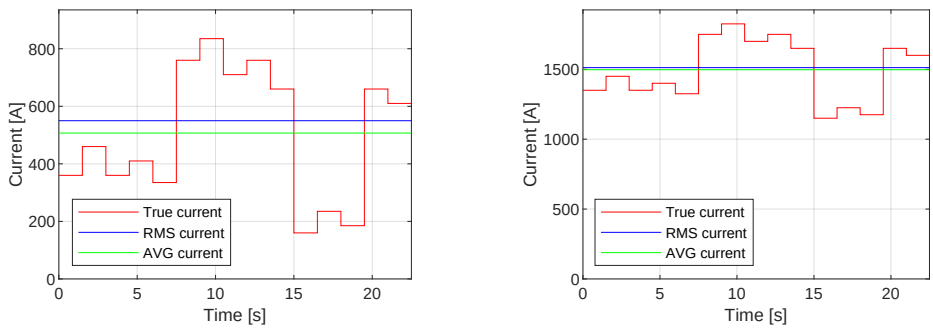


**Figure 3.2:** Shows an example of the average, the RMS and the true current in the main conductors. (a) shows a small DC component and (b) a large DC component.

Due to the difficulty of predicting traffic pattern the average current is used in this thesis. In order to calculate the RMS value a traffic pattern needs to be defined. The absolute worst case is if all of the trucks group together, increasing the current substantially for a period of time. However, it is not likely that all of the trucks group together in one long line, and if they do, the ASSE can protect itself from overheating by limiting the power to the vehicles.

### Solid state switch

There are two types of losses in an solid state switch, conduction losses and switching losses. Conduction losses occur when a current flows through a non-ideal electrical conductor, i.e. a material with less than infinite electrical conductivity. The average conduction losses in the solid state switch therefore depend on the collector-emitter voltage, $V_{CE}$, the current flowing through the switch, $I_C$, and the duty cycle, and can be estimated with (3.13). $V_{CE}$ is either given or can be calculated based on the information provided by the manufacturer in the component's datasheet. In the datasheet the $V_{CE}$ is usually only given for a few

temperatures. Since the switches are not limited to only these temperatures, interpolation of the values from the datasheet can be used to obtain an estimation of the $V_{CE}$ for other temperatures as well, see Fig. 3.3 for an example of such an interpolation.

By assuming that a vehicle draws 100 A and 10 switches are placed in parallel, the voltage drop over the switches is 1.1 V and the resulting instantaneous losses are 110 W. By assuming a 3 % duty cycle the average power loss is 3.3 W. 3 % is roughly the duty cycle if there is one vehicle every two seconds driving at 120 km/h and the contact segments are about 1 m long. A contact segment is active for the time that it takes for a vehicle to travel the distance of two contact segments plus the length of the isolation between the two contact segments.

$$P_{cond} = \frac{1}{T_p} \int_0^{t_{on}} V_{CE} I_C \, dt \tag{3.13}$$

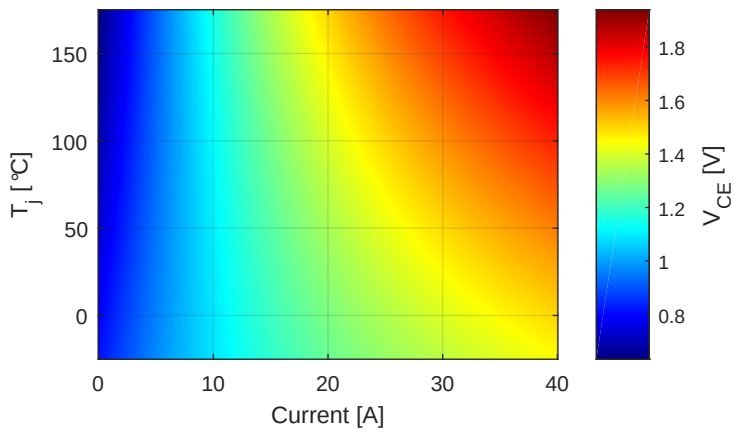


**Figure 3.3:** Shows $V_{CE}$ as a function of current and junction temperature.

Switching losses are the second type of losses in a solid state switch. In fast switched applications switching losses are a large if not the dominant source of losses. In an ASSE the solid state switch switches once per vehicle, which equals to less than one Hz in most cases. Average power loss in a switch due to switching, $P_{sw}$, is estimated with 3.14. The turn on energy, $E_{on}$, and turn off energy, $E_{off}$, are usually in the mJ range. By using the same parameters and component as for the conduction losses, the $E_{on}$ and $E_{off}$ are about 2 mJ each. This results in a power loss of 4 mW for a switching frequency of 1 Hz.

$$P_{sw} = (E_{on} + E_{off}) f_{sw} \tag{3.14}$$

With the average switching loss being orders of magnitudes lower than the conduction loss, the switching losses can be neglected without introducing a significant error in the total loss estimation of the switch.

**Contact point**

The connection between the ASSE and the current collector on the vehicle side is not perfect, implying there is an electric and thermal resistance over the contact. Since the connecting surfaces are not perfectly smooth, the contact area between the two surfaces can be can be significantly smaller than the apparent contact area.

For an ASSE, the contact point is located outdoors in an uncontrolled environment. Therefore the contact resistance can change over time and also along the ASSE due to e.g. dirt or rust on the contact segments. At present time there is no finished design for the current collector, making it difficult to evaluate the contact resistance in the final design.

In an attempt to evaluate the electric contact resistance for a sliding contact on an ASSE, a rotating test rig is built to improve the existing knowledge of the electrical properties of different sliding contact materials. The concept of the rotating test rig is shown in Fig. 3.4 and is based on a rotating disk on which the contact segment is located. Two stationary current collectors slide against the rotating contact segment to create a closed circuit for the current. A current source is connected between the two current collectors to force a current through the contact point of the first current collector, the contact segment and finally through the contact point of the second current collector. The current and also the voltage drops close to the contact points are measured via a slip ring device in the center of the rig, in order to calculate the contact resistance at the contact points.

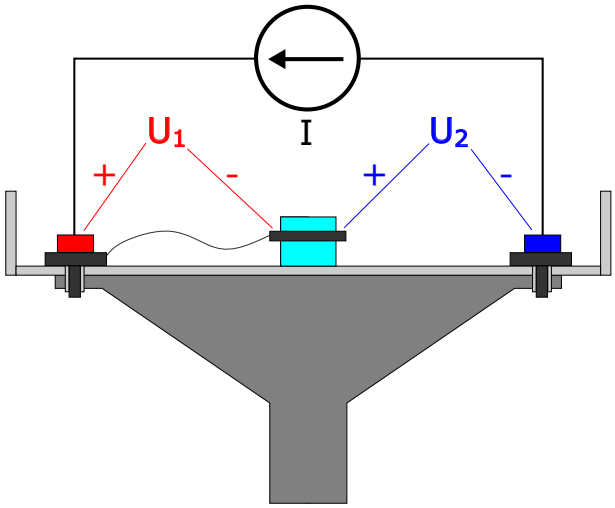


Figure 3.4: Shows a schematic overview of the rotating test rig.

Load cells are mounted on the current collectors to measure the normal forces, in order to get an understanding of how the contact force or pressure affects the performance of the contact. The test rig is also able to measure friction by the use of load cells.

Both the contact segment and the contact material on the current collectors are replaceable to allow for testing of different material combinations. The contact on the current collector is placed on a thin flexing sheet of metal to allow the metal to act as a spring and keep the contact leveled and with good contact to the contact segment, see Fig. 3.5.

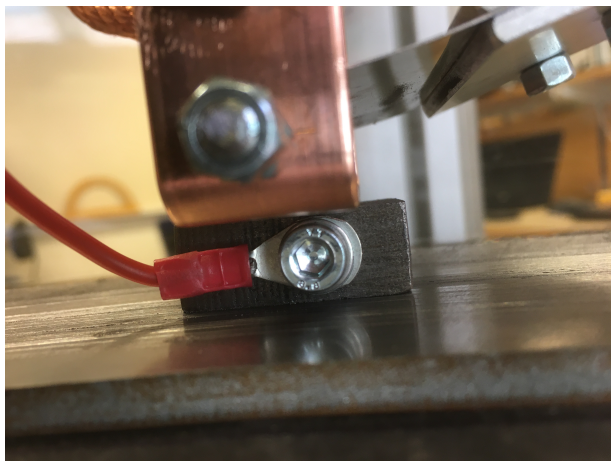

Figure 3.5: Shows a cast iron block used as the contact material on the vehicle side.

Figure 3.6 shows the test rig with two current collectors and a circular contact segment. In this figure the power cables from the current source are not mounted.

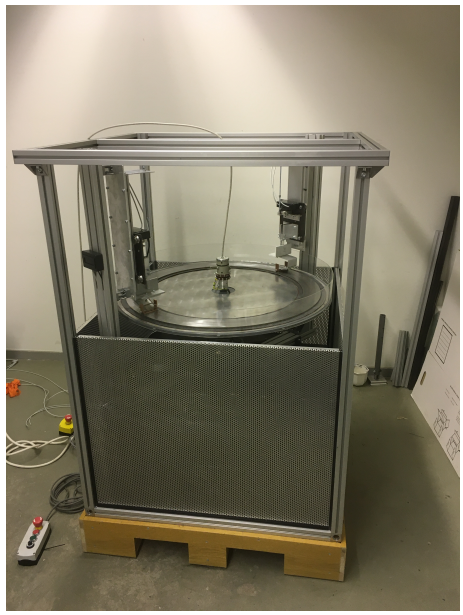

Figure 3.6: Shows the rotating test rig for the contact measurements.

Experiments are conducted with two different materials for the sliding contacts on the vehicle side, cast iron and copper with contact forces of 10 N and 27 N are used. Steel is used for the rotating contact track on the test rig. The apparent contact area of the cast iron contact is approximately 7.3 $cm^2$ and the copper contact 12 $cm^2$. The contact pressure, which is important for the contact resistance, can be calculated as the ratio between the contact force and the area, which is important for the contact resistance. At higher contact pressures more plastic deformation occurs, smoothing the asperities thus creating a better contact. Three different speeds are investigated, 1.7 km/h, 3.8 km/h and 7.5 km/h. These speeds are low compared to a moving vehicle, which can affect the accuracy of the results when extrapolating to speeds outside of the data range. The current is varied between 25 A and 200 A and the results are presented in Fig. 3.7. For all of the combinations the contact resistance decrease with increasing current in the interval of the tests.

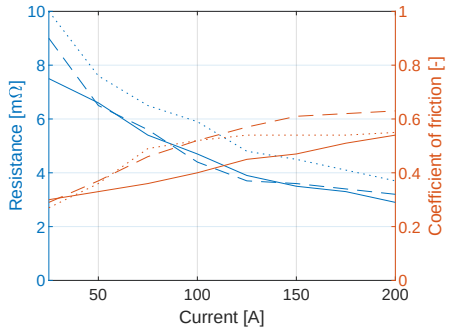


**(a)** Cast iron contact with a contact force of 10 N.

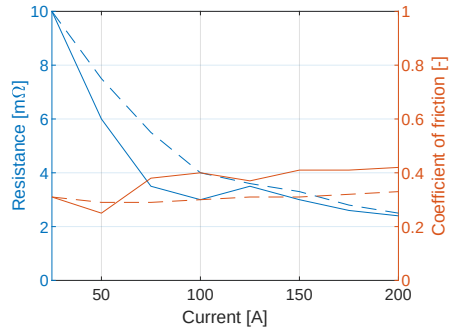


**(b)** Cast iron contact with a contact force of 27 N.

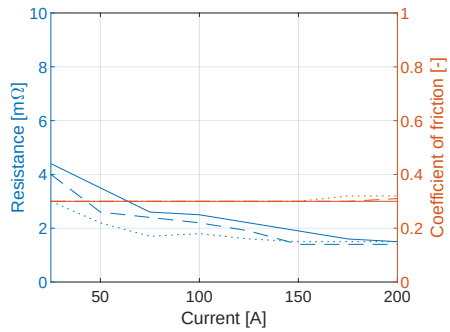


**(c)** Copper contact with a contact force of 27 N.

**Figure 3.7:** Shows contact resistance and coefficient of friction at different current levels. Solid lines represent a sliding speed of 1.7 km/h, dashed lines 3.8 km/h and dotted lines 7.5 km/h.

The contact resistance are measured for a current collector made of stainless steel at Elonroad's test site with the vehicle driving 37-50 km/h. The result from this measurement can be seen in Fig. 3.8 and is about 15-20 mΩ. The peaks in resistance in the figure are due to one of the current collectors sliding up on an insulator piece. When one current collector is on an insulating piece no current is flowing through the contact point and the measurement of the contact resistance is not valid in that point.

Note that a resistance of 20 mΩ conducting e.g. 100 A results in a power loss of 200 W. That is no big problem when a vehicle is moving, but it is a considerable local loss in the contact point when standing still. Thus, there are strong reasons to bring this resistance down by further research and development.

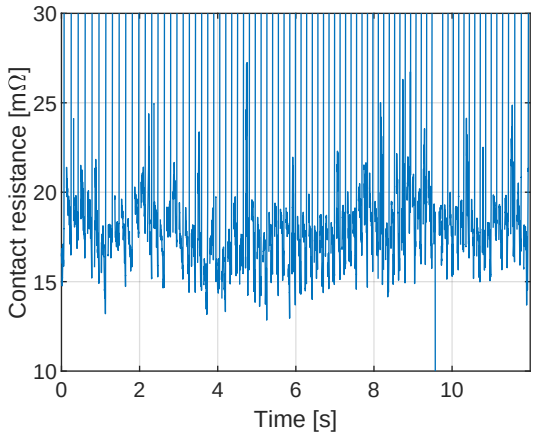


**Figure 3.8:** Shows the measured contact resistance of a stainless steel current collector sliding at 37-50 km/h at Elonroad's test site.

### 3.1.3 Friction

To make an object move, a tangential force is needed. This tangential force needs to be greater than the friction force preventing the object from moving [63]. While the object is at standstill the friction force is called static friction and for a moving object the friction force is called dynamic friction. The most common case is that the dynamic friction is smaller than the static friction [63]. For a conductive ASSE two surfaces, the contact point on the vehicle side and on the ASSE side, slide against each other with the speed of the moving vehicle. The dynamic friction force is then the resulting braking force, which is dependent on the normal force, $F_N$, and the coefficient of friction, $\mu_f$. The normal force is the force pressing the current collector down against the ASSE. The coefficient of friction depends on many parameters, one of them is contact material, see Table 3.3 for some examples of friction coefficients for different materials. Another factor that affect the coefficient of friction is temperature [64].

By knowing the vehicle speed and the friction force the friction power can be calculated by (3.15).

$$P_{friction} = V_{vehicle}\,\mu_f F_N \tag{3.15}$$

Table 3.3: Examples of coefficients of dynamic friction for different material combinations.

| Material combination | $\mu_f$ |
|---|---|
| **Mild steel on mild steel** | 0.57 [65], [66] |
| **Hard steel on hard steel** | 0.42 [65] |
| **Mild steel on cast iron** | 0.23 [65] |
| **Aluminum on mild steel** | 0.47 [65], [66] |
| **Copper on mild steel** | 0.36 [65], [66] |

## 3.2 Heat dissipation

An ASSE is designed to provide vehicles with a large amount of power. This power transfer generates heat in the ASSE, which needs to be dissipated. If the heat is not dissipated well enough the temperature rises and can be a safety hazard or even damage the ASSE itself. The lifetime of the electronic components located inside the ASSE depend on the temperature and the temperature variations of the ASSE. Higher temperatures and temperature large variations reduce lifetime more than lower temperatures and smaller temperature variations.

Heat is dissipated from the ASSE in three ways, convection, radiation and conduction. The ASSE is assumed to be completely flat and positioned horizontally.

### 3.2.1 Convection

Convective heat transfer occurs when there is heat transfer between a surface and a moving fluid [67]. Convective heat transfer includes both free convection and forced convection where free convection is driven by buoyancy forces due to temperature differences in the fluid, and forced convection is driven by external forces moving the fluid.

#### Free convection

Free convection, or natural convection as it is also called, is convection caused by buoyancy forces. The coefficient of thermal expansion is a measure of to what degree a fluid expands when the temperature increases. The mass of the fluid is the same even if the temperature changes but the volume of the fluid changes, resulting in a different density. In the case of an ASSE, the air closest to the ASSE is heated and expands. This air then rises, taking part of the heat with it, and it is replaced by colder air.

In order to calculate the heat transfer coefficient of free convection for a horizontal plate the first step is to calculate the Grashof number, $Gr$, according to (3.16) [68], and the Prandtl number, $Pr$, according to (3.17) for air at the film temperature [68].

$$Gr = \frac{g\,\beta\,(T_s - T_a)\,L_{ch}^3}{{v_{fluid}}^2} \tag{3.16}$$

$$Pr = \frac{C_p\,\mu}{k} \tag{3.17}$$

Grashof's number is a measure of the ratio between buoyancy forces and viscous forces acting on the fluid in question and the Prandtl number is the ratio between momentum diffusivity and thermal diffusivity [67]. These two numbers are then used to calculate the Rayleigh number, *Ra* by (3.18) [68].

$$Ra = Gr\,Pr \tag{3.18}$$

The value of *Ra* is an indication if the boundary layer is laminar or turbulent, and dictates which equation should be used to calculate the Nusselt number [68]. Nusselt number is the ratio between convective and conductive heat transfer and this number is used to calculate the heat transfer coefficient for free convection, (3.21) [69]. For a *Ra* value between $10^4$ and $10^7$, equation (3.19) is recommended and if *Ra* is greater than $10^7$ but lower than $10^{11}$, equation (3.20) is recommended instead [67].

$$Nu = 0.54\,(Gr\,Pr)^{1/4} \tag{3.19}$$

$$Nu = 0.15\,(Gr\,Pr)^{1/3} \tag{3.20}$$

$$h_{freeconv} = \frac{Nu\,k}{L_{ch}} \tag{3.21}$$

**Forced convection**

Forced convection is driven by an external force other than buoyancy, such as e.g. wind generated by pressure differences or a fan. Even at low to moderate fluid speeds the dominant type of convection is usually forced convection.

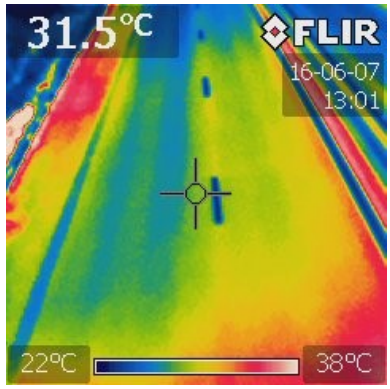


**Figure 3.9:** Shows the effect of forced convection on a freeway outside Lund. The warmer right hand lane is the passing lane in which less vehicles travel. The picture is taken from a bridge above the freeway.

For the ASSE forced convection is very important. Moving vehicles cause a wake behind the vehicle in which the air moves over the ASSE, creating forced convection. The more vehicles the more cooling from forced convection by these vehicles. The effect can be seen in Fig. 3.9 where the passing lane is 1.5 °C warmer than the other lane. It is important to note that this may that this may not only be due to forced convection. Different wear on the road surface can affect the emissivity of the road surface, which in turn affects the reading of the IR camera. Shading is also reducing the absorbed solar heat more in the lane with more vehicles.

The heat transfer coefficient for forced convection can be acquired numerically with the same conditions as the heat transfer coefficient for free convection. The assumption is still that the ASSE is a flat horizontal plate in order to simplify the calculations.

First of all Reynolds number is calculated, (3.22) [69].

$$Re = \frac{v_{fluid} L_{Ch}}{\mu_{fluid} / \rho} \tag{3.22}$$

The higher the speed of the fluid, $v_{fluid}$, the higher the Reynolds number is. $L_{Ch}$ is the characteristic length of the surface where convection takes place (dependent on the correlation used to calculate the convection coefficient) and $\mu_{fluid}$ and $\rho$ are material dependent parameters. The Reynolds number can be used to determine if a flow is laminar or turbulent, and describes the ratio between inertial forces and viscous forces [69]. Laminar flows over a flat plate are characterized by having a Reynolds number less than 500,000 and turbulent flows by Reynolds number higher than 500,000 [69]. To calculate Nusselt number for laminar flow (3.23) is used and for turbulent flow (3.24) is used [69].

$$Nu = 0.664\, Re^{0.5}\, Pr^{1/3} \tag{3.23}$$

$$Nu = 0.037\, Re^{0.8}\, P_r{}^{1/3} \tag{3.24}$$

From the obtained Nusselt number the heat transfer coefficient is calculated from (3.21).

It is worth considering that the presented analytical way of calculating the heat transfer coefficient relies on previous experiments with horizontal flat plates. This is especially troubling when it comes to cooling by moving vehicles as it does not resemble the experiments performed when developing the analytical equations.

**Cooling caused by moving vehicles**

When a vehicle is moving, the air in front of the vehicle is compressed and creates a high pressure zone, and at the same time a low pressure zone is created behind the vehicle [70]. This movement through the air mass creates a wake behind the vehicle that is turbulent [71]. Due to this wake there is an increase in forced convection, acting on both the ASSE and the road. Previous research have shown that vehicles do affect the heat balance of the road and thus the temperature of the road [72, 73]. Because of the wake being turbulent, and the circumstances are different from the circumstances in the experiments performed to obtain the analytical equations for forced convection, the analytical equations are likely inaccurate for this case. The cooling effect by passing vehicles on an ASSE is therefore experimentally investigated in this thesis. The increase in forced convection can also provide increased heating if the ambient air is warmer than the ASSE surface.

The performed measurements are used to calculate the cooling effect, and correlate this to the speed of the passing vehicle. The principle of the experimental setup is to generate a known amount of heat in the setup and measure the temperature of the setup. Based on the temperature difference between the setup and the surrounding air, the cooling coefficient, h-value, can be calculated. Before the system reaches a steady state it is important to consider the thermal mass of the experimental setup to get accurate results from the performed tests. The measurement setup is based on an aluminum foil attached to an electrically and thermally isolated board, see Fig. 3.10. The author wish to extend a big thank you to Lars Lindgren who came up with the idea of using an aluminum foil.

Figure 3.10: The experimental board for measuring the cooling effects by vehicles, figure from [74].

A voltage is applied over the foil to electrically heat the foil by the resulting current flowing through it. By measuring the voltage and the current the power loss in the foil is known and can be used to calculate the h-value. The h-value is a measure of the amount of heat that leaves the system per unit area and degree of temperature difference between the surface and the surrounding air, see (3.25). Even if the equation used to model the heat dissipation corresponds to the convection mechanism (radiation depends on the temperatures to the power of four, and conduction depends on the distance and the material properties), the evaluated h-value also includes the effects of radiation and conduction. To calculate the h-value the heat leaving the system, area of the foil and the temperature difference between the foil and ambient air need to be known. The area of the foil is easily measured and the temperature of the foil is calculated from the change in resistance of the foil. The resistance change can be calculated as the start temperature is known as well as the temperature coefficient of the foil, see (3.26). Figure 3.11 shows the temperature coefficient of the aluminum foil, measured at different temperatures in a temperature cabinet. The gray area in the figure represent the uncertainty in resistivity with a $\pm 1°$C error in the temperature measurement.

$$h = \frac{Q}{A_{surface}\,(T_s - T_{ambient})} \tag{3.25}$$

$$\Delta T = (1 - \frac{R_{start}}{V_{RMS}\,/\,A_{RMS}})\,\frac{1}{\alpha_{al}} \tag{3.26}$$

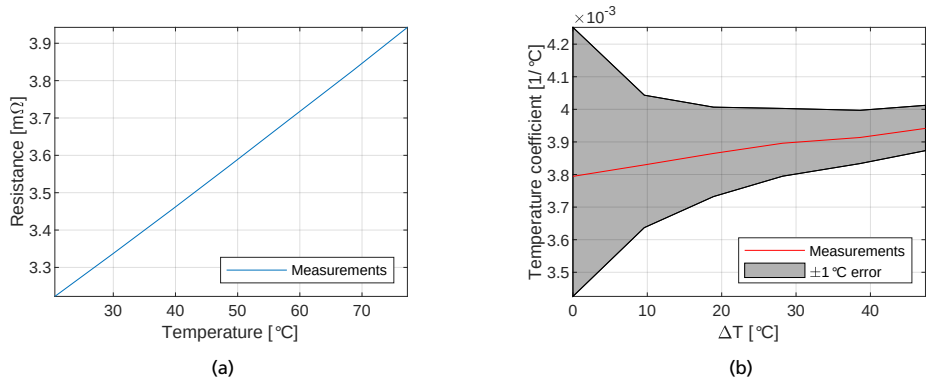


**Figure 3.11:** (a) shows the resistance of a different piece of the aluminum foil used for the experimental setup in Fig. 3.10. (b) shows the temperature coefficient of the aluminum foil based on the measurements in (a). Figure from [74].

The amount of heat leaving the system is the most difficult parameter to estimate as it is the generated heat minus the heat stored in the aluminum foil and the material in close proximity to the foil. In order to estimate the dissipated heat a thermal model is used to model the stored energy in the system during a transient event. A RC-network is used as a thermal model and can be seen in Fig. 3.12. This model takes the stored heat in the material into consideration and is able to identify the cooling coefficient when a vehicle passes over the experimental setup. R1 is the component that should be interpreted as the thermal resistance to the surroundings.

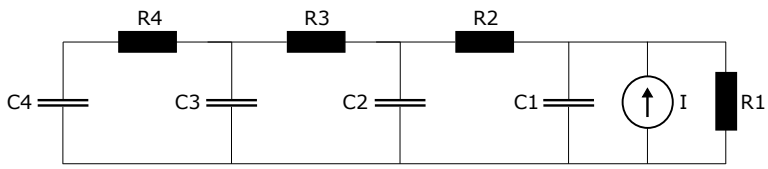


**Figure 3.12:** The thermal RC model used to model the experimental setup, figure from [74].

The parameter identification of the thermal model components is based on fitting the model to a step response. The timescale of the modeled event is the deciding factor of how long the model must fit the step response. Fast events with short timescales require the model to fit in the beginning of the step, compared to events with longer timescales which need the model to be accurate later in the step. Figure 3.13 shows both the calculated temperature from the measurement and the temperature from the thermal model for a step response. The timescale of interest is fairly short, less than 3 seconds, therefore it is important that the thermal model is accurate for times shorter than this. In Fig. 3.14 the first 3 seconds of the step response are visible and it is clear that the model is a good fit to the calculated temperature from the measurement. The model parameters from the model fit to the step response are presented in Table 3.4. The RC-network is not supposed to be a physical

representation of the system, and is only supposed to give an output that agrees with the measurements. With more RC-links more time constants can be introduced in the system. For this model three RC links give a good fit between measurement and thermal model and there is no need for adding further RC-links.

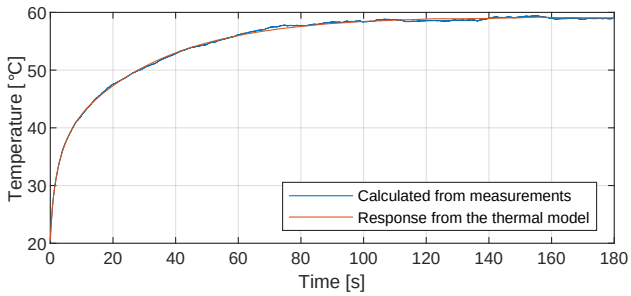


**Figure 3.13:** Shows the temperature for a step response as well as the simulated temperature with the thermal model, figure from [74].

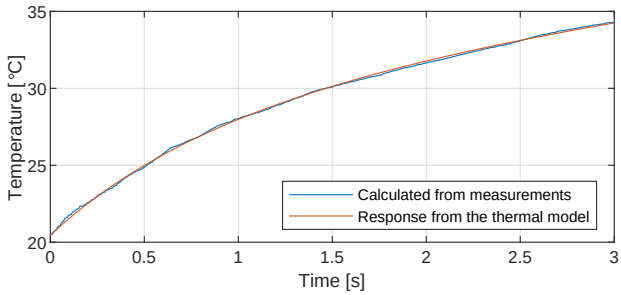


**Figure 3.14:** Shows the first 3 seconds of Fig. 3.13, figure from [74].

**Table 3.4:** Parameters of the thermal model shown in Fig. 3.12.

| Component | Value |
|---|---|
| $R_1$ | 1.0243 K/W |
| $R_2$ | 0.4177 K/W |
| $R_3$ | 0.8815 K/W |
| $R_4$ | 0.0004 K/W |
| $C_1$ | 3.4860 J/K |
| $C_2$ | 5.6960 J/K |
| $C_3$ | 0.0553 J/K |
| $C_4$ | 10.3013 J/K |

A Volvo V70 is used to investigate the cooling caused by a vehicle on an ASSE. The car drives past the experimental setup 6 times, 3 in each direction, for 9 different speeds. During the

experiment current and voltage are logged to know the amount of heat that is generated in the aluminum foil. R1 in the thermal model depends on the cooling coefficient and is removed from the thermal model when the cooling effect of a vehicle is investigated. By removing R1 only the experimental setup itself is present in the thermal model, allowing the model to simulate the heat stored in the setup. Instead of feeding the RC model with a power the model is fed with a temperature, by replacing the current source in Fig. 3.12 by a voltage source. When the temperature changes in the model, the energy in the thermal mass of the system is either increased or decreased. The dissipated power can be calculated by subtracting the power stored in the system from the generated power. Based on the dissipated power and the temperature difference between the foil and ambient, together with the area of the foil the h-value is calculated.

When the vehicle pass by the experimental setup, a significant increase of the h-value can be seen, see Fig. 3.15. With higher vehicle speeds the h-value peaks at a higher number. During the experiment the wind had a wind speed of roughly 1 m/s, this is together with radiation and free convection the reason for the DC offset of the h-value.

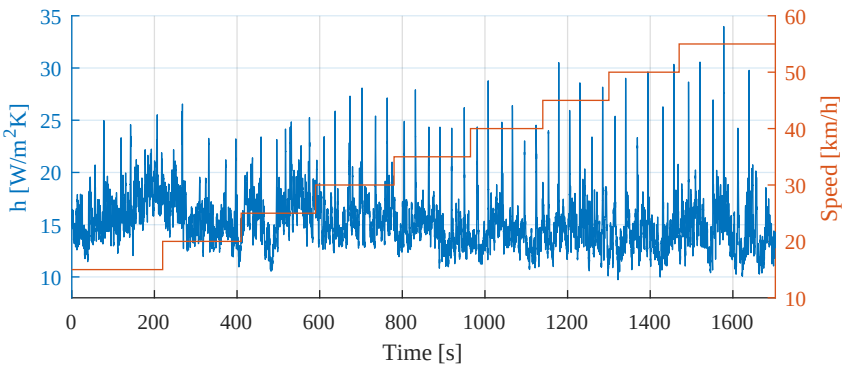


Figure 3.15: Shows the resulting h-value for multiple vehicle passes over the experimental setup, figure from [74].

A closer look on the individual pulses resulting from the vehicle passing by the experimental setup is presented in Fig. 3.16. Speeds below 30 km/h are not included in the figure due to the baseline of the h-value being too unstable. The average h-value for each speed is presented as a thick red line. In order to get a worst case scenario, the cooling from the vehicle is calculated based on the increase in h-value, i.e. not taking into account the cooling existing regardless of the vehicle pass. If there would have been no wind during the measurements the h-value before the vehicle arrives to the setup would have been lower. It is possible that the h-value peak also would have been lower. When the vehicle passes over the test setup the h-value increases rapidly for the first second and is elevated for roughly 1.5-2 seconds in total. Based on this data, a reasonable h-value increase is 10 W/m$^2$K for 1 second, which is the cooling factor used in the thesis. The experimental data only includes

speeds up to 55 km/h, which makes it necessary to extrapolate the data to higher speeds. The extrapolation in this case is that the added cooling stays at 10 $W/m^2K$ for 1 second. More data at higher vehicle speeds and also with different vehicles are needed to obtain more reliable results that represent the different vehicles present on the roads.

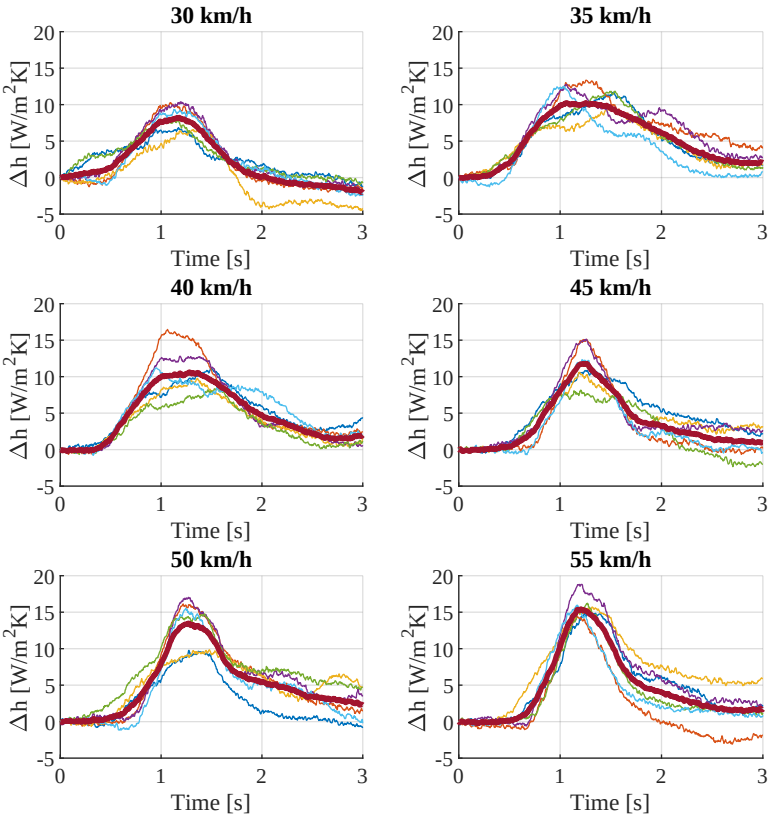


Figure 3.16: The passages from Fig 3.15 put on top of each other for 30 km/h to 55 km/h, showing the increase in h-value during a passage. The average in each subplot is presented as a thicker red line, figure from [74].

### 3.2.2 Conduction

Conduction is the heat transfer mechanism in which energy is transferred from particles to other adjacent particles with less energy [69]. Different materials have different thermal conductivity, which is a measure of how well a material conducts heat. Most metals are good at conducting heat while insulators have lower thermal conductivity and conducts heat less well [69].

When assembling an ASSE consisting of many different parts, and in many cases made of different materials, it is likely that airgaps between the different parts in the ASSE are introduced due to e.g. manufacturing tolerances and thermal expansion. The temperature difference between the two sides of the airgap should not be more than a few degrees, if the ASSE is well designed. A temperature difference of a few degrees makes the thermal radiation small and the air volume is not large enough for convective heat transfer to be a major heat transfer. Because of this the only relevant heat transfer mechanism is conduction.

For an ASSE located on the ground there is conduction down to the asphalt. If this conduction path is strong, heat can easily flow from the ASSE into the ground or the other way around. A weak conduction path allows for less heat transfer. This also implies that the ASSE is not strongly coupled to the large thermal mass of the ground. This can be an advantage in colder climates if the ASSE needs heating to prevent snow and ice from covering the contact segments. On the other hand a strong coupling to the thermal mass of the ground evens out large temperature swings of the ASSE and reduces the peak temperature of the ASSE during heavy load.

### 3.2.3 Thermal radiation

Materials with a temperature above absolute zero emit thermal radiation. This radiation is temperature dependent and is caused by atoms vibrating inside the material. At higher temperatures the atoms are vibrating more, resulting in a greater amount of thermal radiation. The amount of thermal radiation emitted follows Stefan-Boltzmann law, (3.27), where $A_{surface}$ is the surface area, $\epsilon$ is the emissivity and $\sigma$ is the Stefan Boltzmann constant [69].

$$P = A_{surface}\, \epsilon\, \sigma\, T^4 \tag{3.27}$$

As seen in (3.27) the radiation intensity depends on the temperature to the power of four. At high temperatures this makes thermal radiation a very important cooling mechanism, while at low temperatures the heat radiated from a material is small. For an ASSE, it is desirable to keep the temperatures as low as possible. Looking at (3.27), the only parameter that can be changed for a specific ASSE design is the emissivity, since the area is fixed for a specific design and the temperature should be as low as possible. Emissivity is material and surface dependent, which means a material with high emissivity is preferred in order to emit more thermal radiation. By selecting materials with high emissivity more thermal radiation is emitted from the ASSE.

The net cooling effect caused by thermal radiation is difficult to estimate as it depends on the thermal radiation from the surroundings towards the ASSE. For example during clear

skies the incoming thermal radiation is low while during cloudy skies the incoming thermal radiation is high. This incoming thermal radiation can be estimated with (3.28) which is the Swinbank model with updated coefficients [75]. This model includes cloud height, cloud coverage, relative humidity and ambient temperature. Due to the complexity of this model and the uncertainty in estimating the parameters for the model together with the surroundings of the ASSE, a worst case approach is assumed. The worst case is when the incoming thermal radiation is from ambient temperature. This gives the lowest net cooling effect of the ASSE from thermal radiation.

$$E_{thermal} = (1 + KC^2)\, 8.78 * 10^{-13}\, {T_{ground-level}}^{5.852}\, RH^{0.07195} \tag{3.28}$$

## 3.3 Thermal model

The thermal model developed is a 3D finite element model capable of simulating dynamic and static charging using the ASSE. The model is based on a somewhat simplified geometrical model of the first generation of Elonroad's ASSE, which is a road bound conductive ERS placed on top of the asphalt. This design features the power electronics built into the structure of the ASSE, making it particularly challenging when it comes to cooling. The possibility for active cooling is limited while at the same time all of the heat generated by the power electronics is generated inside the ASSE. The added heat to the structure affects both the power electronics as well as the temperature of the entire ASSE structure.

The internal structure of Elonroad's ASSE is complex, with screws, airgaps and electronics, which is very computationally heavy to simulate in detail. In order to reduce the computational intensity of the model, simplifications are made to the geometry. These simplifications include removing screws, airgaps and other complex details, which need a fine mesh to represent properly. These simplifications reduce the amount of mesh elements needed, reducing the computational time for a simulation.

### 3.3.1 Elonroad's ASSE

Elonroad's ASSE is an ERS placed on top of the asphalt, see Fig. 3.17. The ASSE is approximately 5 cm high and 32 cm wide with a flat top and sloping edges. It is built in 10 m subsections that are joined together to create one long continuous ASSE. By having 10 m subsections placed on top of the asphalt, the installation of the ASSE is simple. The subsections are joined together by screws that can easily be removed if there is a need to replace a subsection.

The contact segments are 1 m long and are separated by 10-15 cm of plastic insulation. Every other contact segment is directly connected to the negative main conductor that runs along the entire ASSE. This negative main conductor is grounded in the feed-in station to keep the contact segments connected to the negative conductor at or close to ground potential. A positive main conductor also runs along the entire ASSE and is just like the negative conductor only fed in one end. The contact segments that are not directly connected to the negative conductor are connected through IGBTs either to the positive or the negative main conductor. Due to the limited space inside the ASSE discrete IGBTs with TO-247 packaging are used in parallel, allowing for high current capability in a limited space. Under every other contact segment, a PCB containing the IGBTs and the circuitry needed to drive these is installed. These PCBs also contain e.g. voltage and current measurement and other control circuitry needed for the ASSE.

Figure 3.17: The Elonroad ASSE.

### 3.3.2 Geometry and simplifications

The geometry presented in this thesis is a simplification of Elonroad's ASSE, and it is also the geometry that is simulated. Figure 3.18 shows the simplified cross-section of the ASSE, with the different parts visible.

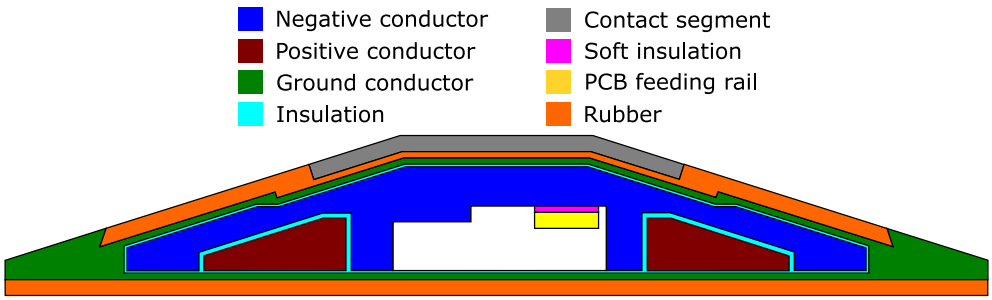


Figure 3.18: A slice of the ASSE showing the different parts on the inside of the ASSE.

- The **PCB**s, located in the white space in the middle of Fig. 3.18, contain a large amount of small components that do not affect the thermal result noticeably, but to model these small components a fine mesh is required. The finer the mesh the more mesh elements are required, which results in longer computational time. The important components on the PCB are the main switching elements, as they are the main source of heat on the PCB. In order to remove the PCB from the model an assumption must be made of where the heat enters the ASSE structure. In this case there are two major thermal paths. The first one is the path to the heatsink of the IGBTs. The IGBTs are attached to a copper PCB feeding rail, which acts as a heatsink. The second thermal path is through the screws connecting the PCB with the contact segment (not shown in Fig. 3.18, but running vertically from the PCB to the contact segment). In the simulations it is assumed that the heat generated in the PCB is applied to the PCB feeding rail and a thermal resistance is added between the PCB feeding rail and the contact segment. The result of this is that the PCB temperature is not included in the model, which is not a problem as the actual temperature distribution on the PCB is of low importance for this study. Measurements also show that the temperature of the PCB feeding rail is a good approximation of the maximum PCB temperature. By knowing the temperature of the PCB feeding rail the temperature of the IGBTs can be estimated. The total thermal mass of the ASSE is reduced when the PCB is removed but the PCB is only a small fraction of the entire thermal mass of the ASSE that the difference in result is small.

- **Rounded corners** need a lot of mesh elements to be represented accurately. In this model corners are of low interest and are made into sharp corners. This reduces the number of mesh elements and also the computational time it takes to run the model.

- The **current collector**, see Fig. 3.19, is modeled as a copper block with a copper rod attached to it. This is obviously not an accurate model of a current collector but it adds thermal mass and cooling to the contact point. This simplification is used because there is currently no existing final design of a current collector. The current collector is only added to the model when static charging is simulated.

- **Small details and components** both externally and internally of the ASSE are neglected. These small details include screws, wires, milling details, and many other details and components in the ASSE.

With these simplifications of the geometry the number of mesh elements are reduced without affecting the results to a large extent in the regions of high interest. The regions of highest interest are the contact segment surface as well as the PCB feeding rail. Figure 3.19 shows the full model including the ground and the current collector of interest from a vehicle. The ground is modeled as a 15 cm thick layer of asphalt on top of a 35 cm layer of gravel, extending 1 m on either side of the ASSE.

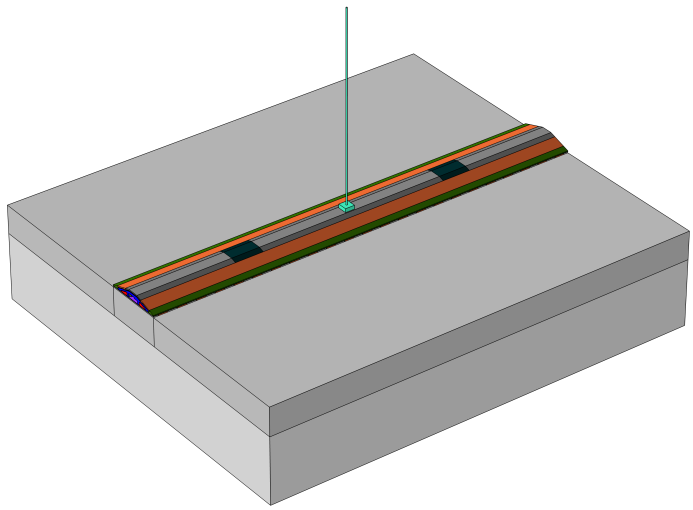

Figure 3.19: Showing the full model of the ASSE, including the ground.

### 3.3.3 Model parameters and assumptions

This section explains how the different heat sources and other boundary conditions are applied to the model. Table 3.5 lists the different materials and their parameters used in the ASSE.

Table 3.5: Material parameters of the ASSE.

| Material | $k$ [W/mK] | $\rho$ [kg/m$^3$] | $C_p$ [J/kgK] |
|---|---|---|---|
| **Aluminum** | 204 | 2700 | 900 |
| **Asphalt** | 1.25 | 2100 | 920 |
| **Copper** | 400 | 8960 | 485 |
| **Hard electric insulation** | 0.18 | 1190 | 1470 |
| **Gravel** | 0.36 | 1840 | 840 |
| **Plastic** | 0.18 | 1190 | 1470 |
| **Rubber (top)** | 0.18 | 1190 | 1470 |
| **Rubber (bottom)** | 0.75 | 1190 | 1470 |
| **Soft electric insulation** | 0.6 | 1470 | 900 |
| **Steel** | 44.5 | 7850 | 475 |

Peak ambient temperature normally occurs in the afternoon around 15:00-16:00. This happens a few hours after the peak solar irradiance as the ground is a large thermal mass, thus changing its temperature slowly. For this thesis ambient temperature is assumed to be a sinusoidal curve with a peak value of 30 °C at 15:00 and a low of 20 °C.

### Convection

To give a worst case scenario it is assumed that there is no wind, and the only convective cooling comes from free convection and forced convection from passing vehicles. Note that forced convection from wind is added in the calibration and validation cases later in this chapter where the model is compared to measurements. Figure 3.20b shows the convective heat transfer coefficient for free convection for the asphalt and Fig. 3.20a for the ASSE. These figures are based on the calculations presented in Section 3.2.1 with the assumption of a flat ASSE. Cooling by both free and forced convection is related to the characteristic length, which is difficult to accurately estimate, therefore two different zones are recognized. The asphalt which is wide and long and the ASSE which is narrow and long. These two are modeled with different characteristic lengths, 1 m for the asphalt for both free and forced convection and 15 cm for the ASSE for free convection and 1 m for forced convection. Cooling from passing vehicles do not use characteristic length and is explained in Section 3.2.1. The same amount of cooling from passing vehicles is assumed for both the ASSE and the asphalt. It could be argued that the wind can cancel out or reduce the cooling from the free convection or from the vehicles but it is an unlikely scenario and is not taken into consideration in this thesis. It is also assumed that no cooling from free convection occurs if the surface is colder than ambient temperature. A surface temperature colder than ambient temperature can occur if the ambient temperature changes fast. This is not the case in this thesis, thus the assumption does not affect the simulations.

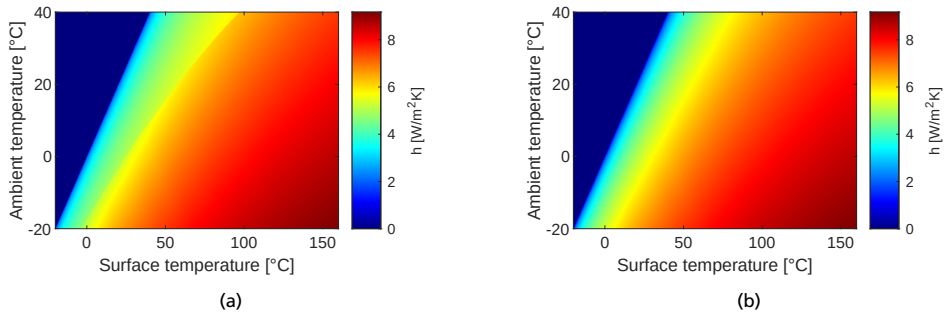


Figure 3.20: Shows the convective heat transfer coefficient for the ASSE, (a), and the asphalt, (b).

### Solar irradiation and thermal radiation

Solar irradiance is applied to every surface facing the sun. It is important to note that the higher the traffic intensity the more shade the vehicles provide for the ASSE, hence lowering the total amount of heat absorbed. For static charging the solar irradiation is assumed to be negligible and is not considered as a source of heat. Solar irradiance is calculated by the equation in Section 3.1.1 with the assumptions of a flat ASSE, a latitude of 55 degrees, 8 % diffuse irradiance, and the day of the year with the most solar irradiance. Figure 3.21 shows both the direct and the global irradiance for the day with the most solar irradiance. The global irradiance is the sum of the diffuse and the direct solar irradiance, which peaks slightly over 840 W/m$^2$.

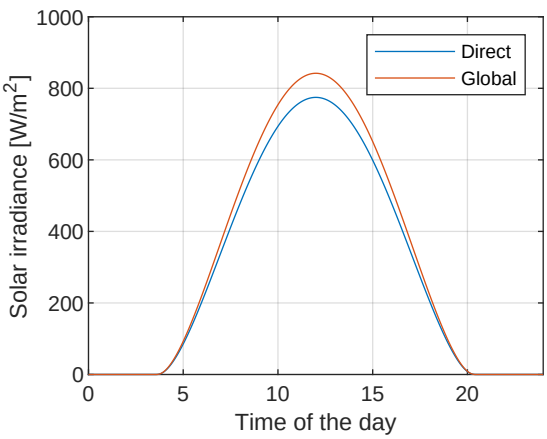


Figure 3.21: Shows the solar irradiance for the day of the year with the most solar irradiance at a latitude of 55 degrees.

Incoming thermal radiation is assumed to be from ambient temperature with the same

emissivity as the surfaces on the ASSE facing the sky. This results in a net cooling effect according to (3.29) and vehicles are not considered to affect the thermal radiation.

$$P = A_{surface}\,\epsilon\,\sigma\,(T^4 - {T_{ambient}}^4) \tag{3.29}$$

Solar absorptivity and emissivity of the surface materials are listed in Table 3.4. These parameters are hard to estimate as they are directly related to the surface of the material. For example dirt, rust or other imperfections affect these parameters, resulting in changing solar absorptivity and emissivity over time.

Table 3.6: Emissivity and solar absorptivity of the surfaces of the ASSE.

| Surface | $\alpha_s$ | $\epsilon$ |
|---|---|---|
| **Steel contact segment** | 0.47 | 0.14 |
| **Plastic insulator** | 0.95 | 0.95 |
| **Rubber** | 0.3 | 0.9 |
| **Aluminum** | 0.16 | 0.03 |
| **Asphalt** | 0.875 | 0.94 |

### Conductors

The resistive losses in the conductors are modeled as volumetric heat sources. These losses are related to the resistivity of the conductor material, which is temperature dependent. This relationship between temperature and resistivity is included in the model. There are two positive main conductors feeding the contact segments with high potential. These two conductors are assumed to share the current evenly.

The current in the conductors is assumed to be the average current as explained in Section 3.1.2. To use the proper RMS current the exact traffic flow needs to be determined.

### IGBTs

There are two thermal paths the heat from the IGBTs can take. The heat from the IGBTs can go either into the PCB feeding rail or via the PCB and the screws connecting the PCB to the contact segment. In the model the losses in the IGBTs are represented by a heat flux applied to the boundary of the PCB feeding rail, which the IGBTs are attached to. A thermal resistance of 5 K/W is added between the PCB feeding rail and the contact segment representing the screws, to allow some of the heat to flow directly to the contact segment.

There are multiple IGBTs connected in parallel. It is assumed that these components share the current equally and have the same voltage drop. Considering the low frequency of the switching the switching losses are negligible and thus not considered.

### Airgaps

Airgaps are thin layers of air between two surfaces. These exist in the ASSE between almost every pair of surfaces in contact, as the fit is not perfect. It is assumed that the airgaps are thin enough for convection as well as thermal radiation to be neglected, as explained in Section 3.2.2. Heat can therefore only pass through these layers by conduction. With air being a poor thermal conductor even a thin airgap increase the thermal resistance noticeably. Figure 3.22 shows the location of the airgaps, where the airgaps marked with a blue color are between the internal surfaces of the ASSE and the red color is used for the airgap between the asphalt and the ASSE. For the internal airgaps a thickness of 0.05 mm is assumed and 0.25 mm for the airgap between the ASSE and the asphalt.

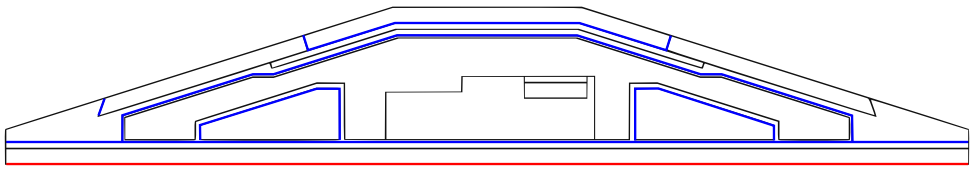

Figure 3.22: Shows the airgaps in the model.

### Friction

Heating by friction is applied as a boundary heat source on the top of the contact segments and the plastic insulators. It is unknown what fraction of the total friction heating power heats up the ASSE and what fraction heats up the current collector, therefore all of the heat from friction is assumed to heat up the ASSE to give a worst case scenario. The coefficient of friction used is 0.2, which is the result of experimental measurements between a steel contact segment and a stainless steel braid. This number is measured by dragging a stainless steel braid across a contact segment and measure the force needed to keep a constant speed.

### Contact point

Based on the measurements in lab conditions and at Elonroad's test track that are explained in Section 3.1.2, the electric contact resistance for dynamic charging is assumed to be 10 mΩ. This is worse than the lab tests but better than the tests at the test track. It is reasonable to

use a lower contact resistance than the one measured for a stainless steel current collector, as it is likely that a material with better electrical properties is used in a commercialized design. Improvements in the current collector design can also reduce the contact resistance further. For static charging the contact resistance is assumed to be 2 mΩ. In [76] a contact resistance of 2 mΩ is measured at 200 A for a cast iron block. Multiple blocks can be used as well as different materials, reducing the contact resistance to less than 2 mΩ. If the current collector is only supposed to be used for static charging, then as long as a material has good electrical characteristics, a material with lower durability compared to the material used for dynamic charging can be used.

The thermal contact resistance is based on an assumed 50 $\mu$m of air between the two contact surfaces.

## 3.4 Thermal model calibration and validation

In order to improve the accuracy of a model, it needs to be calibrated. After the calibration process the model needs to be validated to prove that it is accurate enough for the intended usage. For both calibration and validation, real world data from a 120 m long test track is used. Due to the location of the test track inside a gated off area, dynamic charging tests at realistic power levels and traffic intensities are not possible to perform. The reason for this is the limited amount of traffic that can be on the test site at the same time. In order to characterize the ASSE's thermal behavior under dynamic charging the ASSE utilization needs to be high and be present for several hours. At the test track the amount of passages with a vehicle charging from the road can be at most 2-3 vehicles per minute, which is a very low traffic intensity. Such a low intensity makes it difficult to detect any temperature changes inside the ASSE. A more practical difficulty is that the test vehicles must use the ASSE for several hours straight. Instead of dynamic charging tests, static charging is used to calibrate and validate the thermal model. For static charging only one vehicle is needed and the charging power is limited by the ASSE and not the load, which in the case of the measurements is a trailer, see Fig 3.23c, equipped with a resistive load capable of dissipating up to 200 kW.

### 3.4.1 Measurements at the prototype track

A trailer equipped with resistive heaters capable of dissipating 200 kW is used as a load during the measurements. Figure 3.23a shows the schematic of the test setup. The trailer is connected to one positive and two negative contact segments, where the second negative contact segment is connected to the negative conductor through IGBTs. The result of this is that the main part of the current flows through the negative contact segment, which

is directly connected to the negative conductor and not through the one connected by IGBTs. The measurements are used to calibrate and validate the thermal model of the ASSE structure, which do not include external heat sources, such as current collector related heat sources and solar irradiation. An exception to this is for one calibration and one validation case when the solar irradiance is included in the measurements. The influence of the current collector is reduced by placing two copper plates on the far end of either side of the contact segment under investigation, see Fig. 3.23b. By applying a high contact pressure the electric contact is as good as possible. The trailer is also positioned 3 m away from the contact segment under investigation to minimize the influence from the return path of the current. To reduce the impact of solar irradiance a solar cover is positioned over the ASSE for the measurements performed during summer conditions. For spring conditions a solar cover is not used and the solar irradiation is estimated by the equations in 3.1.1. A full overview of the test setup is shown in Fig. 3.23c. The resistive shunt marked as number 3 is used to monitor the current during the experiment close to the measurement point. This is to make sure there are no major leakage currents between the current measurement in the feed-in station and the test point.

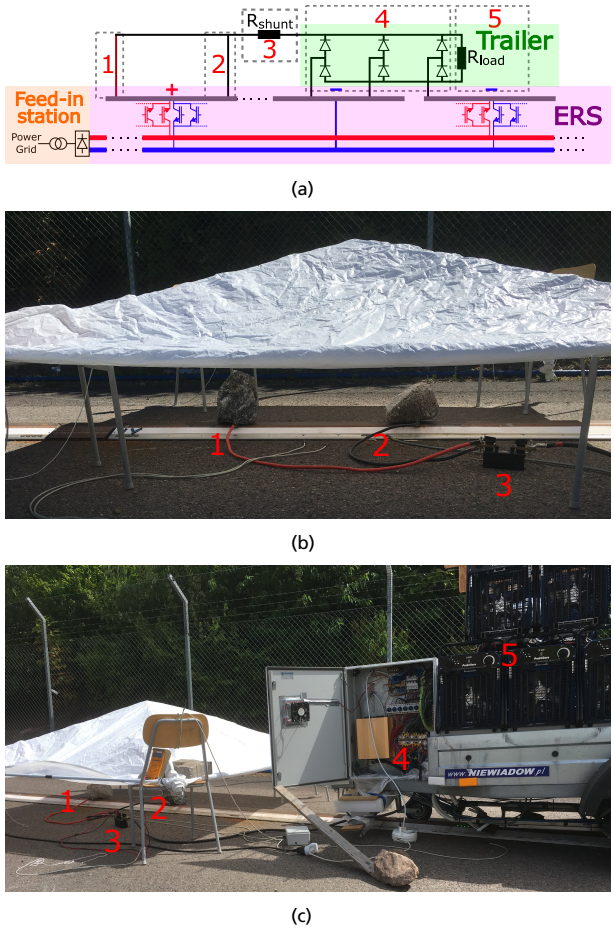


Figure 3.23: (a) shows a schematic of the experimental setup. On either side of a positive contact segment two contact points are placed as far away from the PCB as possible. This is to minimize the effect of the contact losses on the measurements. (b) shows a close up view of the contact segment under investigation. (c) shows the full experimental setup.

Seven different measurements are performed at different current levels and weather conditions. Four of the measurements are used for calibration of the thermal model and the other three are used to validate the model after it is calibrated. These measurements are listed in Table 3.7 where C stands for calibration case and V for validation case. Case $V_2$ is different from the other cases in the sense that the current is turned on and off with 5 minute intervals. Case $C_2$ and $V_3$ are performed on a different 10 m section of the ASSE.

Each test is stopped when the measurements show a PCB temperature of 85 °C or when the temperature is quasi-stationary. During the measurements the ambient temperature, asphalt temperature as well as the wind speed are recorded to be able to replicate the external parameters in the simulation model. For case $C_2$ and $V_3$ a solar cover is not used, which

results in heating from solar irradiance. The tests are performed the 20th and 22nd of march around 9:00-11:30 and 14:00-15:00. The equations in Section 3.1.1 are used to calculate the solar irradiance on a clear day but during the tests clouds were present, reducing the solar irradiance. Due to this 50 % of the clear day irradiance is assumed for both tests, see Fig. 3.24 for the assumed solar irradiance. Note that the 50 % is not measured and is a guess based on observations during the day of the measurements.

**Table 3.7:** Different measurement cases used for calibration and validation of the model.

| Case | Current [A] | Ambient [°C] | Asphalt [°C] | Wind [m/s] |
|---|---|---|---|---|
| C1 | 152 | 20 | 30 | 3.5 |
| C2 | 197 | 5 | 5 | 5 |
| C3 | 248 | 22 | 30 | 3 |
| C4 | 296 | 22 | 30 | 3.5 |
| V1 | 202 | 25 | 35 | 4.5 |
| V2 | 202 | 26 | 36 | 5.5 |
| V3 | 293 | 8 | 8 | 5 |

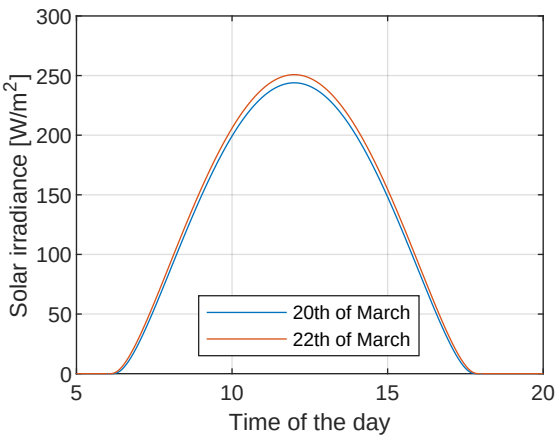


**Figure 3.24:** Shows the solar irradiance for cases $C_2$ and $V_3$. 50 % of the irradiance a cloudless day is assumed based on the equations in Section 3.1.1.

### 3.4.2 Calibration

The FE model is calibrated against four different measurements. During the calibration process the thickness of the airgaps, the thermal conductivity of the bottom rubber, the thermal resistance between PCB feeding rail and contact segment, and the thermal conductivity of the insulation material between the negative conductor and the PCB feeding

rail are adjusted to improve the model's fit to the measured temperatures from the calibration cases. The values presented in this thesis are the calibrated values.

Figure 3.25 shows that the simulation results agree well with the measurements. The PCB is not modeled and a point on the PCB feeding rail is used for the estimation of the PCB temperature. The approximate location of the different measurement points can be seen in Fig. 3.26.

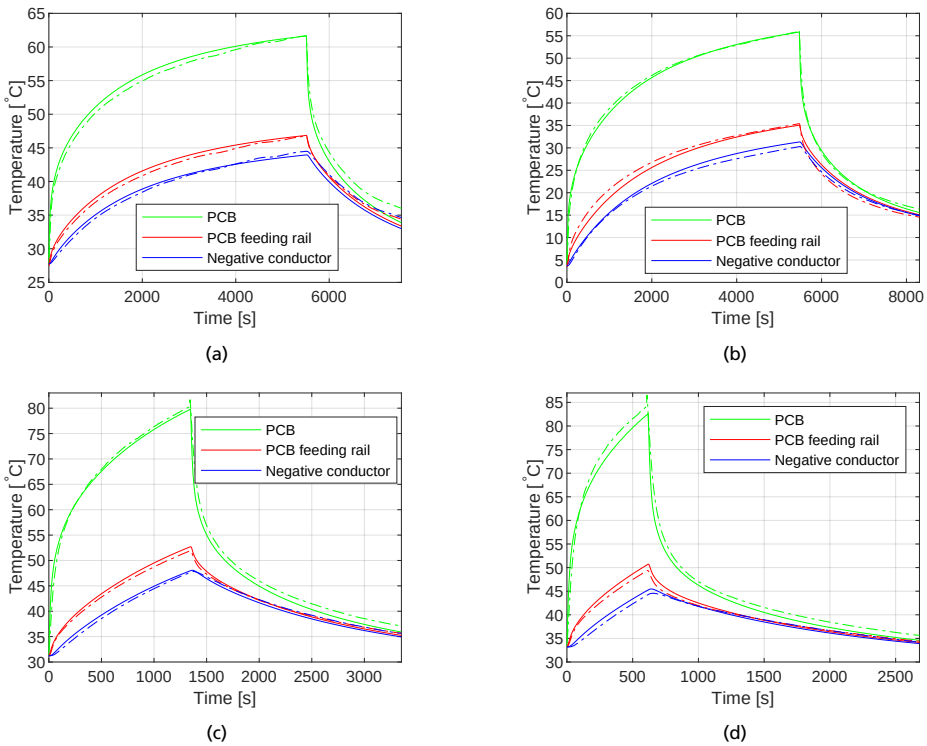


Figure 3.25: Dashed lines are measured temperatures and solid lines are from the thermal model. (a) is for a charging current of 150 A, (b) is for 197 A,(c) is for 248 A and (d) is for 296 A.

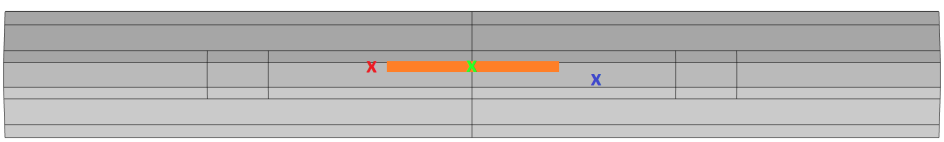

Figure 3.26: The area where the heat from the IGBTs enter the ASSE structure is marked with orange. The red x marks the sensor location of the PCB feeding rail, the blue x the sensor for the negative conductor and the green x the PCB temperature.

### 3.4.3 Validation

The three remaining cases in Table 3.7 are used for validation of the model. The thermal model uses the calibrated parameters from the calibration with the exception of the external parameters, such as wind and ambient temperature.

For case $V_1$ and $V_2$, which are presented in Fig. 3.27a and Fig. 3.27b the model and the measurements align well. For case $V_3$ the model is not as accurate, with a maximum error of 8.6 °C compared to the measurement, see Fig. 3.27c. The maximum error is defined as the maximum deviation from the measured value throughout the entire measurement. By reducing the characteristic length for the forced convection in case $V_3$ to 10 cm, about the width of the contact segment, the error is significantly reduced. This shows the importance and sensitivity of using an appropriate characteristic length for the convection.

The maximum errors of the thermal model for the validation cases are presented in Table 3.8. The large errors for the PCB are due to the quick drop in temperature when the charging stops.

Validation case $V_2$ is interesting as it is similar to an endstop charger for a buss. Due to the large thermal mass of the main conductors in the ASSE the temperatures of the negative conductor and the PCB feeding rail are smoothed and the result is similar to the one obtained for continuous charging with 100 A. For the PCB the temperature swing is larger than for the PCB feeding rail and the negative conductor. This is because the heat is mostly generated on the PCB in the IGBTs, together with the PCB having a small thermal mass.

**Table 3.8:** Model accuracy for the validation cases.

| Case | Negative conductor [°C] | PCB Feeding rail [°C] | PCB [°C] |
|---|---|---|---|
| **V1** | 0.8 | 0.5 | 3.5 |
| **V2** | 0.7 | 0.7 | 4.2 |
| **V3** | 4.9 | 8.6 | 6.0 |
| **V3 ($L_{ch}$ = 10 cm)** | 1.5 | 3.1 | 6.7 |

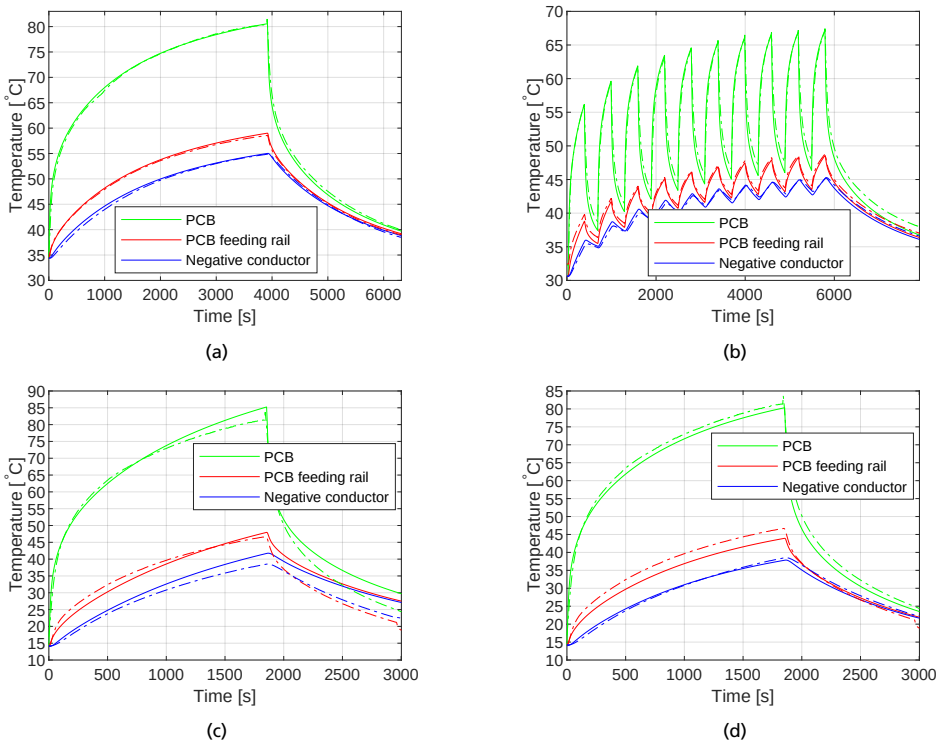


Figure 3.27: Dashed lines are measured temperatures and solid lines are from the thermal model. (a) is for a charging current of 202 A, (b) is for 202 A for 5 minutes and then no charging for the next 5 minutes, (c) is for 293 A and (d) is the same as (c) but the characteristic length of forced convection is reduced to 10 cm.

### 3.4.4 Sensitivity analysis

In order for a thermal model to be trusted it is important to know how the model responds to variations in the input parameters. A robust model with regards to the input parameters is easy to use even with uncertainty in the inputs. The sensitivity analysis in this section is based on case $V_1$. It should be noted that the sensitivity presented in this section is for the locations of the sensors. Closer to the PCB the model is likely more sensitive to variations in the inputs. One parameter is changed at a time from 0.4 p.u. to 3 p.u. where 1 p.u. corresponds to the value of the calibrated model. The following parameters are changed one at a time:

- Airgap thickness ($d_{Airgap}$)
- Convection coefficient ($h_{Convection}$)
- Electrical resistance of the PCB ($R_{PCB}$)

- Asphalt thickness ($d_{Asphalt}$)
- Thermal conductivity of the aluminum ($k_{Aluminum}$)
- Thermal conductivity of the soft insulation between the negative conductor and the PCB feeding rail ($k_{Insulation}$)
- Thermal conductivity of the asphalt ($k_{Asphalt}$)
- Thermal conductivity of the rubber inside the ASSE structure ($k_{Rubber}$)

Figure 3.28 presents the results for the negative conductor, the PCB feeding rail and the PCB. The temperature difference presented is the maximum difference to the 1 p.u. case. The PCB is the major source of the generated heat, therefore the temperature for the PCB is more affected by changing model parameters. With multiple inputs to the model, the total error can add up to a significant error even if the model is only slightly affected by individual changes in the inputs.

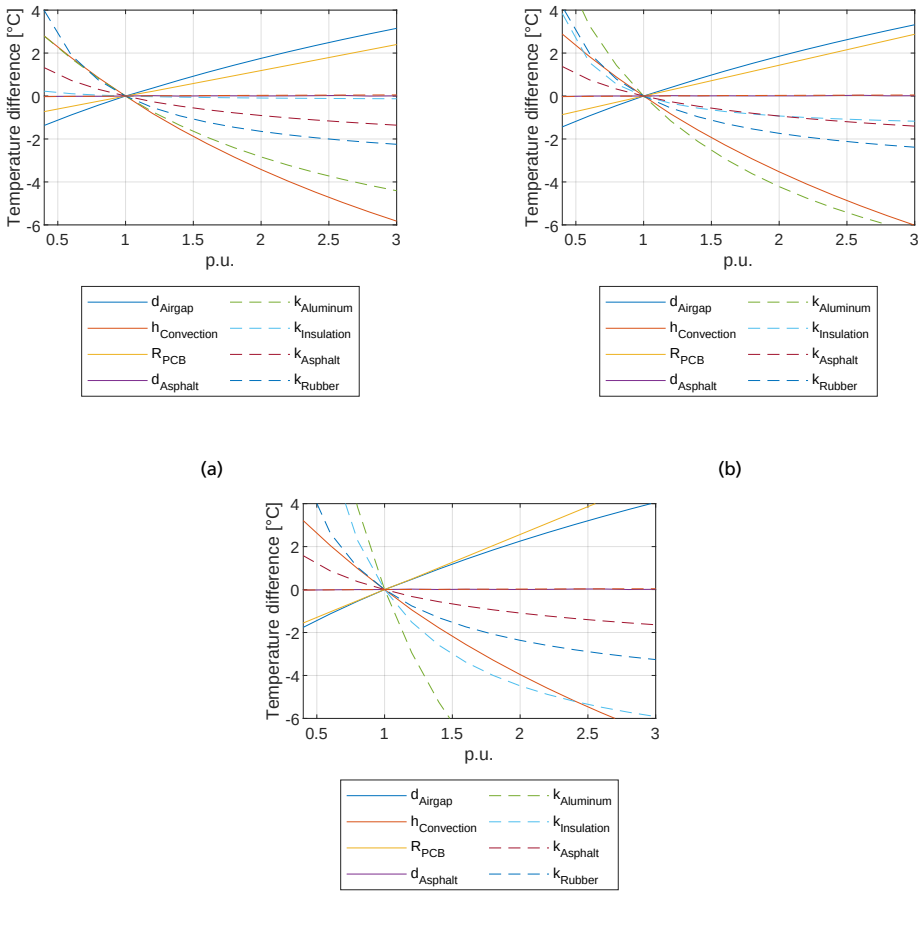


**Figure 3.28:** Shows how the temperature at different locations in the model are affected by changing input parameters. (a) shows the negative conductor, (b) the PCB feeding rail and (c) the PCB.

## 3.5 Chapter summary

In this chapter the heat sources affecting an ASSE are presented together with how heat is dissipated from the ASSE. These sources of heat are both external, e.g solar irradiance, and internal, e.g resistive losses in the main conductors.

Experimental tests are performed to obtain important information about the sources of heat and the cooling mechanisms that are hard to estimate by analytical equations. A rotating test rig is developed to be able to measure electric contact resistance for a sliding contact under different conditions. The test rig is based on a rotating steel track and a stationary current collector, with the steel track connected to a slip ring to allow measurements while the track is rotating. Another experiment is performed to measure the cooling effect caused by a passing vehicle on the ASSE. In order to do this an aluminum foil with a low thermal mass is heated by resistive losses from a known current. When a vehicle passes over the foil the temperature of the foil changes and a thermal model can be used to estimate the cooling effect.

The developed thermal model is a 3D FE model capable of simulating both dynamic and static charging with an ASSE. The model have been calibrated and validated with data from a real ASSE test track. This data include different charging powers and also different external conditions.

# Chapter 4: Lifetime modeling

Lifetime modeling is important to understand how aging of the main semiconductors switches is related to different load cases. By understanding the aging and being able to estimate the expected lifetime of a switch, both cost and performance can be improved. In this chapter existing lifetime models are compared to experimental tests and recalibrated to fit this experimental data.

## 4.1 Mechanisms of failure

There are many different mechanisms of failure affecting IGBTs. In this thesis only power cycling is investigated and therefore only failure mechanisms affected by power cycling are considered. A power cycle is a cycle where the IGBT is heated internally by losses in the component itself. This creates a temperature difference between the chip and the layers further away from the chip. Figure 4.1a illustrates the internal structure of a discrete IGBT without an insulating ceramic substrate and Fig. 4.1b shows the inside of a discrete IGBT of type TO-247. These layers are made of different materials with different coefficients of thermal expansion, which results in mechanical stresses within the component when there is a temperature gradient. The stress causes fatigue and can eventually cause e.g. bond wire liftoff or solder fatigue.

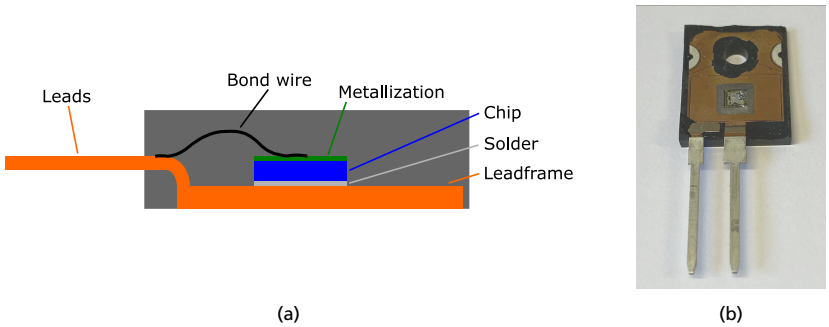


**Figure 4.1:** (a) shows an illustration of the inside of a discrete IGBT and (b) shows the inside of a discrete IGBT.

Bond wire lift off is the result of the chip and the bond wires having mismatched thermal expansion coefficients. This cause sheer stress in the junction between the chip and the bond wires and with repeated cycles the junction between the bond wire and the chip can break. Flexing and sheer stress is the most common reason for a bond wire to fail [77]. A failed bond wire causes a redistribution of the current to the remaining bond wires and within the device, accelerating the aging [78].

Solder fatigue is when the solder interface is degrading, causing a rise in the thermal resistance. An increased thermal resistance results in larger thermal cycles, which in turn accelerate the aging. A higher temperature also increase the forward voltage drop, increasing the cycle depth even further. These larger temperature cycles have a negative impact on bond wire lift-off and accelerates this failure phenomena even more [78].

During power cycling reconstruction of the chip metallization occurs when the temperature swing is large [52]. This metallization layer is usually an aluminum layer, which have a different coefficient of thermal expansion compared to the silicon in the chip it is attached to. The thermal coefficient of expansion for aluminum is 23.5 ppm/K and for silicon 2-4 ppm/K [52], this results in the chip is preventing the aluminum layer from expanding causing stresses. Reconstruction of the metallization increase the electric resistance in the metallization layer and the forward voltage drop is slightly increased [79].

When the IGBT ages from power cycling the voltage drop rises over the component, increasing the power losses for a fixed current. The increased power loss increases the magnitude of the temperature cycles of the component, which cause faster aging and can even cause the component to fail due to overheating if the current is not reduced.

For the ASSE there are also thermal cycles, a thermal cycle is when the IGBT is heated externally, which results in a more even temperature distribution within the IGBT. Thermal cycling is not investigated in this thesis.

## 4.2 Models to estimate lifetime

Commonly used lifetime models are developed for power modules and not discrete components, which are used in the ASSE. In this thesis the lifetime of the discrete IGBTs is calculated based on the lifetime models for power modules, modified with a compensation factor obtained from experimental tests on discrete components. In a future ASSE implementation, power modules could be an option to discrete IGBTs in order to reduce the complexity of having many parallel discrete IGBTs. The main issue with modules in this ASSE is the limited available internal space, which makes it very difficult to fit a power module.

The utilization of an ASSE, even at high traffic volumes, results in rather low duty cycles for the IGBTs compared to more common applications such as power converters. Since neither the lifetime models nor the tests performed to compute the experimental compensation factor are developed for these operation conditions, the results must be extrapolated, adding uncertainty as the models and compensation factor are not validated for the range they are used in.

### LESIT

LESIT is a project from the 1990s, which tested power modules with a standard package with $Al_2O_3$ as ceramic layer. A number of power cycles are recorded for different cycling depths at different average chip temperatures. The result from this project is (4.30) with the parameters $K_{LESIT} = 302500^{-\alpha}K$, $\alpha_{LESIT} = -5.039$, $E_a = 9.89 * 10^{-20}$ and $k_b$ Boltzmann constant [52].

$$N_f = K_{LESIT}\,\Delta T_j{}^{\alpha_{LESIT}}\, e^{\left(\frac{E_a}{k_b T_m}\right)} \tag{4.30}$$

By looking at (4.30) it can be seen that the only parameters that can be affected without modifying the component is $\Delta T_j$ and $T_m$, where $T_m$ is the average temperature during a power cycle. $T_m$ is calculated in (4.31), Fig. 4.2 shows how the $T_{low}$, the lowest temperature during a power cycle, as well as the temperature swing, $\Delta T_j$, of the chip affects number of cycles according to the LESIT model.

$$T_m = T_{low} + \frac{\Delta T_j}{2} \tag{4.31}$$

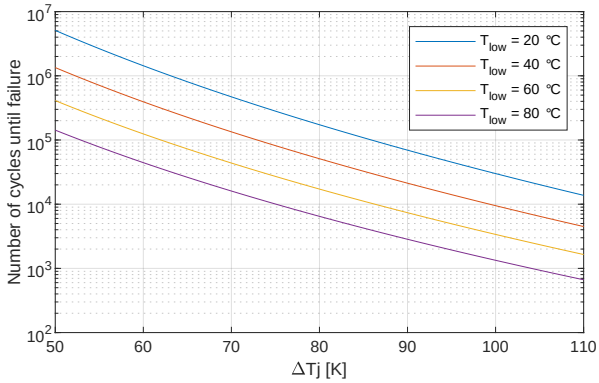


**Figure 4.2:** Expected lifetime according to the LESIT model for different $\Delta T_j$ and $T_{low}$

## CIPS

The CIPS model is derived from a large number of power cycling tests with IGBT modules. Several parameters affecting lifetime of an IGBT module are identified and resulting in (4.32), where $\beta_1 = -4.416$, $\beta_2 = 1285$, $\beta_3 = -0.463$, $\beta_4 = -0.716$, $\beta_5 = -0.761$ and $\beta_6 = -0.5$. $t_{on}$ refers to the on time of the IGBT which is when it conducts, $I_{bondwire}$ is the current per bond wire, $V_{rating}$ is the voltage rating of the chip divided by 100 and $D_{bondwire}$ is the diameter of the bond wires in $\mu$m [80]. $K_{CIPS}$ is a constant with the value $2.03 * 10^{14}$ for standard IGBT modules according to [81]. Advanced IGBT modules have either improved die attach or bond wire parameters or even both of these and the $K_{CIPS}$ for these kind of modules is $9.30 * 10^{14}$ [81]. The discrete devices are assumed to be most similar to standard IGBT modules and a $K_{CIPS}$ of $2.03 * 10^{14}$ is used.

$$N_f = K_{CIPS}\,\Delta T_j{}^{\beta_1}\, e^{\left(\frac{\beta_2}{T_{low}+273}\right)}\, t_{on}{}^{\beta_3}\, I_{bondwire}{}^{\beta_4}\, V_{rating}{}^{\beta_5}\, D_{bondwire}{}^{\beta_6} \tag{4.32}$$

Figure 4.3 shows the expected number of cycles until failure according to the CIPS model with $t_{on} = 0.1$, $I_{bondwire} = 10$, $V_{rating} = 12$ and $D_{bondwire} = 400$. Out of these parameters $V_{rating}$ and $D_{bondwire}$ are defined by the IGBT module and can not be changed by the application. The other parameters are interrelated, which makes it hard to make an accurate figure, e.g. in order to increase $\Delta T_j$ either $t_{on}$ or $I_{bondwire}$ must be increased.

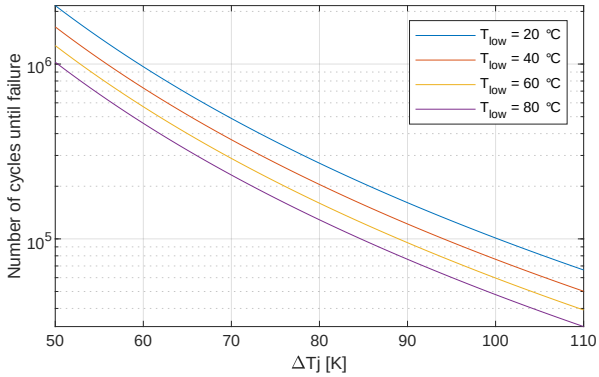


**Figure 4.3:** Expected lifetime according to the CIPS model for different $\Delta T_j$ and $T_{low}$

## 4.3 Compensation factor for discrete IGBTs

The lifetime models are developed for power modules and not discrete IGBTs, making a compensation factor necessary in order for the lifetime estimations to be accurate. The compensation factor is acquired by experimental tests of discrete IGBTs with input parameters from the datasheet of the component. The idea of the compensation factor is to be able to use datasheet values together with the compensation factor to estimate the lifetime of a discrete IGBT. The parameters given in the datasheet, such as thermal impedance may change as the component is aging and this change should be taken care of by the compensation factor.

For the tests the amplitude of the pulsed current is kept constant in order to resemble the operation of an ASSE. A constant amplitude of the current results in a changing temperature cycling depth, due to an increase of the on state voltage as the IGBT is aging. For this thesis only one type of IGBT (RGTH40TS65) is investigated for three different current levels. More current levels as well as different IGBTs are needed in order to further validate the compensation factor or create a new lifetime model for discrete IGBTs.

### 4.3.1 Experimental setup

The main function of the experimental setup is to perform power cycling of IGBTs until they fail and to measure relevant parameters throughout the experiment. The setup is based on a linear current supply, controlled by an analog controller. Figure 4.4a shows a schematic drawing of the experimental setup. The voltage supply is capable of delivering up to 300 A and 5 V. A MOSFET is controlled in the linear region in order to control the current and set it to the desired current level without current ripple. This control is fully analog and

compares the reference current to the actual current and changes the gate signal accordingly. Two other MOSFETs are used as switches to direct the current either to DUT1 or DUT2. Whenever switching between the DUTs the current is reduced to zero before the switching occurs in order to reduce any transients. The current is increased again after 15 ms. For each power cycle current (I), on state voltage (V1, V2) and heatsink temperatures are saved for post processing after a completed test. The heatsink temperatures are measured about 5 mm away from the DUTs. Each DUT is attached to its own heatsink which is about 200x200 mm with a fan attached to the middle of it to provide extra cooling, see Fig. 4.4b.

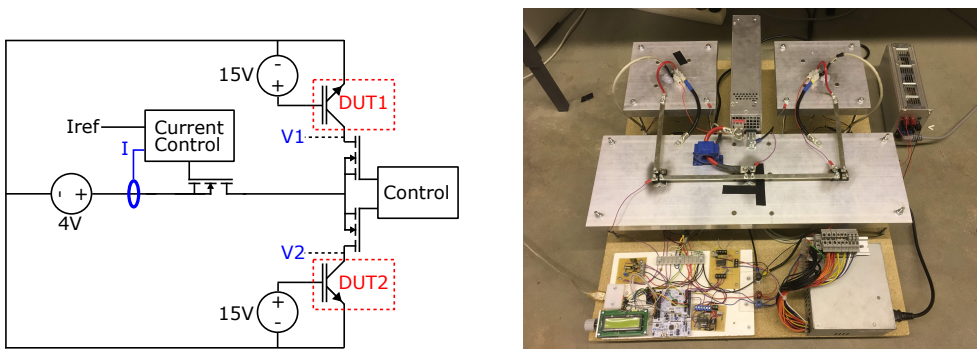


**Figure 4.4:** (a) shows a schematic of the experimental setup and (b) shows the experimental setup.

Parameters from the data sheet are used to analytically calculate the IGBT junction temperature from a known heatsink temperature. In the data sheet of the IGBTs the thermal impedance, $Z_{thjc}$, is given for different pulse lengths. $R_{thch}$ is not given in the data sheet as it depends on the thermal interface material (TIM) between heatsink and case. The TIM used for the experiments is the Wacker P12 [82] and the assumed $R_{thch}$ is 0.3 K/W, this corresponds to a TIM thickness of around 50 $\mu$m when the full copper area is used for heat transfer. With these numbers it is possible to estimate the junction temperature for a cycle with (4.33). When calculating the case temperature an average temperature over the area connected to the heatsink is calculated. Chip size, number of bond wires and so on affects the temperature distribution on the case surface and may also affect the expected lifetime.

$$T_j = P\left(Z_{thjc} + R_{thch}\right) + T_{heatsink} \tag{4.33}$$

### 4.3.2 Experimental results

In total 16 IGBTs for each of four different current levels are cycled until failure, resulting in a total of 64 individual IGBTs. Figure 4.5 shows the number of cycles until failure for

the individual IGBTs. The considered end of life for the IGBTs is defined as an increase of the on state voltage by 20 % from the level reached at 10000 cycles. It takes a few thousand cycles before the heatsink is at a stable temperature, which affects the on state voltage.

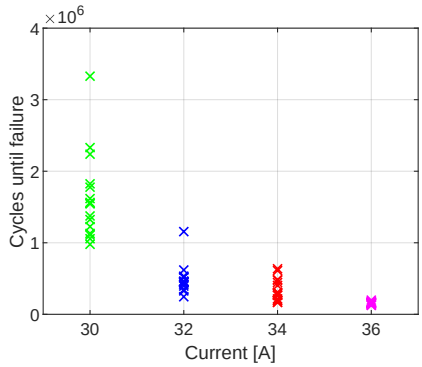


**Figure 4.5:** Shows the number of cycles until failure for different currents.

When the IGBT ages the on state voltage increases. The on-state voltage for 16 IGBTs can be seen in Fig. 4.6 and they all share the same behavior when aging. These results do not give a definite answer to what the reason is for the behavior of the on-state voltage. One factor that could increase the on-state voltage is reconstruction of the metallization. Reconstruction of the metallization increases the resistivity of the layer, resulting in a greater on-state voltage [79]. Another factor can be bond wire liftoff, which could also explain the jumps in the voltage if the bond wire is loose and have a glitching contact to the chip.

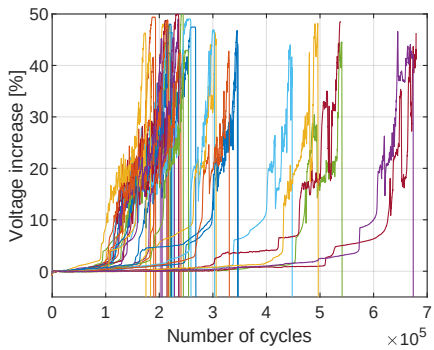


**Figure 4.6:** The on-state voltage changes when an IGBT is subjected to power cycles. The change in on-state voltage for 16 individual IGBTs can be seen in the figure.

Figure 4.7 shows how long the cycled IGBTs last compared to the CIPS and LESIT models. The height of the bars represent a variation of thermal resistance between case and heatsink between 0.2 - 0.4 K/W. A lower thermal resistance makes the model predict a

longer lifetime. This results in a lower lifetime compensation factor. The average lifetime compensation factors, which are represented as straight lines in the figure, are presented in Table 4.9. A lifetime compensation factor of e.g. 0.6 is equal to a lifetime of 60 % compared to what the model predicts.

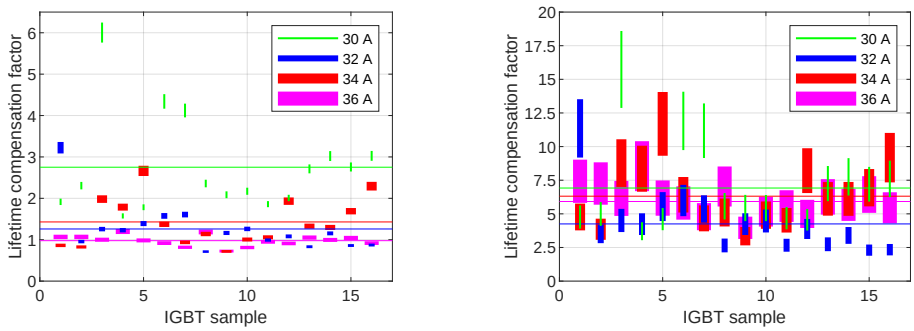


**Figure 4.7:** (a) shows the lifetime compensation factor with regards to the CIPS model and (b) with regards to the LESIT model. The straight lines represent the average value.

**Table 4.9:** Shows the average lifetime compensation factors for the LESIT and CIPS models at different current levels.

| | 30 A | 32 A | 34 A | 36 A |
|---|---|---|---|---|
| **CIPS** | 2.75 | 1.26 | 1.43 | 0.98 |
| **LESIT** | 6.92 | 4.25 | 6.31 | 5.92 |

It is clear from the table that there is a spread in the average compensation factor at the different current levels. Each individual sample is different and to obtain a statistically reliable result more IGBTs must be tested. Lower temperature swings are also needed to be investigated to allow accurate compensation factors even at small temperature swings. Figure 4.8 shows the lifetime compensation factors for the LESIT and CIPS models with a $R_{thch}$ of 0.3 K/W, and it seems like the compensation factors increase with lower current. The exception is the compensation factor for 32 A, which seems to be lower than for both 30 A and 34 A. To obtain a case that is likely the worst case the lowest compensation factor, from Fig. 4.7, for each model is used, 0.71 for the CIPS model and 2.30 for the LESIT model. A curve can be fitted to the data in Fig. 4.8 to obtain a specific compensation factor for a specific current level. Due to the limited amount of data this is not used in the thesis. The lowest compensation factors for each current level is presented in Table 4.10. Another reason to use the minimum compensation factor is because there are multiple IGBTs connected in parallel. Exactly how these IGBTs share the current, which in turn affect the lifetime is not known. When one IGBT ages the on state voltage rises, forcing more current to the other IGBTs and making all of the IGBTs age together but at an

increased rate. The individual IGBTs also have different on state voltages when brand new, and this can further cause an uneven current distribution between the IGBTs.

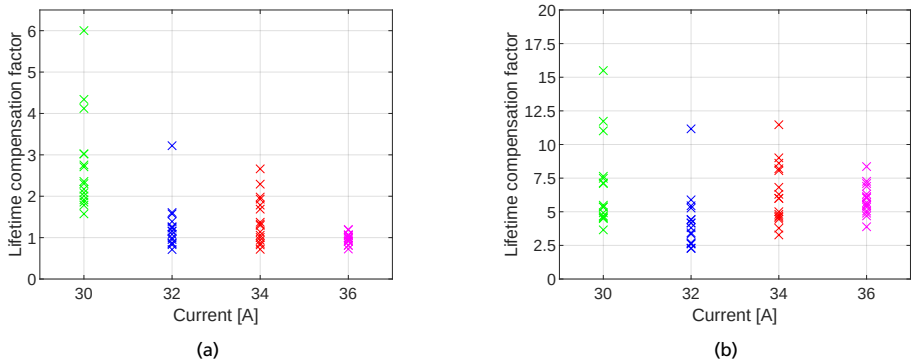


Figure 4.8: Shows the lifetime compensation factor against current where (a) is for the CIPS model and (b) for the LESIT model.

Table 4.10: Shows the minimum lifetime compensation factors for the LESIT and CIPS models at different current levels.

| | 30 A | 32 A | 34 A | 36 A |
|---|---|---|---|---|
| **CIPS** | 1.57 | 0.71 | 0.72 | 0.72 |
| **LESIT** | 3.65 | 2.30 | 3.28 | 3.88 |

It should be noted that, due to time constrains (one million cycles take almost 3 days), only a small amount of IGBTs have been tested and only one type if IGBT. More experimental tests are needed to find a compensation factor for a greater range of currents and for different IGBT models. More samples are also needed to reduce the statistical uncertainties as there is a significant spread between different IGBTs even when they are brand new.

## 4.4 Lifetime model linked to the thermal model

The purpose of the lifetime models is to be able to predict the lifetime of the IGBTs used in the ASSE. Both the CIPS and LESIT lifetime models are based on temperature swings of the IGBT junction and the temperature before or after a cycle. The junction temperature of IGBTs have fast thermal dynamics, which require small timesteps to capture accurately in the thermal model. To avoid small timesteps the IGBTs are not included in the thermal model and only the heatsink of the IGBTs is modeled. This results in that only the slow thermal dynamics of the IGBTs are simulated. The temperature increase over the TIM and IGBT is superimposed to the heatsink temperature to obtain the junction temperature.

Cars and trucks charge with different powers and therefore the resulting $T_j$ depends on

which type of vehicle is charging. For every vehicle passage $T_j$ will do one cycle with its start and end close to the heatsink temperature. Figure 4.9 shows an example of what $T_j$ can look like on a high traffic road (see the time scale in the x axis), when the increase in chip temperature is added to the heatsink temperature according to (4.33). If a full day or year is simulated there are large cycles due to daily variations as well as seasonal variations in the temperature and traffic profile. These variations are not considered as they are mostly the result of thermal cycling and not power cycling.

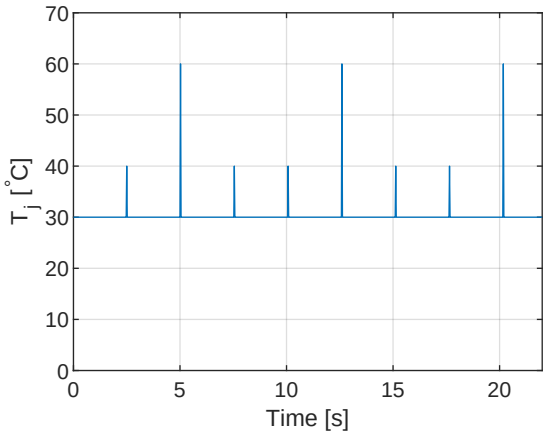


**Figure 4.9:** Shows an example of how the IGBT junction temperature can look like when the junction swing is added to the case temperature.

# Chapter 5: Analysis of Static charging

Static charging is investigated and evaluated based on the requirements presented in Section 2.2. The temperature of exposed metal can not exceed 80 °C and the expected lifetime must be at least 20 years. The expected lifetime of the IGBTs is often over hundreds or thousands of years according to the lifetime models. At such high numbers the expected lifetime is unrealistic but is still presented in the results. The interior temperature of the ASSE is never allowed to exceed 130 °C, according to the thermal requirements in Section 2.2.3. One charging strategy that can increase the transferred energy for a charging event, is to use a charging power that increases the surface temperature over the temperature limit of 80 °C. It is then necessary to allow the surface to cool down before exposing the used contact segment.

## 5.1 Reference cases

Three different charging modes are investigated: fast charging, medium fast charging, and slow charging, see Table 5.11. These three modes are supposed to cover cases ranging from e.g. fast charging of a bus at a bus stop to a charging event lasting for several hours. The time between two vehicles using the charger is called cycle time and is different for the three modes. Four different charging powers are investigated for each mode.

Table 5.11: Charging parameters.

| Parameter | Fast | Medium | Slow |
|---|---|---|---|
| **Charging time** | 5 minutes | 45 minutes | 8 hours |
| **Cycle time** | 10 minutes | 60 minutes | 24 hours |
| **Charging power** [kW] | 50, 100, 150, 200 | 75, 100, 125, 150 | 75, 100, 125, 150 |
| **Number of IGBTs** | 15 | 15 | 15 |
| **Contact resistance** [mΩ] | 2 | 2 | 2 |
| **Cycles per day** | 108 | 18 | 1 |
| **Contact seg. thermal cond.** [W/mK] | 44.5 | 44.5 | 44.5 |
| **Additional power** [W] | 0 | 0 | 0 |

The simulations are initialized with the time of the day being 06:00 and with the entire structure at ambient temperature. Charging events with the same charging and cycle time are assumed from 06:00 to 14:00. The first cycle after 14:00 is considered to be the representative cycle. The exception to this is that for slow charging there is only one cycle and it starts at 06:00. Slow charging during the day gives a tougher case than charging at night An example of raw data from a simulation with different duty cycles are presented in Fig. 5.1. Based on this data important key values are extracted and presented in the rest of this chapter. Cool down time, which is the time a vehicle stays after a charging event ends is only present for the last charging cycle. In previous cycles the vehicles are assumed to leave the charging spot directly after the charging event.

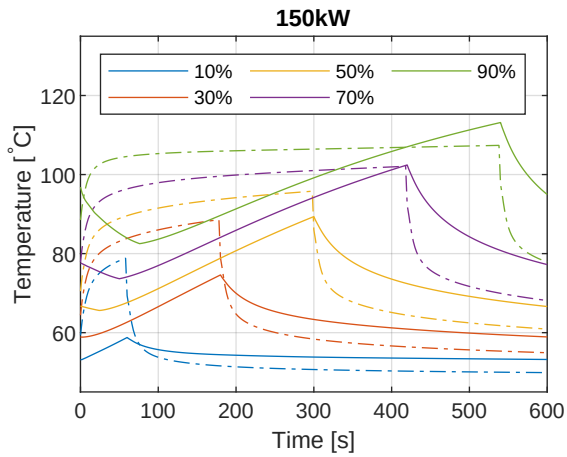


Figure 5.1: The temperature of the surface (solid lines) and the IGBT junction (dashed lines).

### 5.1.1 Fast charging

In the fast charging mode, charging stops shorter than 10 minutes are considered. An example of a charging stop like this is charging of a bus at an endstop. To reduce the number of simulations the cycle time is fixed to 10 minutes and results in e.g. one vehicle charges for 4 minutes and the next vehicle arrives 6 minutes after the first vehicle stops charging. With this kind of charging a relatively small amount of energy is transferred during each charging event. The idea of increasing the transferred energy by using a higher charging power and letting the surface cool down before exposing the warm contact segment is difficult due to the nature of the charging event. In Section 5.2 it is shown that for a short charging event, a large fraction of the charging time is needed to allow the contact segment to cool down.

### 5.1.2 Medium fast charging

Medium fast charging comprises charging stops that last for that lasts for 30-60 minutes. An example of this can be a charging event during a lunch break. The time between charging events is assumed to be fixed at 60 minutes. During a medium fast charging stop the transferred energy is larger than for fast charging and should likely cover the energy need for several hours of driving. In this case there may be a benefit from using a higher charging power than the power resulting in an 80 °C surface temperature and then allowing a warm contact segment to cool down before exposing it.

### 5.1.3 Slow charging

Slow charging is considered to last several hours and only one cycle per day occurs. When charging for several hours the transferred energy can be in the MWh range. If slow charging is assumed to last at least for 4 hours and the battery is charged from 20 % to 100 % the C-rate is 0.2. A C-rate of 0.2 is low and can for most batteries be sustained over the full charging cycle. In the same way as for medium fast charging there can be a benefit in terms of transferred energy during a charging event if the charging power is increased and some time is spent on allowing the contact segment to cool down.

## 5.2 Charging time

Charging time is the time a vehicle is charging. Effectively charging time is directly related to the duty cycle of the utilization of the charger if the cycle time is fixed. For example a charging time of 5 minutes results in a duty cycle of 50 % if the cycle time is 10 minutes. By increasing the duty cycle the average heating power from losses increase while heating from the sun decreases. The resulting temperature of the ASSE can therefore be lower at higher duty cycles if the heating from the sun is higher than heating from electric losses. The amplitude of the temperature swing the IGBTs experience can also be lower at higher duty cycles. This increases the expected lifetime of the IGBTs. The extreme case is at a duty cycle of 100 % as there is no temperature swing, if the external conditions do not change.

For fast charging, medium fast charging and slow charging the temperature of any exposed metal surfaces are investigated. The maximum surface temperature is calculated directly after a charging event. This temperature is plotted as a function of charging time for 4 different charging powers. The same kind of plots are provided for expected lifetime and cool down time, where cool down time is the time it takes before the maximum surface temperature is below 80 °C.

### 5.2.1 Fast charging

At charging powers below 100 kW the surface temperature does not reach 80 °C even at 9 minutes charging time, see Fig. 5.2a. At power levels above 100 kW the surface temperature limits the possible charging time. With a charging power of 200 kW it is only possible to charge for about 1.5 minutes before exceeding 80 °C. At this power level the expected lifetime drops below 20 years with a charging time of 3 minutes or more, see Fig. 5.2b. If a vehicle stays on top of the ASSE (thus protecting the exposed hot surfaces) after it is done charging a higher charging power can be used while still keeping the safety requirement of maximum 80 °C on exposed metal parts. Figure 5.2c shows how long the vehicle must stay at the charging spot in order to physically cover the warm contact segment until the surface temperature of the surface metal parts is below 80 °C. This figure excludes data points where the IGBT junction temperature exceeds 175 °C or if the internal insulation exceeds 130 °C. By staying an extra 2 minutes it is possible to charge with almost 150 kW for 7 minutes. From an energy perspective the benefit of charging with a higher power may not be worth the added effort to make sure the contact segment is at a safe temperature before exposing it.

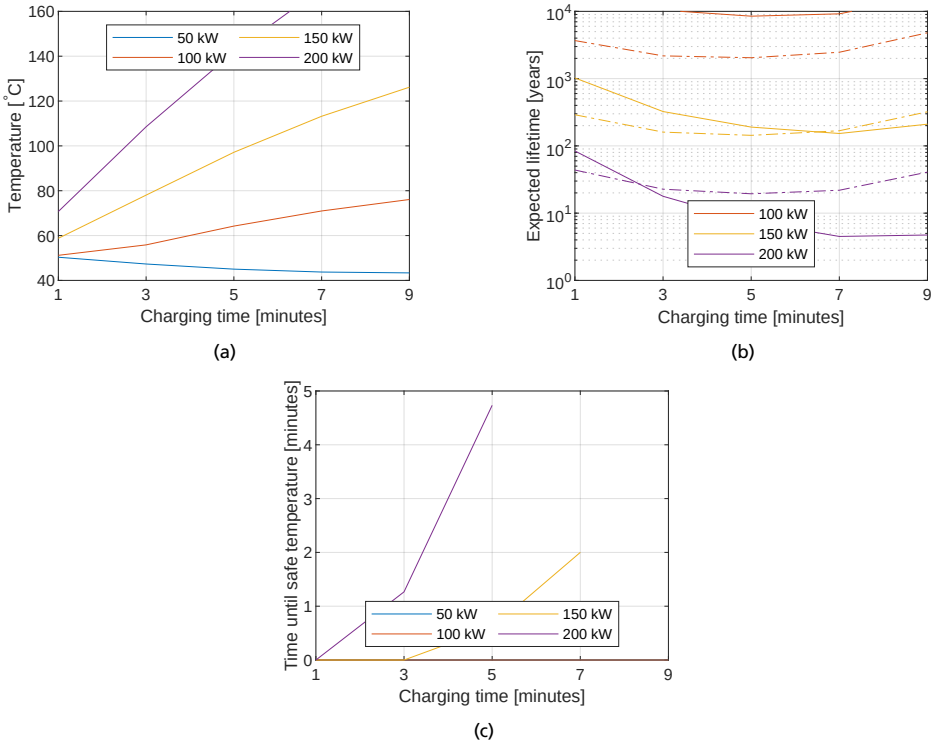


**Figure 5.2:** (a) shows the maximum surface temperature of any exposed metal directly after a charging event. (b) shows the expected lifetime of the IGBTs with dashed lines using the CIPS model and solid lines the LESIT model. (c) shows how long it takes before no surface metal is above 80 °C.

### 5.2.2 Medium fast charging

For medium fast charging a charging power of between 75-100 kW is considered safe, see Fig. 5.3a. At higher charging powers some time is needed to let the ASSE cool down before leaving the charging spot, see Fig. 5.3c. To increase the transferred energy on a charging event lasting e.g. 50 minutes it is better to charge with 125 kW for 47 minutes and let the ASSE cool down for 3 minutes than to charge with slightly less than 100 kW for 50 minutes. Even more energy can be transferred at 150 kW for 42 minutes with an 8 minutes cool down time. IGBT lifetime is not a limiting factor for any of the investigated charging powers or charging times. In Fig. 5.3b it can be seen that longer charging times result in increased expected lifetime as mentioned before, due to a more constant temperature profile (although at a higher average temperature). For medium fast charging the ASSE structure have a larger temperature swing than for fast charging. This temperature swing of the structure of the ASSE is related to the charging time and cycle time and is affecting the expected lifetime.

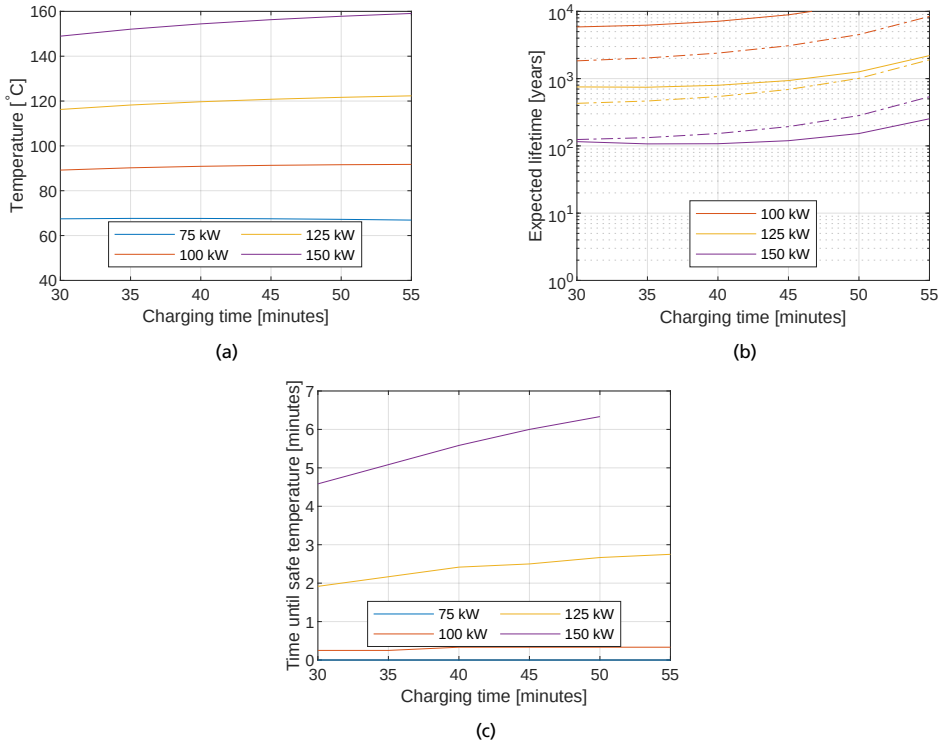


**Figure 5.3:** (a) shows the maximum surface temperature of any exposed metal directly after a charging event. (b) shows the expected lifetime of the IGBTs with dashed lines using the CIPS model and solid lines the LESIT model. (c) shows how long it takes before no surface metal is above 80 °C.

### 5.2.3 Slow charging

The result of slow charging is similar to medium fast charging. Due to the long charging times for both charging categories the temperature of the ASSE structure have started to stabilize, reducing the difference between the two categories. With slow charging starting its charging cycle at 06:00 a charging time of e.g. 4 hours result in a finished charging event at 10:00. This early finish time results in lower temperatures compared to a charging cycle that finish around 14:00 as the ambient temperature is lower. By letting the ASSE cool down after a charging event the transferred energy during a charging event can be increased. The increase in power is over 50 %, from 75-100 kW to over 150 kW, see Fig. 5.4. The longer the charging event is the more can be gained from properly planing the stop with a cool down time.

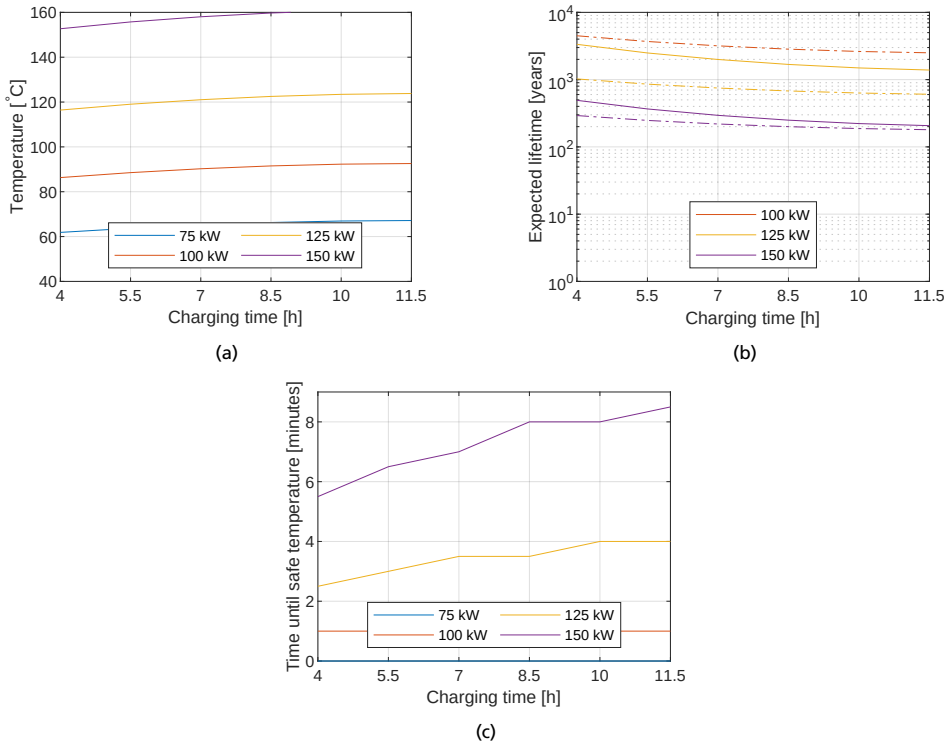


**Figure 5.4:** (a) shows the maximum surface temperature of any exposed metal directly after a charging event. (b) shows the expected lifetime of the IGBTs with dashed lines using the CIPS model and solid lines the LESIT model. (c) shows how long it takes before no surface metal is above 80 °C.

### 5.2.4 Summary

For a fixed cycle time the temperature increases with a longer charging time as the duty cycle is increased. This increase in temperature is also present in the temperature of the IGBT. However, with a higher duty cycle the junction temperature swing of the IGBT is reduced, thus increasing the lifetime of the IGBT.

## 5.3 Number of IGBTs

This section analyzes how the number of IGBTs in parallel affects their lifetime. The same PCB is assumed in all cases, but the number of IGBTs mounted on the PCB is changed. Fewer IGBTs results in a higher current per IGBT, which increases the total generated heat from the IGBTs as the forward voltage increase. This increased heat generation is divided among fewer physical IGBT devices, increasing the stresses on the IGBTs. Added stresses

have a negative impact on the expected lifetime of the IGBTs, which is the main concern when deciding on how many IGBTs in parallel are needed.

The surface temperature of the ASSE is only slightly affected by the number of IGBTs due to the long thermal path between the IGBTs and the surface. With the heat generated inside the IGBTs the heat have time to spread before reaching the surface.

Finding a suitable number of IGBTs for the application is important in order to reduce cost of the ASSE while maintaining good performance.

### 5.3.1 Fast charging

It is clear from Fig. 5.5 that a reduction of the number of parallel IGBTs greatly affects the expected lifetime of the IGBTs. At a charging power of 100 kW 6 IGBTs are needed while at 200 kW 18 IGBTs are needed to fulfill the requirement of 20 year lifetime. When the charging power is doubled the number of parallel IGBTs needed is more than doubled as the heat generated in the IGBTs is increased. To compensate for the increased ASSE temperature the current through each IGBT needs to be lower than in the case for a lower charging power. The small increase in surface temperature and cool down time when the number of IGBTs decrease is mainly because the heat is generated on a smaller area.

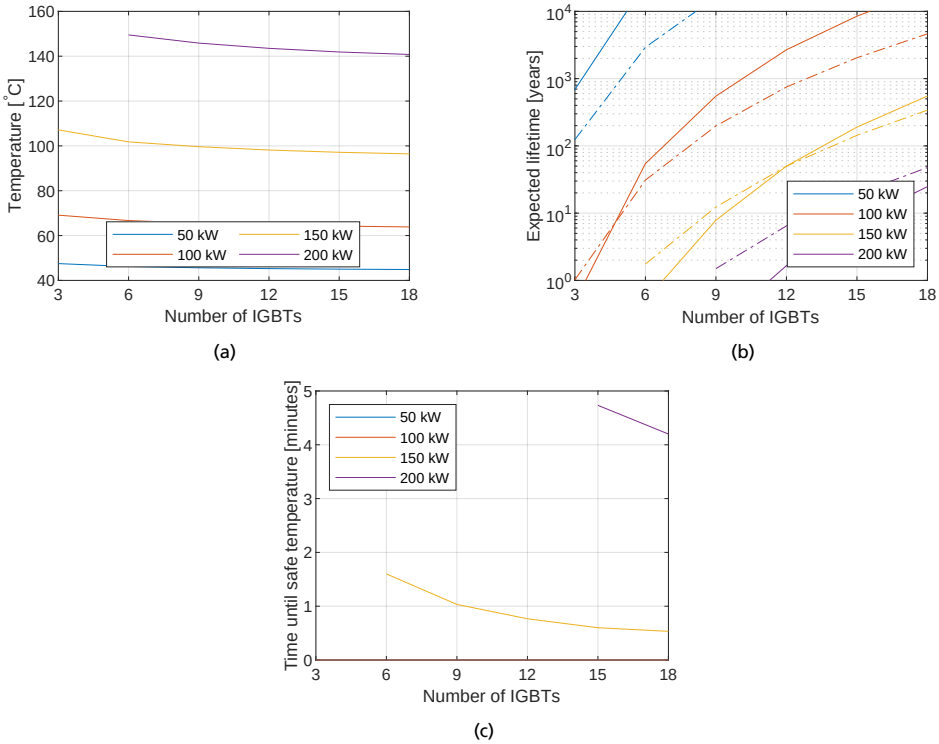


**Figure 5.5:** (a) shows the maximum surface temperature of any exposed metal directly after a charging event. (b) shows the expected lifetime of the IGBTs with dashed lines using the CIPS model and solid lines the LESIT model. (c) shows how long it takes before no surface metal is above 80 °C.

### 5.3.2 Medium fast charging

The number of IGBTs do mostly affect the expected lifetime of the IGBTs in the same way as for fast charging. With a charging power of 125 kW and with 9 IGBTs a cool down time of 3.5 minutes is needed. The expected lifetime of the IGBTs is well above 20 years for this case, see Fig. 5.6. For 150 kW 12 IGBTs and a cool down time of 7 minutes are needed.

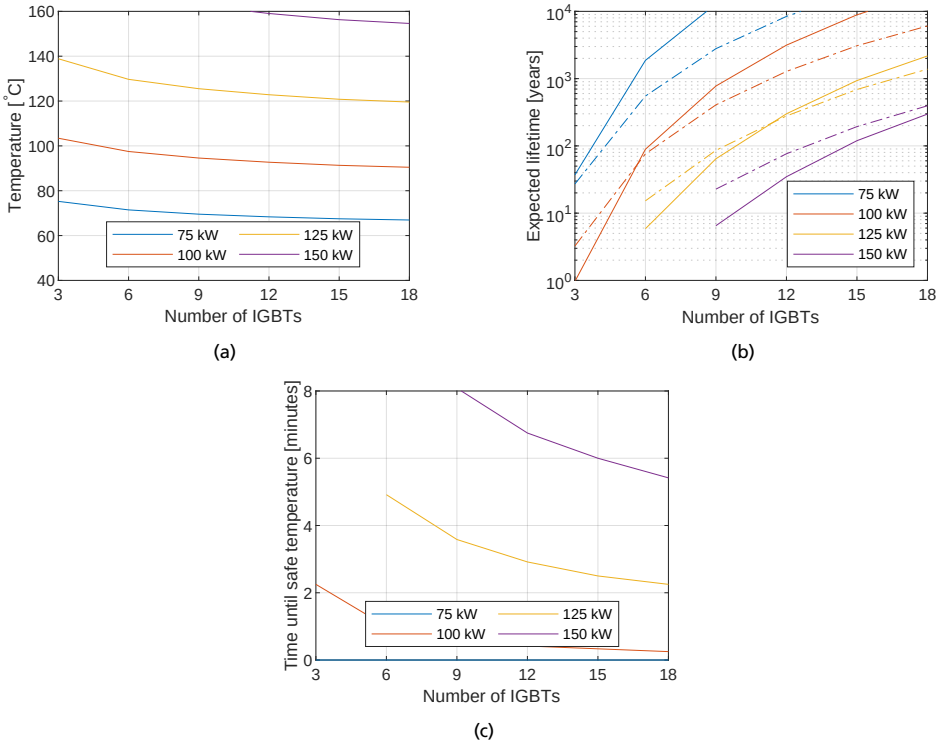


**Figure 5.6:** (a) shows the maximum surface temperature of any exposed metal directly after a charging event. (b) shows the expected lifetime of the IGBTs with dashed lines using the CIPS model and solid lines the LESIT model. (c) shows how long it takes before no surface metal is above 80 °C.

### 5.3.3 Slow charging

Slow charging behaves in the same way as medium fast charging. With only one charging cycle per day the expected lifetime of the IGBTs is longer for slow charging. At 125 kW it is possible to use 6 parallel IGBTs and for 150 kW at least 9 are needed, see Fig. 5.7.

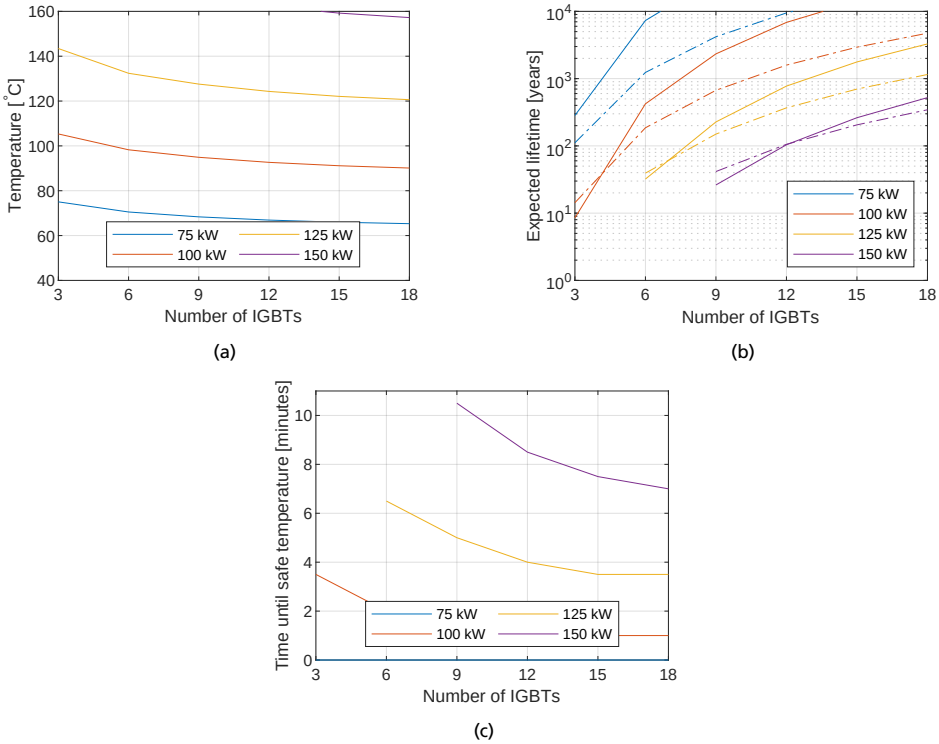


**Figure 5.7:** (a) shows the maximum surface temperature of any exposed metal directly after a charging event. (b) shows the expected lifetime of the IGBTs with dashed lines using the CIPS model and solid lines the LESIT model. (c) shows how long it takes before no surface metal is above 80 °C.

### 5.3.4 Summary

The number of parallel IGBTs is a design parameter that greatly affects the expected lifetime of the IGBTs. In order to determine how many IGBTs to install on a PCB, it is important to consider the application, and if the same hardware should be used for many different applications. Based on the simulations in Section 5.3 a good number seems to be in the range of 9-12 IGBTs to allow a charging power of 150 kW.

## 5.4 Contact resistance

The contact resistance is directly related to the heat generated in the contact point between the current collector on the vehicle side and the contact segment on the ASSE side. For a static charging application the heat generated in the contact point is localized to a small area. This can be an issue at a high contact resistance or at high charging powers as the

temperature in the contact point can become dangerous. By reducing the heat, the charging power is less limited by the temperature in the contact point.

### 5.4.1 Fast charging

The contact resistance is very important when it comes to static charging. With a contact resistance of 0.5 mΩ the surface temperature of the ASSE never exceeds 80 °C, even directly after a charging event of 200 kW, see Fig. 5.8. A low contact resistance increase the importance of the expected lifetime as this may be the limiting factor. This is the case when charging with 200 kW and with a contact resistance of 0.5 mΩ.

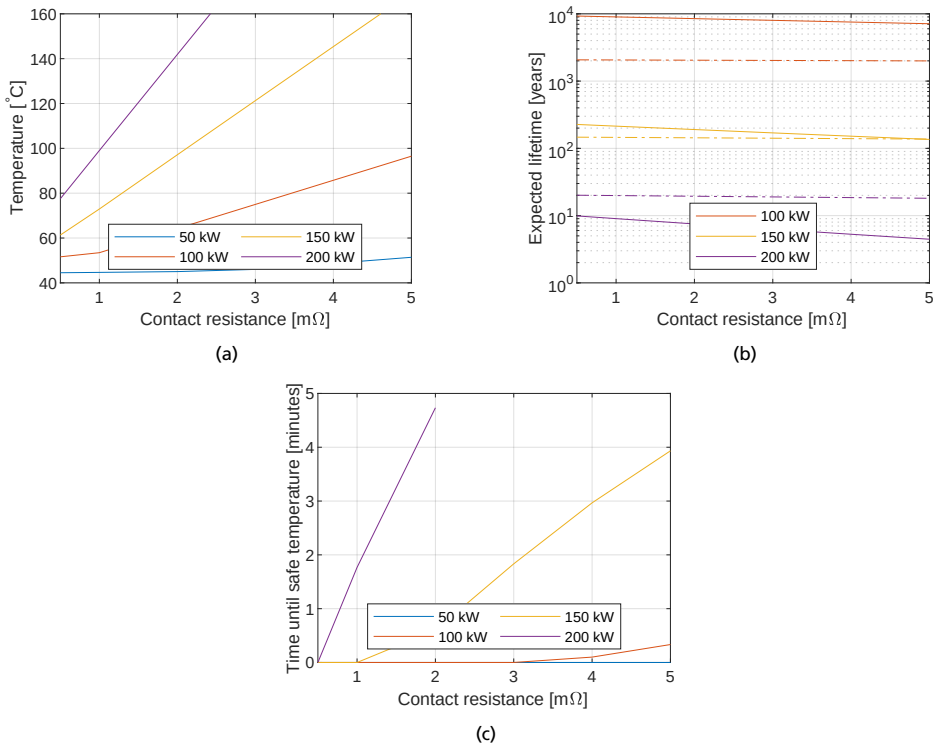


Figure 5.8: (a) shows the maximum surface temperature of any exposed metal directly after a charging event. (b) shows the expected lifetime of the IGBTs with dashed lines using the CIPS model and solid lines the LESIT model. (c) shows how long it takes before no surface metal is above 80 °C.

### 5.4.2 Medium fast charging

A reduction in contact resistance allows for a large increase in charging power. By allowing the used contact segment to cool down a charging power of up to 150 kW can be used with

a contact resistance of 5 mΩ. Even though the surface temperature is well above 130 °C for a charging power of 150 kW and a contact resistance of 5 mΩ the internal insulation does not exceed 130 °C.

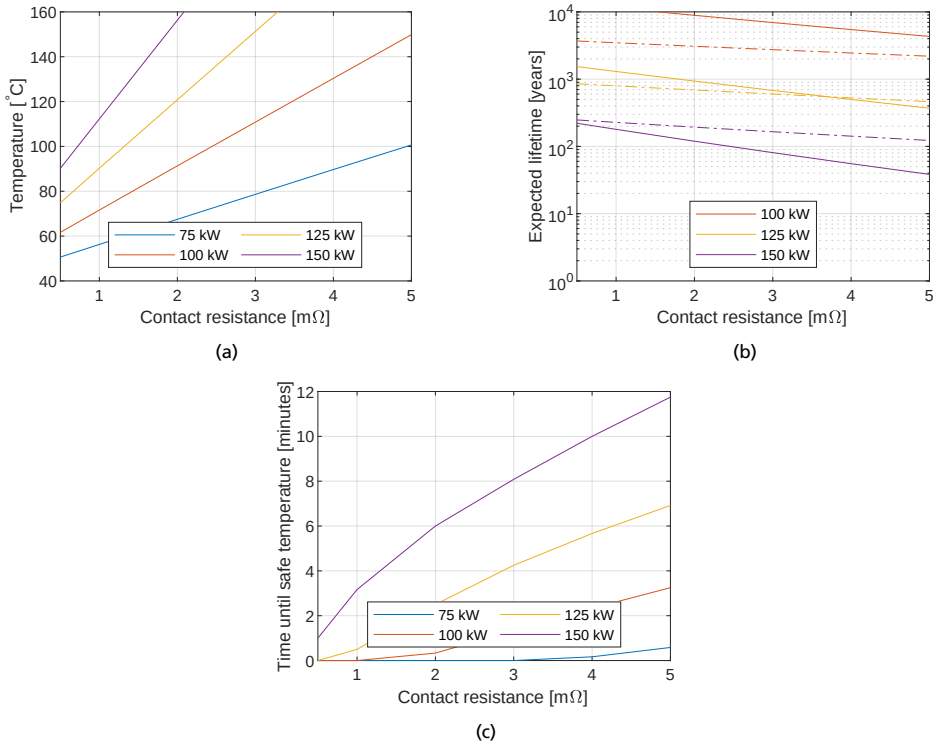


**Figure 5.9:** (a) shows the maximum surface temperature of any exposed metal directly after a charging event. (b) shows the expected lifetime of the IGBTs with dashed lines using the CIPS model and solid lines the LESIT model. (c) shows how long it takes before no surface metal is above 80 °C.

### 5.4.3 Slow charging

Yet again slow charging and medium fast charging exhibit similar behavior. By having a cool down time of 15 minutes the charging power can be up to 150 kW with a contact resistance of 5 mΩ. For this particular case 1.2 MWh of energy is transferred (in 8 hours) from the ASSE to the vehicle.

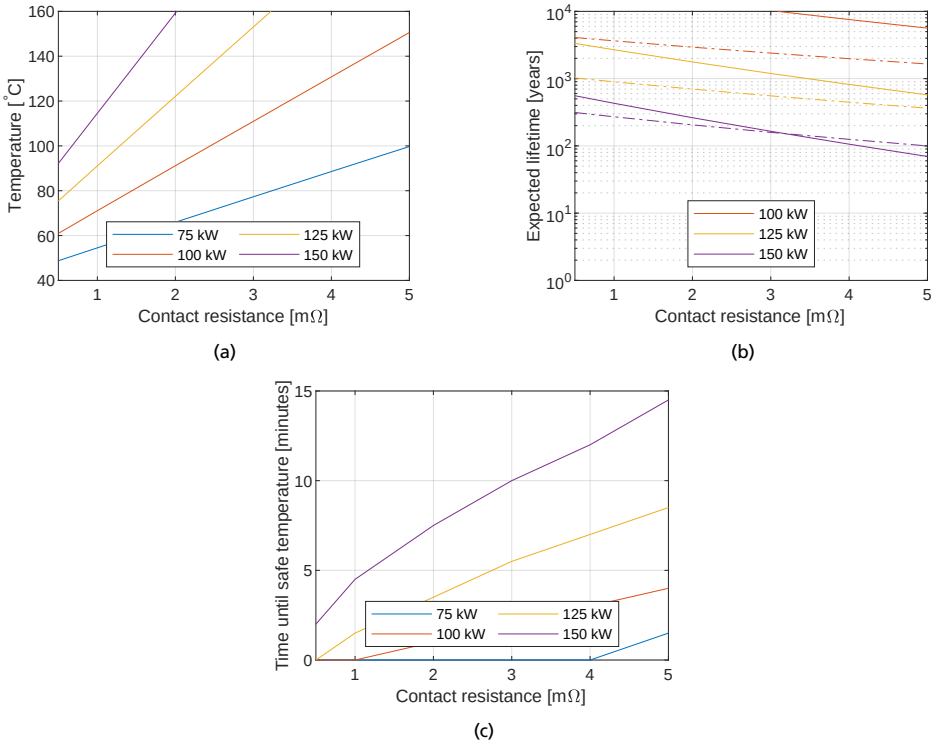


**Figure 5.10:** (a) shows the maximum surface temperature of any exposed metal directly after a charging event. (b) shows the expected lifetime of the IGBTs with dashed lines using the CIPS model and solid lines the LESIT model. (c) shows how long it takes before no surface metal is above 80 °C.

### 5.4.4 Summary

For a poor contact the resistance in the contact point is likely to limit the charging performance. Based on the simulations in Section 5.4 it is clear that the contact resistance is important and should be kept as low as possible. Already at a few mΩ the hot spot on the contact segment can reach more than 150 °C for charging powers over 100 kW.

## 5.5 Thermal conductivity of the contact segment

The thermal conductivity of the material in the contact segments is important for how heat spreads in the material. With a lot of heat being generated in the contact point it is important that the heat can spread longitudinally in the contact segment where it can deliver heat to the surrounding air, to prevent high localized temperatures. The material choice for the contact segment mainly affect the surface temperature and makes next to no impact on

the temperatures within the ASSE structure. Due to this the thermal conductivity of the contact segment is not important for the expected lifetime of the IGBTs but only for the surface temperature itself.

### 5.5.1 Fast charging

By choosing a material with a thermal conductivity of around 150 W/mK the cool down time can be around 1.5 minutes shorter at 150 kW compared to if stainless steel (10 W/mK) is used in the contact segment, see Fig. 5.11. With a material with similar thermal properties as aluminum a charging power of 150 kW can be used without any need for a cool down time, Fig. 5.11.

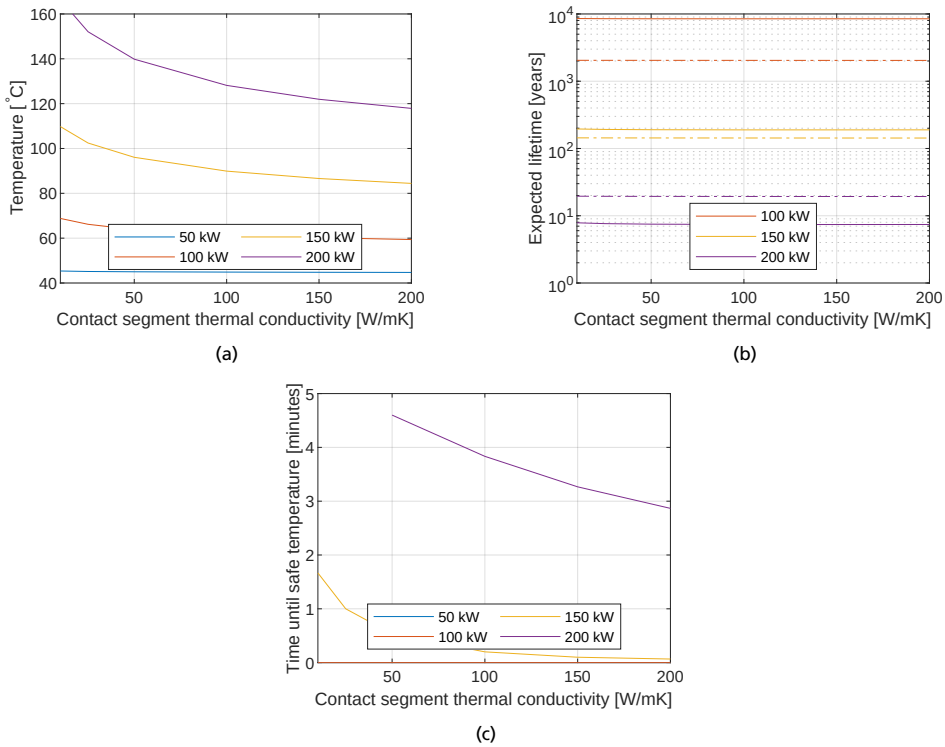


**Figure 5.11:** (a) shows the maximum surface temperature of any exposed metal directly after a charging event. (b) shows the expected lifetime of the IGBTs with dashed lines using the CIPS model and solid lines the LESIT model. (c) shows how long it takes before no surface metal is above 80 °C.

### 5.5.2 Medium fast charging

Medium fast charging can benefit from having a contact segment with high thermal conductivity. By switching from stainless steel to aluminum the charging power can be increased by roughly 25 kW with a cool down time of 4 minutes, see Fig. 5.12. At slightly less than 125 kW a cool down time of only a few seconds is needed with a contact segment made from aluminum but about 4 minutes is needed for stainless steel.

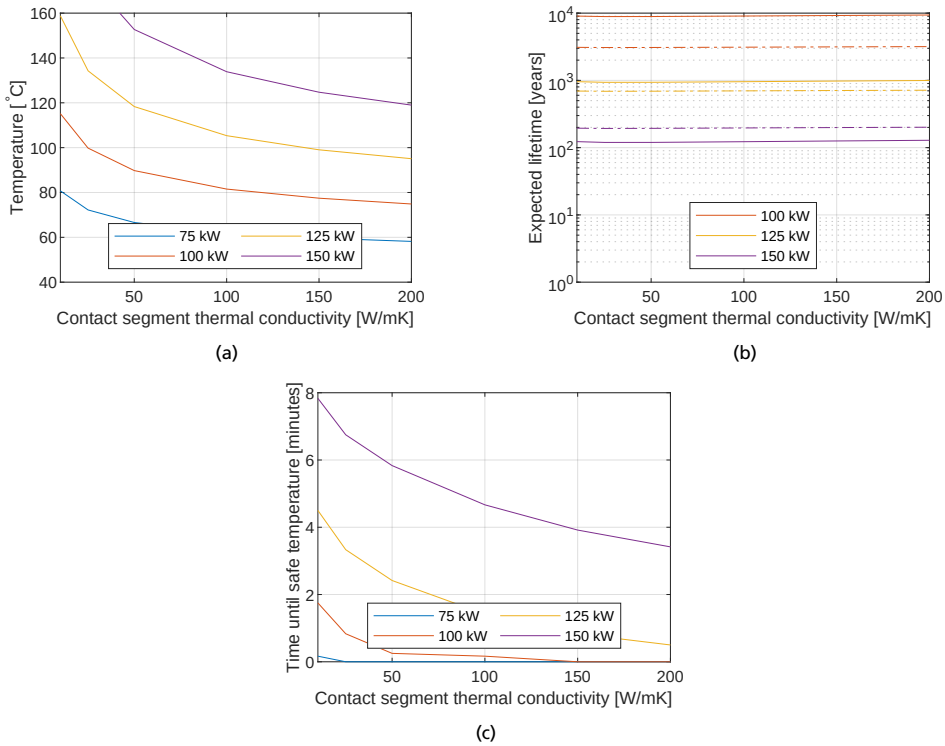


Figure 5.12: (a) shows the maximum surface temperature of any exposed metal directly after a charging event. (b) shows the expected lifetime of the IGBTs with dashed lines using the CIPS model and solid lines the LESIT model. (c) shows how long it takes before no surface metal is above 80 °C.

### 5.5.3 Slow charging

Slow charging and medium fast charging behaves in almost the same way. By increasing the thermal conductivity of the contact segment the power capabilities of the ASSE improves, see Fig. 5.13.

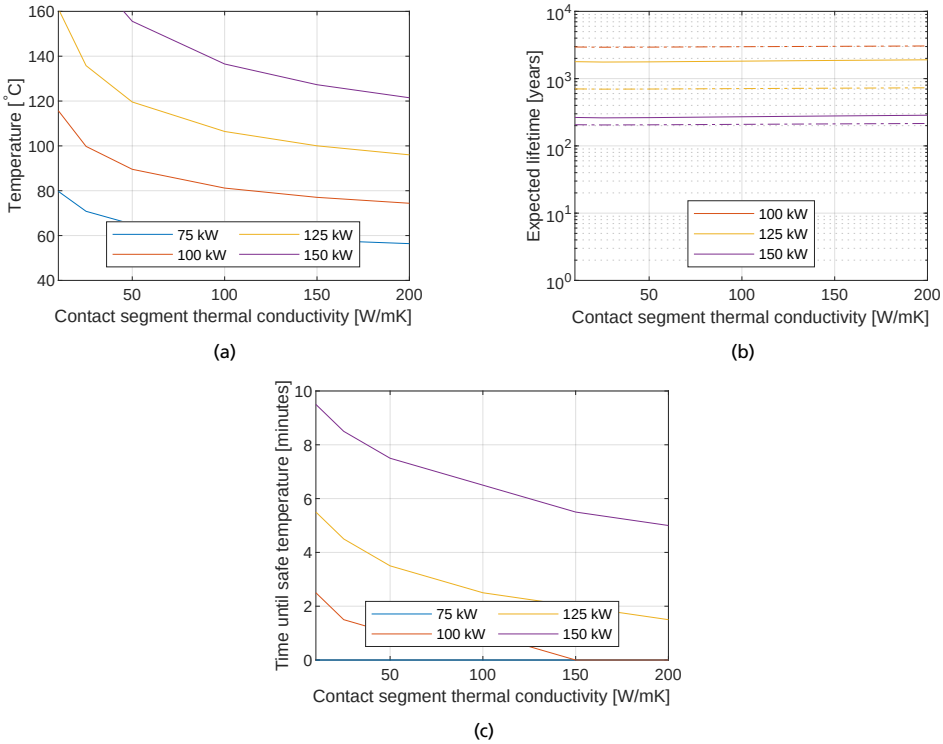


**Figure 5.13:** (a) shows the maximum surface temperature of any exposed metal directly after a charging event. (b) shows the expected lifetime of the IGBTs with dashed lines using the CIPS model and solid lines the LESIT model. (c) shows how long it takes before no surface metal is above 80 °C.

### 5.5.4 Summary

During static charging the losses in the contact point are localized to a small area. By making the contact segments out of a material with high thermal conductivity, the localized heat can spread within the material and reduce the temperature of the hot spot. It may be possible to combine two different materials, e.g. having a steel surface and a copper or aluminum bottom, to reduce hot spots while maintaining a high durability of the contact segment.

## 5.6 External cooling

External cooling is applied to the surface of the current collector and 30 cm of the energized contact segment with the current collector located in the center of the 30 cm section. Since the cooling action is mostly needed on the surface of the ASSE the cooling circuit is most practically placed on the vehicle. This can be achieved by e.g. allowing the air from the air

conditioning unit in the vehicle to flow over the surface of the ASSE. The thermal resistance from the inner parts of the ASSE to the ambient is less affected than the surface to ambient thermal resistance when the external cooling is applied. This makes external cooling the most effective at reducing the surface temperature but not the temperature of the inner parts of the ASSE.

In the simulations added external cooling is only applied to the last charging cycle. This is to reduce the number of simulations needed as otherwise a sweep over cool down time is also needed. The result of this is a worst case scenario where only the vehicle performing the charging cycle of interest is equipped with cooling equipment for the ASSE.

The added external cooling in this section is not correlated to a particular cooling solution. Experimental tests are needed to obtain information about the possible magnitude of the added cooling for different cooling solutions.

### 5.6.1 Fast charging

Added external cooling makes it possible to charge at higher power levels. 150 kW can be used without any cool down time with an added cooling of 40 $W/m^2K$, see Fig. 5.14 (it is worth remembering that with no external cooling, a cool down time of 30 seconds is needed). For 200 kW the lifetime of the IGBTs is the main limiting factor if a cool down time is allowed. If every charging cycle would experience the added external cooling the temperatures of the ASSE would be lower and the expected lifetime of the IGBTs longer.

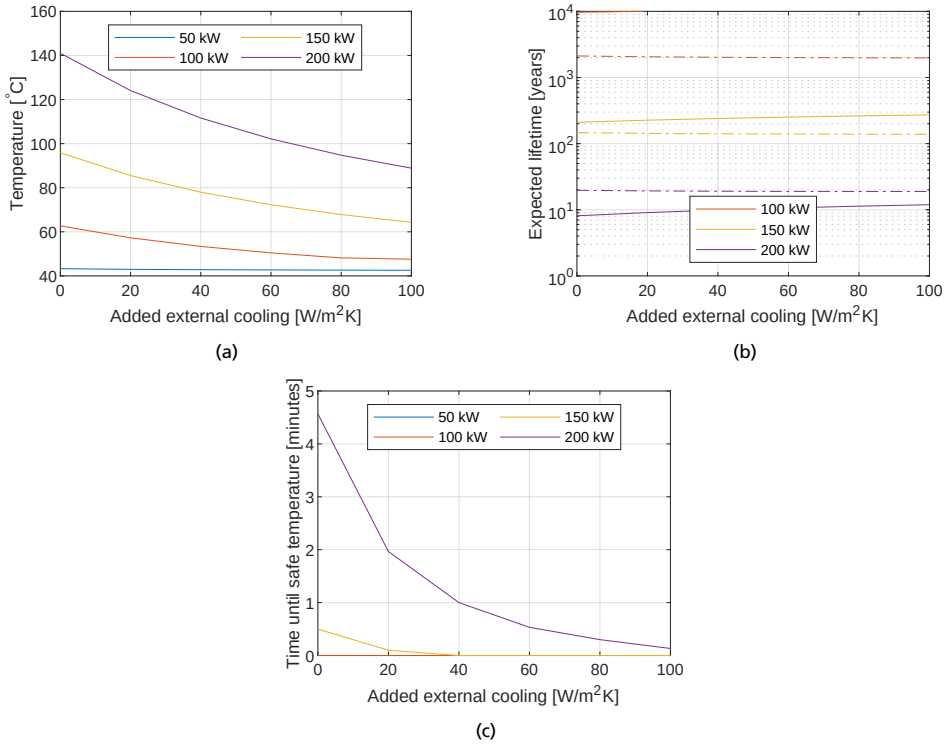


**Figure 5.14:** (a) shows the maximum surface temperature of any exposed metal directly after a charging event. (b) shows the expected lifetime of the IGBTs with dashed lines using the CIPS model and solid lines the LESIT model. (c) shows how long it takes before no surface metal is above 80 °C.

### 5.6.2 Medium fast charging

For medium fast charging the lifetime of the IGBTs is not a limiting factor as the expected lifetime is over 100 years for power levels up to 150 kW. By allowing a few minutes of cool down time after the charging ends about 150 kW can be used even for low level of added cooling, see Fig. 5.15. At 100 W/m$^2$K added external cooling it is possible to charge with 150 kW without a cool down time.

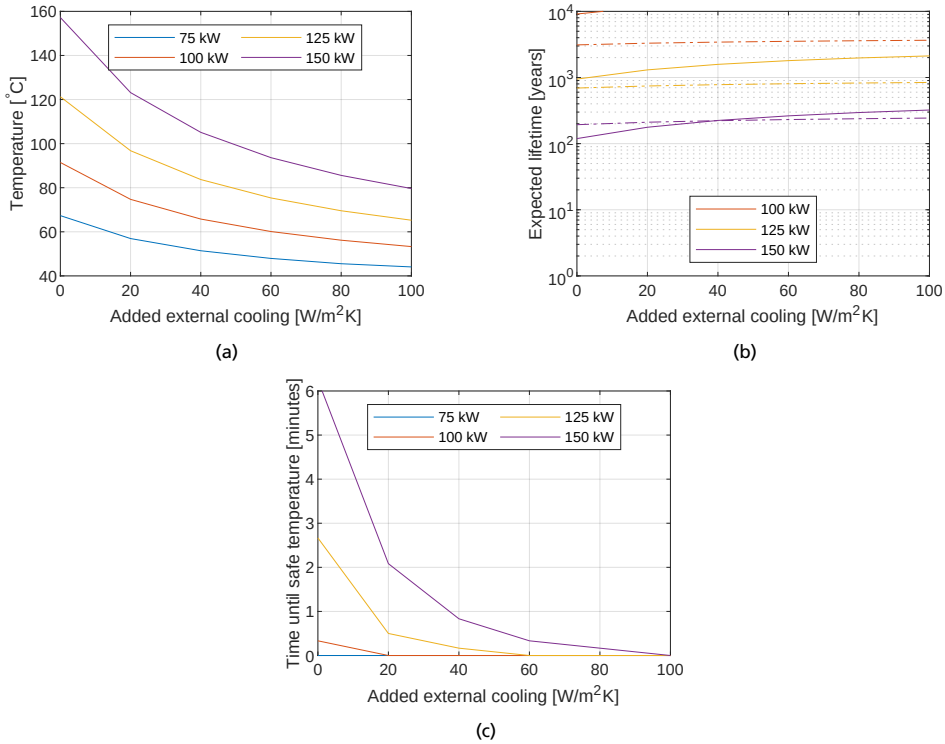


**Figure 5.15:** (a) shows the maximum surface temperature of any exposed metal directly after a charging event. (b) shows the expected lifetime of the IGBTs with dashed lines using the CIPS model and solid lines the LESIT model. (c) shows how long it takes before no surface metal is above 80 °C.

### 5.6.3 Slow charging

Added cooling increases the ASSE power capabilities. If no cool down time is allowed the charging power can be as high as 150 kW if the external cooling is 100 W/m$^2$K, see Fig. 5.16. By allowing a cool down time and applying 100 W/m$^2$K of external cooling the charging power can be well above 150 kW.

The benefit slow charging have from added external cooling depends on the importance of the cool down time. If a vehicle is charging for several hours it is likely that the driver can either reduce the charging time or extend the charging stop with some minutes to bring the surface temperature down to a safe level. If the charging stop can be properly planned the modifications on board the vehicle to allow external cooling is unnecessary.

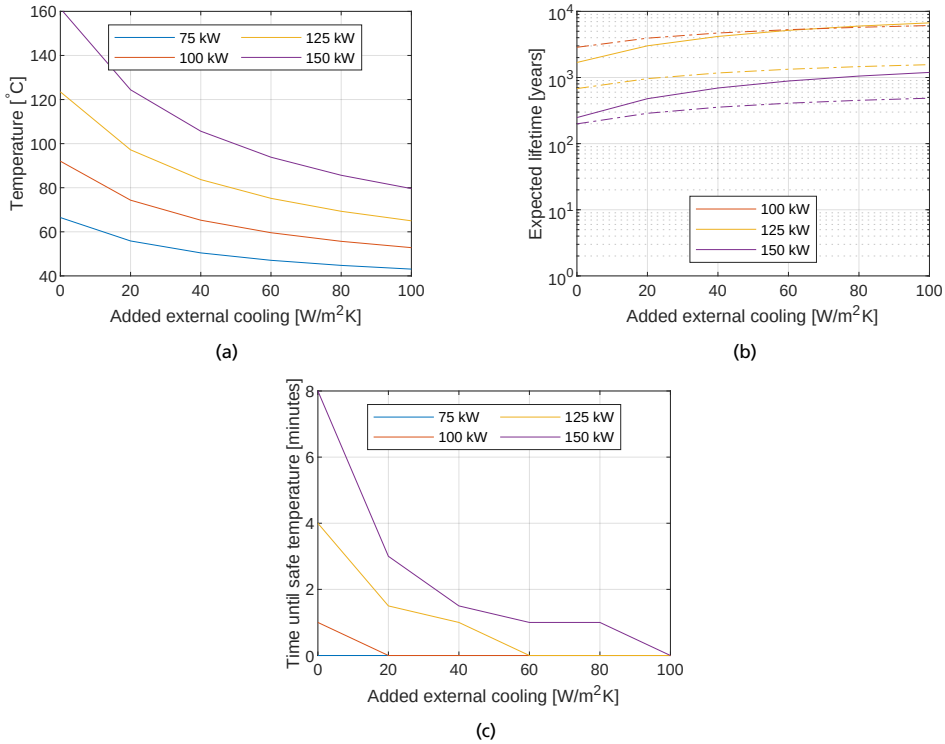


**Figure 5.16:** (a) shows the maximum surface temperature of any exposed metal directly after a charging event. (b) shows the expected lifetime of the IGBTs with dashed lines using the CIPS model and solid lines the LESIT model. (c) shows how long it takes before no surface metal is above 80 °C.

### 5.6.4 Summary

External cooling of the ASSE makes it possible to increase the charging power significantly, depending on the amount of external cooling. By directing e.g. a stream of air from the vehicle to the current collector and contact segment it is possible to increase the charging power with 10's of kW.

## 5.7 Additional power from multiple vehicles

An ASSE is mainly designed for dynamic charging, on which multiple vehicles can draw power simultaneously. This can be utilized for static charging by having one feed-in station feeding a stretch of ASSE from which multiple parked vehicles can draw power from. This type of charger can be beneficial e.g. where multiple taxis or buses are waiting in line. With multiple vehicles drawing power at the same time, but from different contact segments,

the current in the main conductors increase, increasing the losses and temperature of the ASSE. Additional current in the main conductors affect the entire ASSE structure. This current constantly generates heat, keeping an ASSE segment warm even if there is no vehicle drawing power from that specific segment.

### 5.7.1 Fast charging

At a charging power of 150 kW and a 1 minute cool down time an additional 400 kW, can be drawn from the ASSE, see Fig. 5.17. If the charging power is reduced to 100 kW, the additional charging power is around 1.1 MW without any cool down time. For large vehicles, which can charge from 2 energized contact segments at the same time, 6 vehicles drawing 200 kW each can charge from the ASSE.

The difference between the two lifetime models is because of the average IGBT junction temperature. The LESIT model is more affected by the average temperature than the CIPS model.

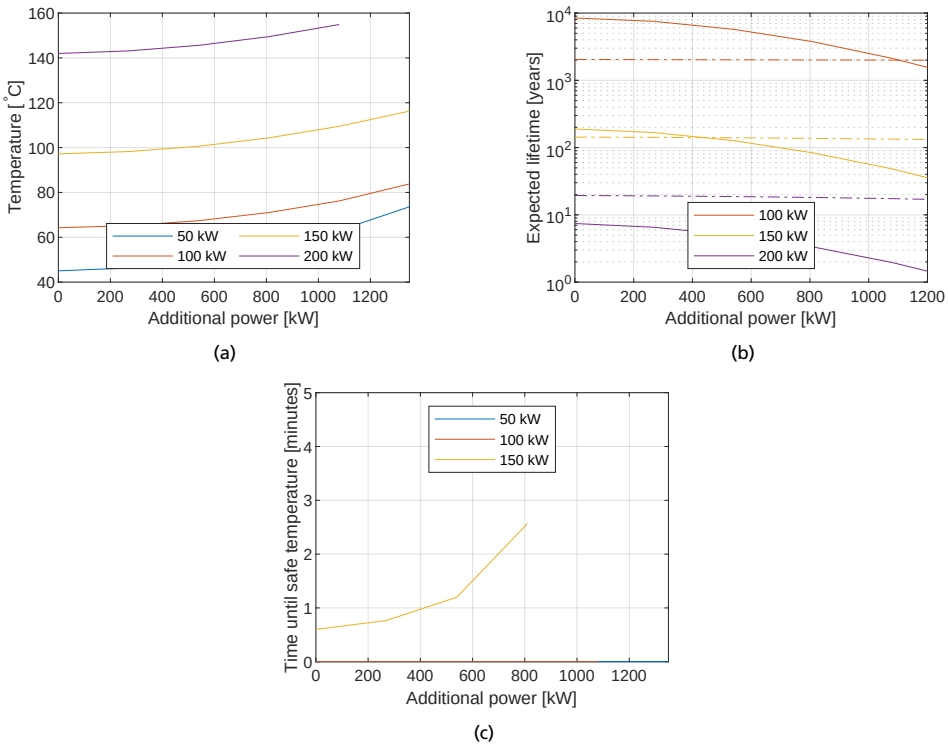


**Figure 5.17:** (a) shows the maximum surface temperature of any exposed metal directly after a charging event. (b) shows the expected lifetime of the IGBTs with dashed lines using the CIPS model and solid lines the LESIT model. (c) shows how long it takes before no surface metal is above 80 °C.

### 5.7.2 Medium fast charging

With a 6 minute cool down time it is possible to charge just one vehicle at a time with 150 kW. By decreasing the charging power to 125 kW the additional power drawn from the ASSE can be 800 kW, see Fig. 5.18. At no cool down time no more than a 75 kW charging power can be used but an additional 900 kW can be supplied by the ASSE.

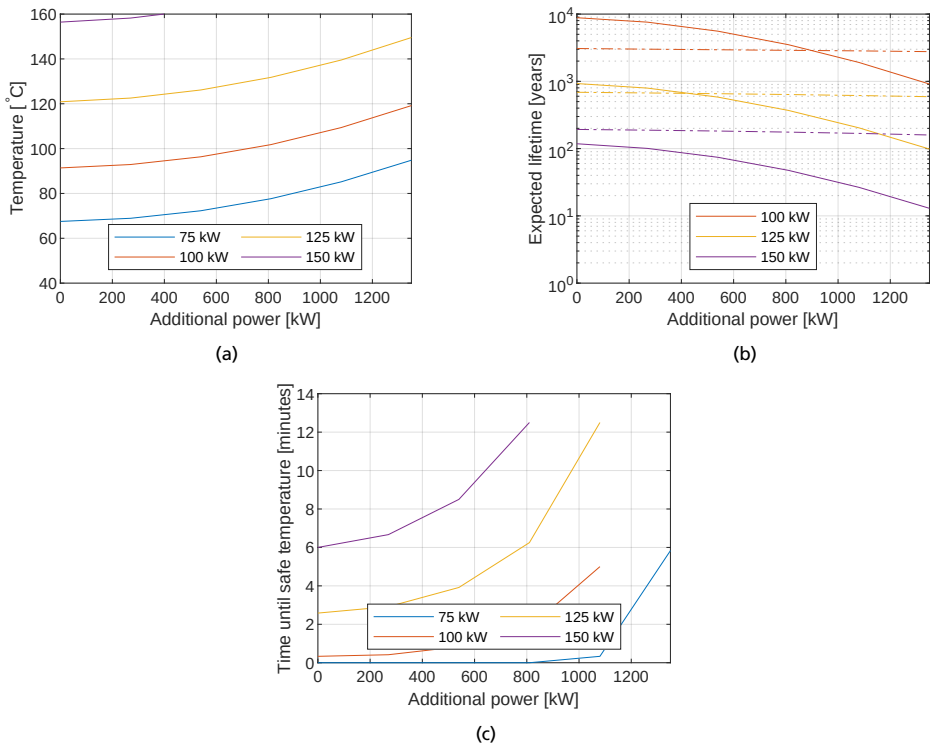


**Figure 5.18:** (a) shows the maximum surface temperature of any exposed metal directly after a charging event. (b) shows the expected lifetime of the IGBTs with dashed lines using the CIPS model and solid lines the LESIT model. (c) shows how long it takes before no surface metal is above 80 °C.

### 5.7.3 Slow charging

For a slow charging event lasting for 8 hours a considerable amount of energy is transferred even at low charging powers. A charging power of 75 kW results in 600 kWh and if two energized contact segments are used 1.2 MWh is transferred. At this charging power with a cool down time of 5 minutes an additional charging power of 1.32 MW is available. If a higher charging power per contact segment is needed, 125 kW allows for an additional 550 kW.

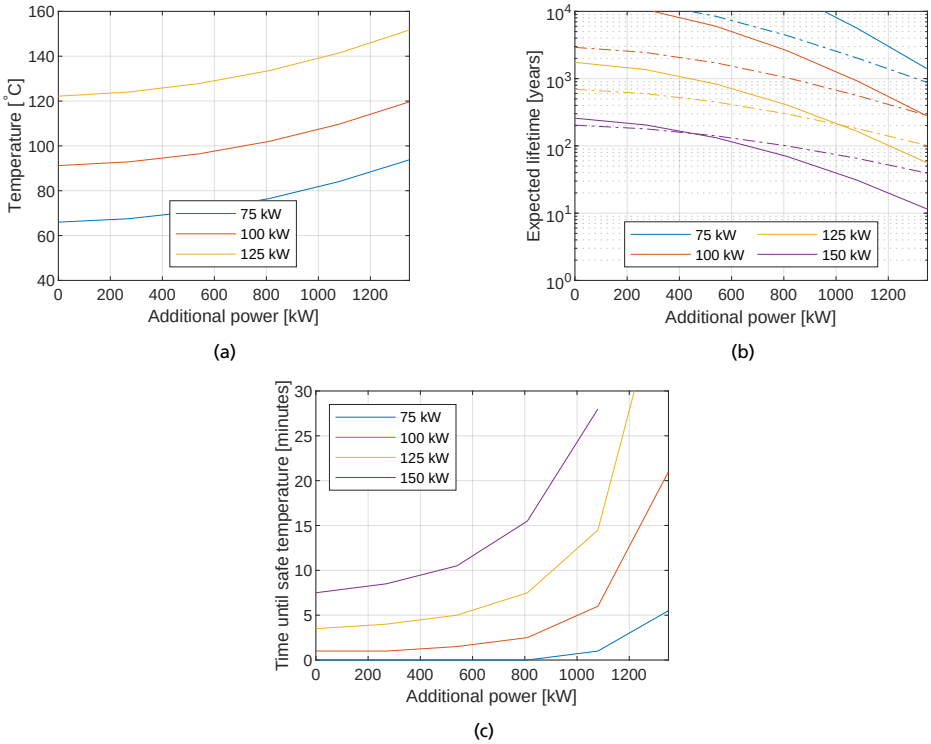


**Figure 5.19:** (a) shows the maximum surface temperature of any exposed metal directly after a charging event. (b) shows the expected lifetime of the IGBTs with dashed lines using the CIPS model and solid lines the LESIT model. (c) shows how long it takes before no surface metal is above 80 °C.

### 5.7.4 Summary

When an ASSE is installed as a static charger it can be made long enough for several vehicles to draw power from it. A special case of this is during a traffic jam when vehicles are stopped on the road and still draw power from the ASSE. The vehicles connect to different contact segments, but the current flows in the shared main conductors. The additional current from the vehicles drawing power, limits the power that can be delivered per contact segment to prevent overheating. As a result of the cumulative current in the main conductors, the contact segments closest to the feed-in point can deliver the least amount of power if no charging strategy is applied. A charging strategy could be e.g. to limit the power of the vehicles further away from the feed-in point.

## 5.8 Conclusions

Static charging with an ASSE is a possibility both for light and heavy vehicles, even if an ASSE is originally designed for dynamic charging where multiple vehicles charge simultaneously. By having one feed-in point and multiple vehicles performing static charging, the maximum possible charging power per contact segment decreases. The reason for this is that even if the vehicles are not connected to the same contact segment they still share the same main conductors. Due to this, the more power drawn from the ASSE the more losses there are in the main conductors and the maximum charging power per contact segment must be reduced. It is important to consider the static charging application to be able to design the ASSE with enough feed-in points. With only one vehicle charging from the ASSE charging powers in excess of 100 kW are possible in most cases if a short cool down time can be applied after the charging event (but before the vehicles leaves the charging spot, leaving the metal surfaces exposed). For light vehicles the charging power is enough under normal circumstances. For heavy vehicles the charging power may be too low for fast and medium fast charging even if a heavy vehicle can connect to 2 energized contact segments.

With 15 parallel IGBTs the surface temperature of the ASSE is most often the limiting factor. The surface temperature is greatly affected by the contact resistance between current collector and ASSE. Due to this it is important to use a well designed current collector to achieve a low contact resistance. The contact resistance is also affected by the surface of the ASSE contact segment, which can be covered by e.g. dirt. If the contact between the current collector and ASSE is poor the contact resistance can easily reach several 10's of mΩ. This increase in contact resistance, which can be unexpected, severely limits the performance of the ASSE. Since the surface temperature is the limiting factor in most cases the number of IGBTs can be reduced to save cost and reduce the complexity of the PCBs located inside the ASSE.

By making improvements to the ASSE design and adding external cooling provided from the vehicle side the power capabilities of the ASSE can be increased substantially. If the medium fast charging case is investigated with e.g. a contact segment with the thermal conductivity of aluminum, an added external cooling of 50 $W/m^2K$ and a contact resistance of 1 mΩ the ASSE can handle up to 175 kW without the need for a cooling time. By allowing a cool down time of 3 minutes the charging power can be up to 200 kW if one additional IGBT is used, making the total number of IGBTs 16. The additional IGBT is needed to increase the expected lifetime of the IGBTs to at least 20 years as the lifetime is the limiting factor at this charging power.

The current collector design is important for the thermal performance of the ASSE. With a poorly designed current collector the current collector may be the limiting factor of a

charging event as the current collector can reach too high temperatures. The temperature of the current collector is not included in this thesis as the current collector design is simplified, consisting of only a block and a cable. An accurate model of the current collector is needed for even more accurate estimations of the thermal behavior of the current collector and ASSE during a charging event.

# Chapter 6: Analysis of dynamic charging

Dynamic charging is evaluated based on the requirements in Section 2.2 in the same way as for static charging. 24 hours are simulated to capture the effect of varying traffic intensity and ambient temperature over the day. The focus is on surface temperature, lifetime of the IGBTs and the efficiency of the ASSE. If the temperature of the insulation inside the ASSE exceeds 130 °C the ASSE is considered permanently damaged and is not evaluated further. The expected lifetime of the IGBTs is often over hundreds or thousands of years according to the lifetime models. At such high numbers the expected lifetime is unrealistic but is still presented as results. Since there is a possibility that the moving vehicles suddenly stop and make it possible for humans and animals to come in contact with the ASSE the cool down time can be at the most a few seconds. Due to this the surface temperature is never to exceed 80 °C. Efficiency is the average energy efficiency of the system defined as the ratio between the energy that enters the vehicles, measured after the on-board rectifier, and the energy supplied to the ASSE, measured after the feed-in station. Sliding friction between the current collector and the ASSE is included but the added air drag from having a current collector is not included in the efficiency. Air drag is difficult to estimate as it depends not only on the current collector but also on the chassis of the vehicle.

## 6.1 Reference parameters

Each of the investigated parameters is varied one at a time with the rest of the parameters fixed. This allows for an understanding of how the ASSE behaves in different cases. The parameters investigated are the distance between feed-in points, the impact of traffic intensity, the number of IGBTs, the vehicle speed, the cooling action from moving vehicles and the location. The distance between feed-in points affects the RMS current in the main conductors, which is the main source of heat at large RMS currents. The impact of traffic is also related to RMS current in the main conductors. The RMS current is calculated based

on an assumed conductor temperature of 60 °C. The reason for using a fixed temperature is because the temperature along the ASSE changes and the whole length of the ASSE is not simulated. More traffic means more vehicles driving on the ASSE, which adds both shading and cooling from wind drag. The wind drag is one of the parameters investigated as this is likely vehicle dependent and the estimation of this parameter in this thesis is based on just one particular vehicle. The number of IGBTs is mainly affecting the expected lifetime of the IGBTs. This is shown and explained for static charging in Section 5.3, and the same happens for dynamic charging. The section on vehicle speed shows how different speed limits or traffic jams affect the temperature of the ASSE. It is assumed that the power the vehicles draw from the ASSE is scaled with the speed to achieve a more realistic scenario. The power is calculated based on the analytical equations presented in Section 2.1.2.

The most important parameters for dynamic charging are summarized in Table 6.12.

Table 6.12: Charging parameters.

| Parameter | Value |
|---|---|
| **Distance between feed-in points** | 1500 m |
| **Number of IGBTs** | 15 |
| **Cooling from moving vehicles** | 10 $W/m^2K$ |
| **Contact resistance** | 10 mΩ |
| **Normal force (car)** | 75 N |
| **Normal force (truck)** | 150 N |
| **Latitude** | 55 |
| **Maximum power (car)** | 75 kW |
| **Maximum power (truck)** | 360 kW |
| **Traffic factor** | 1 |

The assumed original *traffic intensity* is the same as presented in Section 2.1.1 expressed in vehicles/hour. The vehicles are assumed to be at least 2 seconds apart and any extra vehicles are assumed to drive in a different lane. Trucks stay in the ASSE lane if possible and the cars move to other lanes. A multiplier called *traffic factor* is used to scale the original traffic intensity presented in Section 2.1.1. At high traffic factors, i.e. when the amount of traffic on a road is increased, the lane covered with an ASSE is mostly used by trucks as the cars have moved over to a different lane. The fact that some vehicles change lanes and drive at different speeds is neglected in order to not need a traffic simulation model. In this thesis it is assumed that there is an ASSE in the second lane as well to avoid the influence of vehicles switching back to the first lane with a drained battery. The behavior of real traffic can affect the power the vehicles draw from the ASSE if e.g. only one lane is covered by an ASSE and vehicles need to drive in a different lane to overtake other vehicles. The result of this is effectively a lower $k_{ERS}$, which results in a higher power drawn from the ASSE. Out of all of the vehicles driving on the ASSE not all of the vehicles need to draw power from the ASSE. Different *utilization factors* of the ASSE is assumed to investigate how the ASSE is

affected by not all vehicles being equipped to use the ASSE. For the utilization factor no difference is made between cars and trucks, e.g. 30 % means that 30 % of the cars and 30 % of the trucks draw power from the ASSE. Three different utilization factors, 30 %, 70 %, and 100 % are used to resemble three different levels of ASSE adoption. The difference between utilization factor and traffic factor is that the utilization factor dictates how large of a fraction of the total traffic volume is utilizing the ASSE, while the traffic factor is scaling the total traffic volume.

## 6.2 Distance between feed-in points

The distance between feed-in points, defined in Fig. 1.7b, is important both for installation cost and for aesthetics. A long distance means fewer but more more powerful feed-in stations. This likely minimizes the cost for the feed-in stations as it is most often cheaper to construct fewer high power stations compared to many lower power stations. Aesthetics, especially in an urban environment, can benefit by having less feed-in stations.

At 100 % utilization factor the distance between the feed-in points can be about 1500 m before the surface temperature exceeds 80 °C according to Fig. 6.1a. With a lower utilization factor the distance between the feeding points can be even longer and at 30 % utilization factor the distance can be several kilometers. The expected lifetime of the IGBTs is not a limiting factor for the ASSE with the reference parameters, see Fig. 6.1b.

The efficiency is very important for a charging system such as an ASSE. A higher efficiency results in less energy wasted as heat, which is important for a system with limited cooling capabilities. With longer conductors the RMS current increases (due to more vehicles being fed at the same time) but also the distance the current needs to flow in the conductors increases. Due to this, there is a trade-off on how long the distance between the feed-in points should be with regards to temperature, expected lifetime and efficiency. Based on Fig. 6.1c there is about 1.5 % losses that are not depending on the distance between feed-in stations. An estimation of how the losses are distributed is presented in Fig. 6.1c. The main conductors quickly become the dominant source of losses when the distance between feed-in points increase.

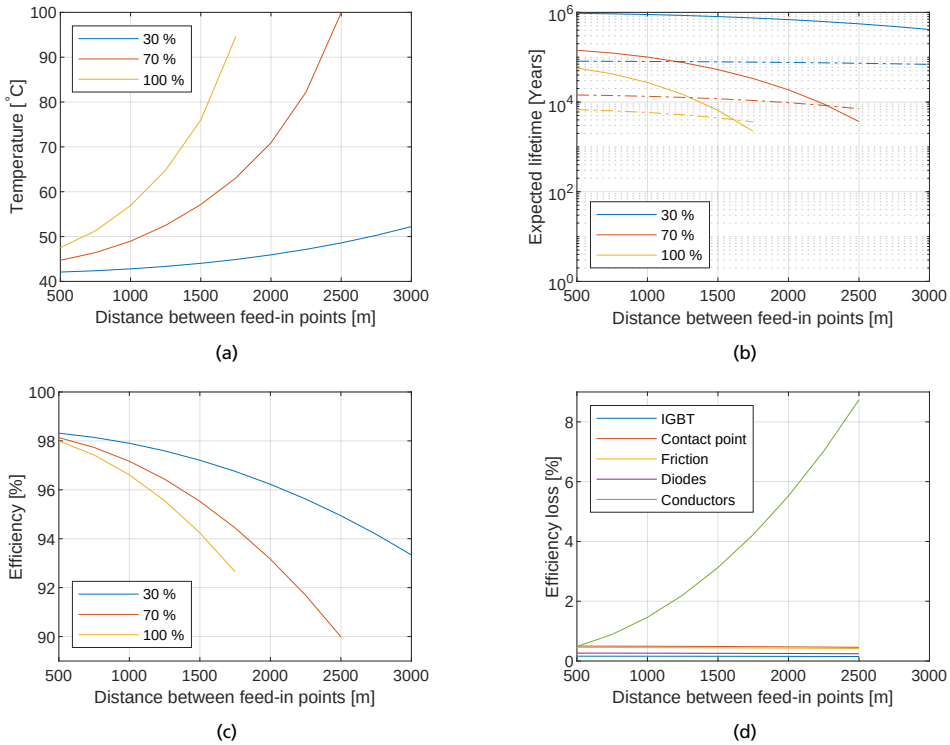


**Figure 6.1:** (a) shows the surface temperature of any exposed metal surfaces. (b) shows the expected lifetime of the IGBTs with dashed lines using the CIPS model and solid lines the LESIT model. (c) shows the efficiency of the ASSE from feed-in point to after the rectifier on-board the vehicle. (d) shows the different efficiency loss components from the 70 % utilization factor from (c).

## 6.3 Impact of traffic

The amount of traffic on the road affects both the cooling and the heating of the ASSE. The more traffic utilizing the ASSE the more power is drawn from the ASSE and the electric losses increase. On the other hand, with more traffic the increased amount of vehicles results in increased cooling from shading and air drag.

As explained earlier, the assumed traffic intensity is the same as presented in Section 2.1.1. When the maximum capacity of the lane with the ASSE is reached, vehicles start to drive in a different lane. The first vehicles to move to a different lane are cars, and when only trucks remain in the lane with ASSE any additional trucks move to a different lane. The result of this is that once only trucks are present in the ASSE lane and the maximum capacity of the lane is reached the number of vehicles do not increase even if the total traffic on the road increase.

An interesting behavior can be observed for low utilization factors where the surface temperature of the ASSE decreases with an increased amount of traffic, see Fig. 6.2. The lifetime of the IGBTs is well beyond 20 years for the investigated cases. Efficiency decreases with increased traffic flow as the power drawn from the ASSE increases. With the reference parameters, the majority of the losses are located in the main conductors of the ASSE. The increased power drawn from the ASSE at higher traffic levels increase the RMS current in the main conductors and therefore also the losses.

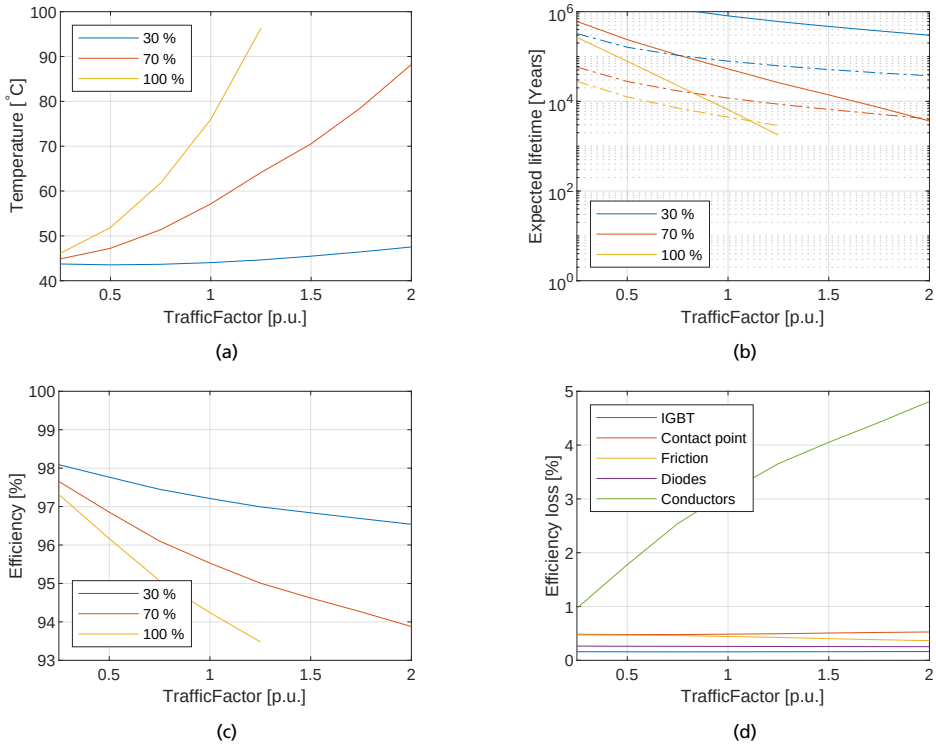


**Figure 6.2:** (a) shows the surface temperature of any exposed metal surfaces. (b) shows the expected lifetime of the IGBTs with dashed lines using the CIPS model and solid lines the LESIT model. (c) shows the efficiency of the ASSE from feed-in point to after the rectifier on-board the vehicle. (d) shows the different efficiency loss components from the 70 % utilization factor from (c).

## 6.4 Number of IGBTs

The number of IGBTs have a small impact on the heat generated by the IGBTs. With fewer IGBTs the voltage drop increase over the remaining IGBTs resulting in an increased heat generation. This can be seen in both the efficiency and surface temperature in Fig. 6.3. With regards to the number of IGBTs, the expected lifetime is the most interesting

parameter. 15 IGBTs, which is the reference case, yields an expected lifetime that is a lot longer than 20 years. For the reference parameters only 7-8 parallel IGBTs are needed even at 100 % utilization factor. This is a significant reduction from the 15 IGBTs used as reference and can simplify the PCBs in the ASSE. A simplification of the PCBs do not only result in cheaper PCBs but also a reduction of components, which can result in better reliability as less components can fail. It should be noted that the required number of IGBTs may be different for dynamic and static charging depending on the charging scenario. An example of this is that static medium fast charging in Section 5.3.2 requires 11 IGBTs for a power level of 150 kW, and for the dynamic charging scenario in this section with a utilization factor of 70 % only 6 IGBTs are needed. This needs to be considered if the ASSE should be able to handle both dynamic and static charging with the same hardware configuration.

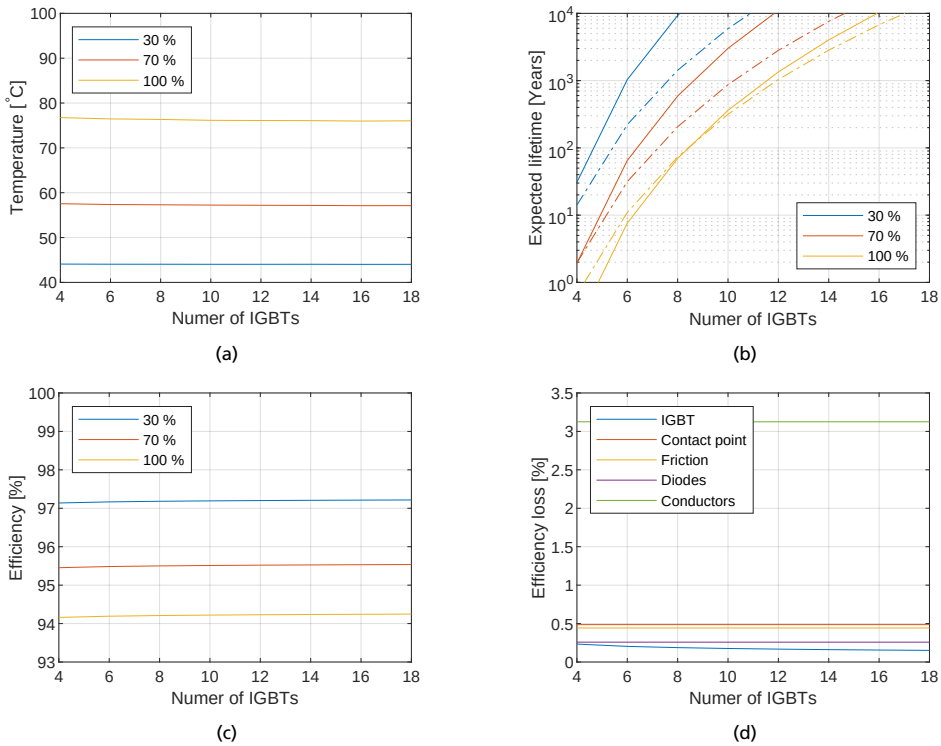


**Figure 6.3:** (a) shows the surface temperature of any exposed metal surfaces. (b) shows the expected lifetime of the IGBTs with dashed lines using the CIPS model and solid lines the LESIT model. (c) shows the efficiency of the ASSE from feed-in point to after the rectifier on-board the vehicle. (d) shows the different efficiency loss components from the 70 % utilization factor from (c).

## 6.5 Vehicle speed

The power a vehicle needs to draw from an ASSE is related to the speed of the vehicle. Since different roads have different speed limits the power drawn from the ASSE differs on different roads. In the simulations the power drawn is based on the analytical equations in Section 2.1.2. This change in power affects temperature, efficiency and expected lifetime of the IGBTs. In Fig. 6.4 the impact of different vehicle speeds are presented and a trend shift can be seen at 90 km/h. This is as the trucks are limited to 90 km/h and can not exceed this speed even if the road allows for higher speeds.

With an increase in efficiency and decrease in surface temperature as the speed decreases, it is possible to use longer distance between feed-in points for a road with a low speed compared to a road with a higher speed. Inside e.g. a city where the speed limit is 40-50 km/h the feed-in points can be several km apart without exceeding the surface temperature limit.

An increase in speed increase the losses in the main conductors and contact point more than the other components of losses presented in Fig. 6.4d. The predominant losses in the main conductors and contact point are resistive losses and are related to the current squared while e.g. losses in the diodes and IGBTs are dependent on the current and forward voltage, where the forward voltage does not increase linearly with the current.

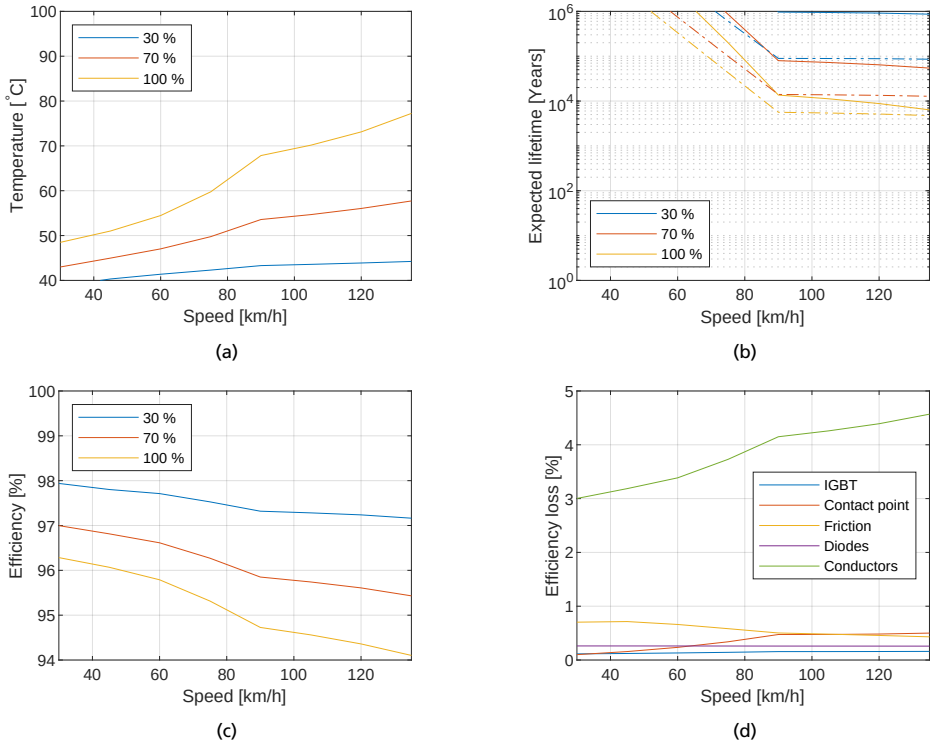


**Figure 6.4:** (a) shows the surface temperature of any exposed metal surfaces. (b) shows the expected lifetime of the IGBTs with dashed lines using the CIPS model and solid lines the LESIT model. (c) shows the efficiency of the ASSE from feed-in point to after the rectifier on-board the vehicle. (d) shows the different efficiency loss components from the 70 % utilization factor from (c).

## 6.6 Cooling from moving vehicles

Cooling from moving vehicles is in this thesis set to a fixed 10 $W/m^2K$ for 1 second after each vehicle passage. These values are obtained from experimental tests with a single vehicle at speeds up to 55 km/h as shown in Section 3.2.1. On a real road there are many different types of vehicles driving at different speeds, making the cooling parameter important to investigate. The temperature of the ASSE is greatly affected by the cooling provided from moving vehicles, see Fig. 6.5.

Added cooling from vehicles does not significantly affect the expected lifetime of the IGBTs. Since the RMS current is calculated based on a fixed conductor temperature of 60 °C (as explained earlier in this chapter), the efficiencies shown in Fig. 6.5c are not varying with the amount of cooling from moving vehicles. However, with added cooling the temperature of the main conductors is decreased and thus the resistance of the conductors is decreased,

increasing the efficiency of the system.

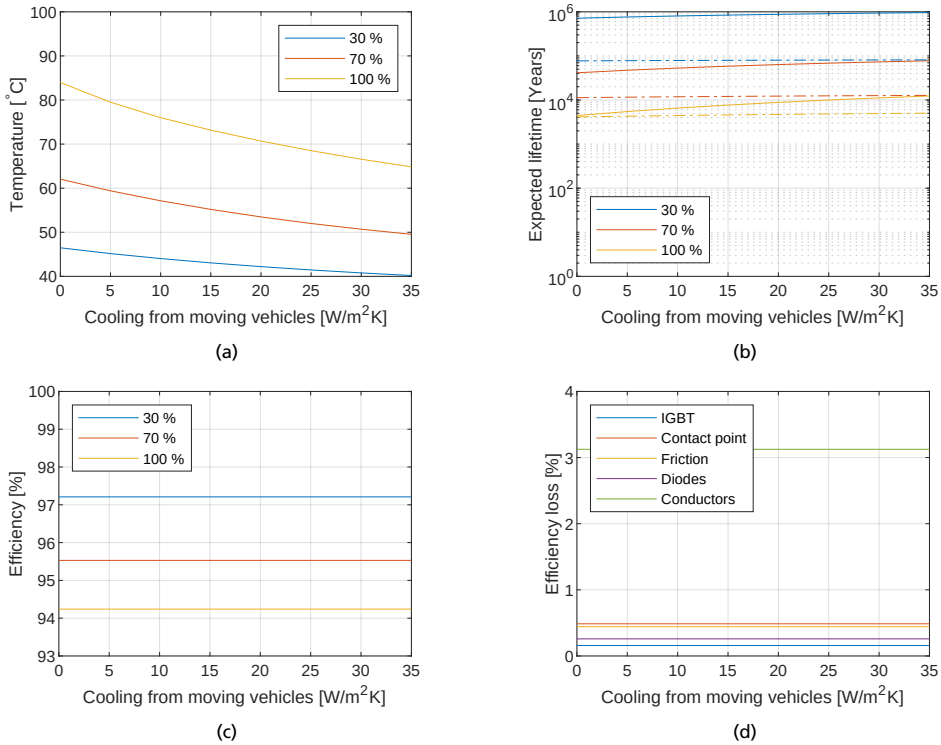


**Figure 6.5:** (a) shows the surface temperature of any exposed metal surfaces. (b) shows the expected lifetime of the IGBTs with dashed lines using the CIPS model and solid lines the LESIT model. (c) shows the efficiency of the ASSE from feed-in point to after the rectifier on-board the vehicle. (d) shows the different efficiency loss components from the 70 % utilization factor from (c).

## 6.7 Location

The location of the ASSE is important to consider as the location affects the ambient temperature, and the amount of heat received from the sun. The important parameter for location is the latitude the ASSE is placed at. At latitudes closer to the poles of the globe the incoming solar irradiance is less. This affects not only the ASSE temperature directly by increasing the heat absorbed by the surface of the ASSE but also the ambient temperature by heating up e.g. the ground. In this section the ambient temperature is not changed from the reference temperature even at different locations as it is difficult to specify a suitable ambient temperature based on latitude.

Based on the results presented in Fig. 6.6 it is clear that the temperature drops at higher latitudes. The differences in how affected the different utilization factors are depends mainly

on the ratio between the heat generated by electrical and mechanical losses and the heat from solar irradiance, but also on the surface temperature of the ASSE. A higher surface temperature yields a higher convection coefficient and also cooling by thermal radiation. The ratio between the losses in the ASSE is important as 24 h is simulated with a varying traffic intensity over these hours. When a significant fraction of the total heat comes from solar irradiance, the highest temperature occurs for most cases around the time when the incoming solar irradiance is close to its peak, which happens about the same time every day if the sky is clear. On the other hand, for low fractions of solar irradiance the highest temperature occurs when the traffic intensity is at its peak, which e.g. can be in the morning or afternoon. In Fig. 6.6a the temperature presents the same behavior for 30 % and 70 % utilization factor, while for 100 % the curve starts to differ significantly at latitude 70°. At this latitude the peak temperature is no longer occurring at lunch time but before lunch around 10:00. The same conclusion as for utilization factor can be made based on distance between feed-in points and other factors affecting the power drawn from the ASSE.

The temperature difference between southern Sweden (where all the experimental tests in this theses were performed) to the equator is about 5 °C with the reference parameters, if the effect of ambient temperature is not included. For a warm summer day it is not unreasonable to assume the area around the equator to be 15 °C warmer than the southern parts of Sweden. The total temperature change of the ASSE caused by changing the latitude can be approximated by the increase in ambient temperature added to the change in temperature caused by solar irradiance. A 15 °C change in ambient temperature would then result in an increased temperature of around 20 °C from the equator to the southern part of Sweden, which is a considerable difference. With an increase in ambient temperature both convection and thermal radiation change, which makes the actual result differ slightly from the approximation.

As explained in the section for cooling by moving vehicles the efficiency presented in Fig. 6.6c is constant due to the temperature of the main conductors is assumed to be 60 °C for the entire ASSE. However, the increased temperature expected at latitudes closer to the equator, will likely lead to higher temperatures of the main conductors and hence to lower efficiencies.

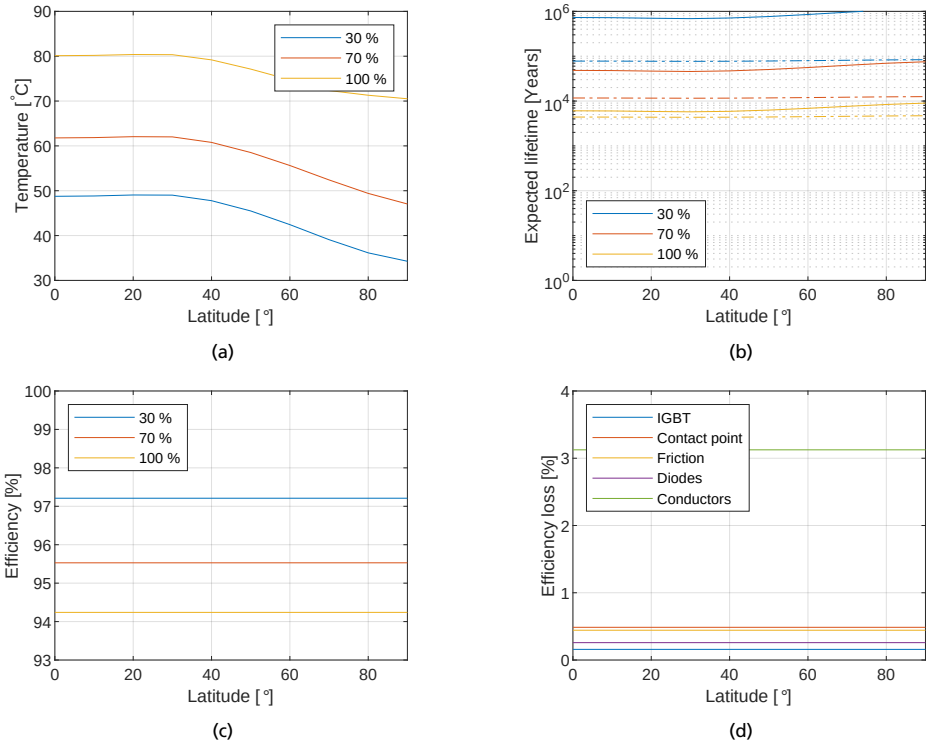


**Figure 6.6:** (a) shows the surface temperature of any exposed metal surfaces. (b) shows the expected lifetime of the IGBTs with dashed lines using the CIPS model and solid lines the LESIT model. (c) shows the efficiency of the ASSE from feed-in point to after the rectifier on-board the vehicle. (d) shows the different efficiency loss components from the 70 % utilization factor from (c).

## 6.8 Conclusions

With an ASSE that is fed in one end and uses internal conductors to transfer the energy over a distance it is important to consider the losses in these conductors. The total losses in the main conductors are related to both the RMS current flowing through the main conductor and also the length of the conductor. While the RMS current affects the losses per meter, which affects the temperature of the ASSE, the length of the conductor affects the total losses. The total losses do not affect the temperature of the ASSE since the losses can be spread out over a long distance. Instead the total losses affect the efficiency of the ASSE and they are relevant to consider when designing a cost efficient solution, and a solution that is good for the environment.

The reference value for the number of IGBTs is set to 15 as stated in Table 6.12. This number is unnecessarily high, and provides an expected lifetime for the IGBTs in excess of hundreds

to thousands of years in most cases. A large portion of the parallel IGBTs can be removed and still fulfilling the requirement of an expected lifetime of 20 years.

In order to reduce cost and environmental impact it may be beneficial to have different ASSE designs for different roads. On a road where vehicles are driving slowly less power is needed, compared to a road where they drive faster. For those roads with a lower power demand, the number of IGBTs can be reduced significantly and the large main conductors can also be reduced. With smaller main conductors the losses increase for a fixed current, which results in a need of more feed-in stations if the losses are to be kept at the same level. A thorough study of cost and environmental impact is needed to optimize the ASSE design based on cost and environmental aspects.

# Chapter 7: Conclusions and future work

In this thesis thermal management of conductive electric road systems is investigated. The main focus is on the ASSE developed by Elonroad, a particular ERS solution with very short contact segments (1 m) and the switching elements integrated in the ERS structure. This chapter presents the main conclusions from this thesis work and gives suggestions for future work.

## 7.1 Conclusions

This thesis presents a thermal model to estimate the temperatures, both internally and on the surface of an ASSE, which has been calibrated and validated with measurements from a full size ASSE test track. These measurements have been performed in different weather conditions and at different charging powers.

A lifetime model for the main switches inside the ASSE is developed and used together with the thermal model to estimate both temperatures of the ASSE and lifetime of the switches for different load cases. The focus of the work is on the ASSE itself and not on the ground beneath the ASSE.

The investigated ASSE is capable of supplying vehicles with power both when they are moving (dynamic charging) and when they are standing still (static charging). The main difference between these two modes of supplying power is that the losses are localized to a small area for static charging. This increases the risk of generating a thermal hot spot, which can cause safety issues for anyone coming in physical contact with the high temperature. For dynamic charging the losses are spread out over a large area, thus reducing the risk of getting a localized hot spot.

For any conductive ERS it is important to have a good electric connection between the

current collector on the vehicle and the contact segment. A good connection implies a low contact resistance, and as a result low contact losses. The difference in electric contact resistance between a good and a poor connection can be of several orders of magnitude. This is especially important to consider for static charging where the losses are localized, to prevent any hot spots caused by the generated heat in the contact point. In the case of a poor connection between the current collector and the contact segment, the maximum power an ASSE can supply to a vehicle in static charging is limited by this connection. The tests made in this thesis point at a contact resistance in the range 1-2 mΩ, but the simulations suggest that contact resistances below 1 mΩ would strongly impact in particular static charging power levels.

For dynamic charging, the long main conductors in an ASSE are usually the largest source of heat, due to the cumulative current from multiple vehicles drawing power from the ASSE. The heat in the main conductors are spread out over a long distance and do therefore not create any hot spots. Due to this, the total losses in the main conductors can be quite large compared to losses that create hot spots without generating dangerous temperatures. The main conductors are also responsible for a major part of the drop in efficiency at higher loads. This drop in efficiency is important to consider, and design choices can be made to increase the efficiency, by e.g. having a closer distance between the feed-in points or changing the material of the conductors. The distance between the feed-in points is important for the system optimization, no matter if the optimization is based on e.g. cost or temperature. A shorter distance results in more feed-in stations, which needs to be weighed against the gain in efficiency and lower temperature.

Cooling is important for both dynamic and static charging. Static charging can greatly benefit from cooling of a small area around the current collector. Adding additional cooling, e.g. an air stream from within the vehicle, to this area reduces the surface temperature of the contact segment significantly, which allows for a higher static charging power. Cooling around the current collector has a smaller effect for dynamic charging as the losses are not localized and the surface temperature is often lower. Moreover, dynamic charging provides a cooling effect from drag that reduce the need for an additional air flow from e.g. within the vehicle.

With the knowledge and the modeling tools resulting from this thesis work an ASSE can be dimensioned for different load cases. The thermal model allows for both optimization of the ASSE structure and the number of parallel switches, but also of the distance between the feed-in points from a thermal and lifetime perspective.

This thesis presents efficiency numbers for different combinations of parameters. These numbers can be used to optimize both the design of the ASSE and cost for deploying the ASSE on a road network. The results presented lay the ground for a cost optimization of a large scale deployment of an ASSE like the one developed by Elonroad.

## 7.2 Future work

Future research is needed to further calibrate and validate the thermal model. More measurements with different external conditions are needed to gather data for a wide range of usage conditions. With the fast development of the ASSE technology the geometry of the model needs to be continuously updated to keep up with the changes made in the geometry of the ASSE. The same applies for the lifetime compensation factors, which have been obtained from a limited data set. Below is a list of the main areas in need for future research.

- **Cooling from moving vehicles** is experimentally investigated in this thesis with the use of a car driving at different speeds. More types of vehicles and more speeds are needed to properly represent the vehicle fleet providing cooling for the ASSE. The influence of different current collector designs is another aspect of cooling from moving vehicles that needs to be investigated. The current collector is extending out from the vehicle and affects the airflow around the chassis of the vehicle. A change in the airflow may have an effect on how well a moving vehicle cools down the ASSE.
- **Air drag losses** from adding a current collector is not investigated in this thesis. The effect on overall air drag for the vehicle is not only due to the air drag from the current collector, but rather on how this added equipment affects the aerodynamics of the entire vehicle. A suggestion for future work is to study the effect on the vehicle energy consumption as a function of the added drag due to the current collector.
- **Contact resistance** needs further investigation both for dynamic and static charging. A rotating test rig is used in this thesis to evaluate two different current collector materials at low speeds. There is however a large uncharted territory related to how material choices, contact pressures, contact design, presence of e.g. water/snow/ice/dirt, affect the contact resistance, noise emissions, and particulate emissions.
- **Expected lifetime of discrete IGBTs** is in this thesis calculated by using a compensation factor in combination with existing lifetime models for modules and not discrete components. In the application of dynamic charging the junction temperature swing is a lot smaller than what the lifetime models and compensation factors are developed for. Due to this the models and compensation factors need to be validated for the junction temperature swings that occurs from dynamic charging. The compensation factors do need to be evaluated for different types of discrete IGBTs.

# References


[1] International Energy Agency, "CO2 Emissions from Fuel Combustion 2019." IEA, November 2019.

[2] International Energy Agency, "Global EV Outlook 2019: Scaling up the transition to electric mobility." IEA, May 2019.

[3] European Commission, "Report on Raw Materials for Battery Applications." November 2018.

[4] J. Gordon, "Cobalt: the dark side of a clean future." Raconteur, `https://www.raconteur.net/business-innovation/cobalt-mining-human-rights`, Accessed: 2020-03-10.

[5] J. Nastu, "Shortage of Ethically Sourced Cobalt from Congo Causes Trouble for GE, Apple, Tesla…and More." Environmental leader, `https://www.environmentalleader.com/2017/05/shortage-ethically-sourced-cobalt-congo-causes-trouble-ge-apple-tesla/`, Accessed: 2020-03-10.

[6] S. M. Knupfer, R. Hensley, P. Hertzke, and P. Schaufuss, "Electrifying insights: How automakers can drive electrified vehicle sales and profitability." McKinsey & Company, January 2017.

[7] F. Lambert, "Tesla confirms base Model 3 will have less than 60 kWh battery pack option, cost is below $190/kWh and falling." Electrek, `https://electrek.co/2016/04/26/tesla-model-3-battery-pack-cost-kwh/`, Accessed: 2020-03-27.

[8] D. Hall and N. Lutsey, "Effects of battery manufacturing on electric vehicle life-cycle greenhouse gas emissions." ICCT, February 2018.

[9] M. G. H. Gustavsson, F. Hacker, and H. Helms, "Overview of ERS concepts and complementary technologies." Swedish-German research collaboration on Electric Road Systems, April 2019.

[10] G. Domingues, *Modeling, Optimization and Analyss of Electromobility Systems*. Media-Tryck, 2018.

[11] Tesla, `https://www.tesla.com/sv_SE/blog/introducing-v3-supercharging`, Accessed: 2020-03-20.

[12] European Council for Automotive R&D, "Battery requirements for future automotive applications." EUCAR, July 2019.

[13] G. Bower, "Tesla Model 3 2170 Energy Density Compared To Bolt, Model S P100D." INSIDEEVs, `https://insideevs.com/news/342679/tesla-model-3-2170-energy-density-compared-to-bolt-model-s-p100d/`, Accessed: 2020-06-12.

[14] K. Field, "BloombergNEF: Lithium-Ion Battery Cell Densities Have Almost Tripled Since 2010." CleanTechnica, `https://cleantechnica.com/2020/02/19/bloombergnef-lithium-ion-battery-cell-densities-have-almost-tripled-since-2010/`, Accessed: 2020-06-12.

[15] I. Hore-Lacy, *Nuclear Energy in the 21st Century: The World Nuclear University Primer*. World Nuclear University Press, 2006.

[16] M. Hanazawa and T. Ohira, "Power transfer for a running automobile," in *2011 IEEE MTT-S International Microwave Workshop Series on Innovative Wireless Power Transmission: Technologies, Systems, and Applications*, pp. 77–80, May 2011.

[17] S. Hall, "Capacitive power transfer to car through wheel – is it possible?." Master thesis, 2012.

[18] P. Fyhr, G. Domingues, M. Andersson, F. J. Márquez-Fernández, H. Bängtsson, and M. Alaküla, "Electric roads: Reducing the societal cost of automotive electrification," in *2017 IEEE Transportation Electrification Conference and Expo (ITEC)*, pp. 773–778, June 2017.

[19] J. D. Boeij, E. Lomonova, J. Duarte, and A. Vandenput, "Contactless Energy Transfer to a Moving Load Part II: Simulation of Electrical and Mechanical Transient," in *2006 IEEE International Symposium on Industrial Electronics*, vol. 2, pp. 745–750, July 2006.

[20] G. A. Covic and J. T. Boys, "Inductive Power Transfer," *Proceedings of the IEEE*, vol. 101, pp. 1276–1289, June 2013.

[21] M. Alaküla and F. J. Márquez-Fernández, "Dynamic charging solutions in Sweden: An overview," in *2017 IEEE Transportation Electrification Conference and Expo, Asia-Pacific (ITEC Asia-Pacific)*, pp. 1–6, Aug 2017.

[22] D. Bateman, D. Leal, S. Reeves, M. Emre, L. Stark, F. Ognissanto, R. Myers, and M. Lamb, "Electric Road Systems: A solution for the future?." World Road Association (PIARC), 2018.

[23] S. Tongur, "The role of business models in the transition to Electric Road Systems." Sustainable Horizons in Future Transport, Shift Policy Brief, 2019/2020.

[24] Elonroad, `http://elonroad.com/`, Accessed: 2020-03-08.

[25] Elways, `http://elways.se/`, Accessed: 2020-03-08.

[26] A. Singh, "Electric Road Systems: A feasibility study investigating a possible future of road transportation." Master thesis, 2016.

[27] M. Gustavsson, C. Börjesson, R. Eriksson, and M. Josefsson, "Automatic Conductive Charging of Electric Cars." RISE Viktoria and Volvo Cars, 2017.

[28] T. Tajima, W. Noguchi, and T. Aruga, "Study of a Dynamic Charging System for Achievement of Unlimited Cruising Range in EV." SAE Technical Paper 2015-01-1686, 2015.

[29] T. Tajima, H. Tanaka, T. Fukuda, Y. Nakasato, W. Noguchi, Y. Katsumasa, and T. Aruga, "Study of High Power Dynamic Charging System." SAE Technical Paper 2017-01-1245, 2017.

[30] F. J. Márquez-Fernández, "Power conversion challenges with an all-electric land transport system." Swedish Electromobility Centre, 2019.

[31] P. Abrahamsson, F. J. Márquez-Fernández, and M. Alaküla, "Thermal Modeling and Analysis of an Alternating Short-Segmented Conductive ERS," vol. 5, pp. 1078–1086, 2019.

[32] Swedish Transport Administration, `http://vtf.trafikverket.se/SeTrafikinformation.aspx`, Measure point: 3210370, Direction: Forward, Date: 2015-03-18 12:00 – 2015-03-19 12:00, Accessed: 2020-02-20.

[33] Conference of European Directors of Roads, "Safe distance between vehicles." CEDR, April 2010.

[34] Audi, `https://www.audi.se/se/web/sv/models/a4/a4-sedan.html#layer=/se/web/sv/models/a4/a4-sedan/layer/layer-dimensions.html`, Accessed: 2020-02-20.

[35] Volvo, `https://www.volvocars.com/se/bilar/modeller/v60/specifikationer/dimensioner`, Accessed: 2020-02-20.

[36] EUR-LEX, https://eur-lex.europa.eu/, CELEX:01996L0053-20150526, Accessed: 2020-03-19.

[37] P. Slowik, N. Pavlenko, and N. Lutsey, "Assessment of next-generation electric vehicle technologies." ICCT, October 2016.

[38] F. Rodríguez, O. Delgado, and R. Muncrief, "Fuel consumption testing of tractor-trailers in the European Union and the United States." ICCT, May 2018.

[39] J. Bilo, H.-G. Burghoff, H. dos Santos, J. Engbring, E. Erich, P. Gresch, F. Harrmann, T. Heckenberger, N. Hees, I. Hegedüs-Bite, H. Kalb, M. Kriegel-Gemmecke, C. Kuper, A. Leone, M. Nalbach, B. Piller, H. Rechberger, N. Schnocks, R. Schöttle, H.-J. Schröder, U. Sinner, W. Stabroth, J. Weitzel, and M. G. Zeyen, "48-Volt Electrical Systems – A Key Technology Paving to the Road to Electric Mobility." German Electrical and Electronic Manufacturers' Association, April 2016.

[40] A. D. Wearing, J. Haybittle, R. Bao, J. W. Baxter, C. Rouaud, and O. Taskin, "Development of High Power 48V Powertrain Components for Mild Hybrid Light Duty Vehicle Applications," in *2018 IEEE Energy Conversion Congress and Exposition (ECCE)*, pp. 3893–3900, Sep. 2018.

[41] D. Eshete, "Automotive 48V Power Supply, finally a reality?." ON Semiconductor, https://www.onsemi.com/blog/automotive/automotive-48v-power-supply, Accessed: 2020-06-24.

[42] H. S. Turner, "Human responses to electricity: A literature review." The Aviation Medicine Research Laboratory, January 1972.

[43] H. Dahlin and Åsa Eliasson, "Jämförelse mellan asfalt- och betongbeläggningar. Uppdatering av kalkylmodellen 2Ö." Master thesis, 2007.

[44] 3M™, "3M™ Heat Shrink Tubing and Devices - Product Catalog." Accessed: 2020-02-20.

[45] S. Ohta, "Temperature Classes of Electrical Insulators." Three Bond Technical News, December 1985.

[46] A. M. Stoll, M. A. Chianta, and J. R. Piergallini, "Thermal Conduction Effects in Human Skin: I. Experimental data acquisition." 15 January 1979.

[47] S. Timsit, "Electrical contact resistance: properties of stationary interfaces," in *Electrical Contacts - 1998. Proceedings of the Forty-Fourth IEEE Holm Conference on Electrical Contacts (Cat. No.98CB36238)*, pp. 1–19, 1998.

[48] P. Fyhr, *Materials and Manufacturing Economics*. Media-Tryck, 2018.

[49] E. Csanyi, "Insulating materials in electrical equipment." Electrical Engineering Portal, https://electrical-engineering-portal.com/insulating-materials-in-electrical-equipment, Accessed: 2020-10-9.

[50] J. Magnusson, *On the design of hybrid DC-breakers consisting of a mechanical switch and semiconductor devices*. Universitetsservice US AB, 2015.

[51] C. Blake and C. Bull, "IGBT or MOSFET: Choose Wisely." International Rectifier.

[52] J. Lutz, H. Schlangenotto, U. Scheuermann, and R. D. Donker, *Semiconductor Power Devices: Physics, Characteristics, Reliability*. Springer International Publishing, 2018.

[53] I. Batarseh and A. Harb, *Power Electronics: Circuit Analysis and Design*. Springer International Publishing, 2018.

[54] Z. Sen, *Solar Energy Fundamentals and Modeling Techniques*. Springer-Verlag London Limited, 2008.

[55] J. Widén and J. Munkhammar, *Solar Radiation Theory*. 2019.

[56] R. Kittler and S. Darula, "Determination of time and sun position system," *Solar Energy*, vol. 93, pp. 72 – 79, 2013.

[57] P. Tzoumanikas, E. Nikitidou, A. Bais, and A. Kazantzidis, "The effect of clouds on surface solar irradiance, based on data from an all-sky imaging system," *Renewable Energy*, vol. 95, pp. 314 – 322, 2016.

[58] N. Nijegorodov and P. V. C. Luhanga, "Air mass: Analytical and empirical treatment; an improved formula for air mass," *Renewable Energy*, vol. 7, no. 1, pp. 57 – 65, 1996.

[59] F. Kasten, "A New Table and Approximation Formula for the Relative Optical Air Mass," *Archiv für Meteorologie, Geophysik und Bioklimatologie, Serie B*, vol. 14, no. 2, pp. 206 – 223, 1965.

[60] A. B. Meinel and M. P. Meinel, *Applied solar energy: an introduction*. Addison-Wesley series in physics, Addison-Wesley Pub. Co., 1976.

[61] M. Försth and A. Roos, "On the importance of spectrally resolved absorptivity data in fire technology." SP Technical Research Institute of Sweden, 2009.

[62] J. H. Henninger, "Solar Absorptance and Thermal Emittance of Some Common Spacecraft Thermal Control Coatings." NASA Reference Publication 1121, April 1984.

[63] G. Straffelini, *Friction and Wear. Methodologies for Design and Control*. Springer International Publishing, 2015.

[64] J. Lenard and S. Kalpakjian, "The Effect of Temperature on the Coefficient of Friction in Flat Rolling," *CIRP Annals*, vol. 40, no. 1, pp. 223 – 226, 1991.

[65] A. M. S. Eugene A. Avallone, Theodore Baumeister, *Marks' Standard Handbook for Mechanical Engineers*. McGraw-Hill, 2006.

[66] W. G. Beare and F. P. Bowden, "Physical properties of surfaces I - Kinetic friction," *Philosophical Transactions of the Royal Society of London. Series A, Mathematical and Physical Sciences*, vol. 234, no. 741, pp. 329–354, 1935.

[67] T. L. Bergman, A. S. Lavine, F. P. Incropera, and D. P. DeWitt, *Fundamentals of Heat and Mass Transfer, 7th Edition*. John Wiley & Sons, 2011.

[68] B. Sundén, *Introduction to Heat Transfer*. WIT Press, 2012.

[69] Y. A. Cengel, *Heat Transfer: A Practical Approach*. Mcgraw-Hill (Tx), 2002.

[70] J. Levin and R. Rigdal, "Aerodynamic analysis of drag reduction devices on the underbody for SAAB 9-3 by using CFD." Master thesis, 2011.

[71] Y. J. Wang and K. M. Zhang, "Coupled turbulence and aerosol dynamics modeling of vehicle exhaust plumes using the ctag model," vol. 59, pp. 284 – 293, 2012.

[72] A. Fujimoto, A. Saida, and T. Fukuhara, "A New Approach to Modeling Vehicle-Induced Heat and Its Thermal Effects on Road Surface Temperature," vol. 51, pp. 1980–1993, 11 2012.

[73] A. Fujimoto, A. Saida, T. Fukuhara, and T. Futagami, "Heat transfer analysis on road surface temperature near a traffic light," 2010.

[74] P. Abrahamsson, F. J. Márquez-Fernández, and M. Alaküla, "Thermal Modeling of an ERS during Dynamic Charging," in *2019 IEEE Vehicle Power and Propulsion Conference (VPPC)*, pp. 1–6, 2019.

[75] M. A. Goforth, G. W. Gilchrist, and J. D. Sirianni, "Cloud effects on thermal downwelling sky radiance," in *Proc.SPIE*, vol. 4710, 2002.

[76] P. Abrahamsson and M. Alaküla, "Thermal modeling of an ERS during static charging," in *2018 IEEE International Conference on Electrical Systems for Aircraft, Railway, Ship Propulsion and Road Vehicles International Transportation Electrification Conference (ESARS-ITEC)*, pp. 1–6, 2018.

[77] M. Ciappa, "Selected failure mechanisms of modern power modules," *Microelectronics Reliability*, vol. 42, pp. 653–667, 2002.

[78] J. Ottosson, *Thermal Modelling of Power Modules in a Hybrid Vehicle Application*. Tryckeriet i E-huset, 2013.

[79] J. Lutz, T. Herrmann, M. Feller, R. Bayerer, T. Licht, and R. Amro, "Power cycling induced failure mechanisms in the viewpoint of rough temperature environment," in *5th International Conference on Integrated Power Electronics Systems*, pp. 1–4, March 2008.

[80] R. Bayerer, T. Licht, T. Herrmann, J. Lutz, and M. Feller, "Model for Power Cycling lifetime of IGBT Modules – various factors influencing lifetime," in *Proceedings of the 5th International Conference on Integrated Power Electronic Systems*, pp. 37–42, 2008.

[81] A. Wintrich, U. Nicolai, W. Tursky, and T. Reimann, "Application Manual Power Semiconductors." SEMIKRON International GmbH, 2015.

[82] Wacker, "WACKER® SILICONE PASTE P12." Revised: 11.11.2019.

Printed by Media-Tryck, Lund 2020 NORDIC SWAN ECOLABEL 3041 0903

Div. Industrial Electrical Engineering and Automation
Department of Biomedical Engineering
Faculty of Engineering
Lund University
ISBN: 978-91-985109-0-4
CODEN: LUTEDX/(TEIE1093)/1145/(2020)